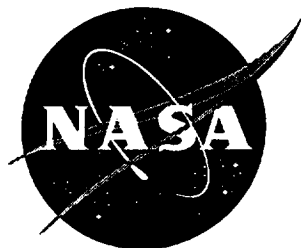NASA Technical Memorandum 110204

Structural Test Documentation and Results for the McDonnell Douglas All-Composite Wing Stub Box

Dawn C. Jegley and Harold G. Bush
Langley Research Center, Hampton, Virginia

April 1997

Structural Test Documentation and Results for the McDonnell Douglas All-Composite Wing Stub Box

Dawn C. Jegley
and
Harold G. Bush

Abstract

The results of a series of tests conducted at the NASA Langley Research Center to evaluate the behavior of an all-composite full-scale wing box are presented. The wing stub box is representative of a section of a commercial transport aircraft wing box and was designed and constructed by McDonnell Douglas Aerospace Company as part of the NASA Advanced Composites Technology (ACT) program. Tests were conducted with and without low-speed impact damage and repairs. The structure with nonvisible impact damage carried 140 percent of Design Limit Load prior to failure through an impact site.

Introduction

To evaluate the potential of a stitched graphite-epoxy material form for use in commercial transport aircraft wings, a short section of a wing box was designed and fabricated by the McDonnell Douglas Aerospace Company as part of the NASA Advanced Composites Technology Program (ACT) contract NAS1-18862. This short wing-box section is referred to herein as the "wing stub box." The wing stub box was tested at the NASA Langley Research Center to evaluate its structural performance. The present paper describes the results of a series of tests designed to investigate the effects of applied bending and vertical shear loading conditions that simulate a 2.5g flight maneuver, visible and non-visible impact damage, and a repair on the response and failure of the wing-stub-box test specimen.

Wing-Stub-Box Test-Specimen Description

The wing-stub-box test specimen consists of a metallic load-transition structure at the wing root, a composite wing stub box, and a metallic extension structure at the wing tip as shown in figure 1a. The load-transition structure and the wing-tip extension structure are metallic end fixtures required for appropriate load introduction into the composite wing stub box during the test. The load-transition structure is located inboard of the composite wing stub box (between the composite wing stub box and the vertical reaction structure at the wing-stub-box root), and the wing-tip extension structure is located outboard of the composite wing stub box. The load-transition structure is mounted on a steel and concrete vertical reaction structure resulting in a nominally clamped end condition. Details of the fixtures are shown in figure 1b.

The composite wing stub box and the wing-tip extension structure are each approximately 11.6 feet long. The load-transition structure is approximately 2 feet long. The wing stub box is approximately 8 feet wide and 28 inches deep at its inboard end, and 5 feet wide and 15 inches deep at its outboard end. The load-transition structure is 8 feet wide and 28 inches deep throughout. The wing-tip extension structure is approximately 5 feet wide and 15 inches deep at its inboard end, and 3 feet wide and 15 inches deep at its outboard end. The entire structure, including the composite wing stub box and the metallic fixtures, is approximately 25 feet long.

The composite wing stub box was fabricated from Hercules, Inc. AS4/3501-6 and IM7/3501-6 graphite-epoxy materials which are stitched together using E. I. DuPont de Nemours, Inc. Kevlar thread. IM7 graphite fibers are only used for the 0 degree fibers in the lower cover panel skin. The composite skin and stiffeners are composed of layers of the graphite material forms that were prekitted in nine-ply stacks which have a $[45/-45/0_2/90/0_2/-45/45]_T$ stacking sequence. Each nine-ply stack is approximately 0.058 inches thick. Several nine-ply stacks of the prekitted material are used to build up the desired thickness at each location. The composite wing stub box was fabricated using the Resin Film Infusion (RFI) process which is described in reference 1. The metallic structures are made from steel and aluminum. The composite wing

stub box weighs approximately 1,200 lb and the entire wing-stub-box test specimen weighs approximately 7,700 lb.

The composite wing stub box consists of upper and lower cover panels (each of which has stringers and intercostals stitched to the skin), ribs and spars. All of these parts are made from graphite-epoxy material. The skin of the upper and lower cover panels range in thickness from approximately 0.3 to 0.9 inches. The upper cover panel has nine stringers oriented along the length of the wing box and parallel to the rear spar. The lower cover panel has eleven stringers oriented along the length of the wing box and parallel to the rear spar. The skin in the upper cover panel varies in thickness and contains from five to ten of the nine-ply stacks, depending upon the location on the wing. The skin in the lower cover panel also varies in thickness and contains from six to fifteen of the nine-ply stacks, depending upon the location on the wing. The stringers are made from eight nine-ply stacks (except at stiffener runout details where the number of stacks is reduced from eight to two). The stringers are blade stiffeners which are approximately 2.3 inches tall and 0.46 inches thick with a 1.12-inch-wide flange on either side of the web.

In addition, the composite wing stub box contains front and rear spars and five ribs. The ribs are connected to the cover panels at intercostals which are attached to the skins. The intercostals are approximately 2.3 inches tall and 0.116 inches thick. The geometry of the upper and lower cover panels is shown in figure 2. The locations of the ribs and stringers and rib and stringer identification numbers are shown in the figure. Ribs are numbered from 4 to 8, starting at the inboard end of the wing stub box. Stringers in the lower cover panel are numbered from 1 to 11, starting at the rear spar, and are spaced uniformly seven inches apart. Stringers in the upper cover panel are numbered from 1 to 10, starting at the rear spar. Stringers in the upper cover panel are uniformly spaced seven inches apart except for the bay which contains the access door. Inboard of rib 7, the stringers on either side of the access-door bay are 18 inches apart. Stringer 6 is in the center of this bay outboard of rib 7 only. Stringer 6 is run out by tapering the web and flange thicknesses as the stringer approaches rib 7. To provide additional support, an aluminum T fitting was bolted to the web of stringer 6 and to the intercostal at rib 7. One composite blade stiffener and two metal angles, oriented parallel to

the ribs, were placed between ribs 5 and 6 and between ribs 6 and 7, respectively, to prevent the skin from buckling prematurely. However, since no axial stiffeners are included in this region, this region is referred to herein as the "unsupported region."

Loading   Conditions

The test specimen was loaded in bending by slowly applying a single concentrated vertical load to the outboard end of the wing-tip extension structure. This loading condition caused the upper cover panel of the wing stub box to be loaded predominately in compression and the lower cover panel to be loaded predominately in tension. The Design Ultimate Load for the wing box was determined by the applied load that was predicted to generate 40 ksi of stress in the upper cover panel and 50 ksi of stress in the lower cover panel. These stress levels were predicted to correspond to an applied load at the jack position of 166,000 lb, as discussed in reference 2. The Design Limit Load was 110,600 lb. A series of four tests was conducted. The test specimen was loaded to failure in the last test.

Instrumentation

Displacements were recorded at 15 locations on the test specimen and at one location on the vertical reaction structure under the rear spar of the test specimen. Direct Current Displacement Transformers (DCDTs) were placed at six locations on the lower cover panel and at six locations on the upper cover panel of the wing stub box, as shown in figures 3 and 4, respectively. DCDTs were placed at three locations on the extension structure, including the loading point, as shown in figure 3. The location of these 16 DCDTs was not changed through the test series and data measured by all DCDTs were recorded during each test.

A total of 254 strain gages were used to record strains in the test specimen. Strain gages were placed on the load-transition structure, on the composite wing stub box, and on the wing-tip extension structure. Strain gages were placed on interior surfaces prior to final specimen assembly and on exterior surfaces after final assembly. Most strain gages were applied prior to testing,

but some strain gages were added between tests (such as those around impact sites). Strain gage locations for the wing stub box cover panels are shown in figures 5-11. Strain gage locations on the upper cover panel are shown in figure 5. Strain gage locations on the lower cover panel are shown in figure 6. Strain gage locations on the stringer blades and flanges are shown in figure 7. Strain gage locations on two stiffener runouts on the upper cover panel are shown in figure 8. Strain gage locations on the metal-to-composite splices between the upper cover panel and the load-transition and wing-tip extension boxes are shown in figure 9. Strain gage locations on the intercostals are shown in figure 10. Strain gage locations in the vicinity of impact sites are shown in figure 11. All strain gages on the upper and lower cover panels measure strain in the 0 degree direction, which is parallel to the rear spar, except for strain gages which are part rosettes, strain gages which are located at the front spar and strain gages around the access door.

Strain gage locations on the front and rear spars are shown in figures 12 and 13, respectively. Strain gage locations on the ribs are shown in figure 14. Strain gage locations on the metallic load-transition structure are shown in figure 15. Strain gage locations on the metallic wing-tip extension structure are shown in figures 16 and 17. Additional details of strain gage locations are shown in reference 3.

Fixtures and Accessories

Fixtures to attach to load-transition structure to the vertical reaction structure, a 300-kip actuator assembly, four support poles, and an impact apparatus were required to position, load and damage the test specimen.

Mounting and Loading Apparatus

All fixtures and support structures are shown in figure 1b. To apply proper boundary conditions at the root end of the composite wing stub box, fixtures were designed and built to attach the inboard end of the test specimen to the vertical reaction structure. The fixtures were designed to provide a nominally clamped end condition. The vertical reaction structure contains a slotted steel platen with slot centers that are three inches apart. T-bolts were positioned in

the slotted plate to attach steel attachment and bearing plates to the vertical reaction structure. Two rows of bolts were used to hold the lower cover panel of the transition structure to the vertical reaction structure. The load-transition structure was bolted to the vertical reaction structure through the bearing and attachment plates as shown in figure 18. The metal fixtures are represented in the figure by the unfilled regions on the figure and the locations of contact between the load-transition structure and the bearing and attachment plates are represented by the filled regions on the figure. All dimensions in the figure are in inches.

To hold the test specimen in position prior to testing and between tests, four aircraft jacks and four steel support poles were placed beneath the wing-tip extension box. These jacks were required to prevent sagging of the test specimen due to gravity. These jacks were adjusted so that the upper cover panel skin of the wing stub box was level. That level position was the starting point for all tests.

For the load to be introduced correctly into the test specimen, a 300-kip actuator assembly was required. This assembly contained the 300-kip actuator, a load cell, a swivel on each end of the actuator to allow rotation during loading, a load reaction plate attached to the lower cover panel and front spar of the wing-tip extension structure, and a support truss. The actuator, load cell and swivels were connected together, and then positioned inside the support truss. The support truss not only held the actuator upright prior to its connection to the load reaction plate, but also was strong enough to prevent the actuator from falling to the floor if the test specimen broke apart at failure. The support truss and actuator apparatus was moved under the wing tip and the top of the swivel was attached to the wing-tip extension box.

Impact Apparatus

A dropped-weight impactor was designed and built to inflict impact damage to the upper cover panel of the composite stub box. A photograph of the dropped-weight impactor is shown in figure 19. In this figure, the impactor is shown resting on steel beams which are positioned to allow the one-inch-diameter tup of the impactor to rest on the cover panel when it is at its lowest

6

position. The square plate at the bottom of the impact apparatus was clamped to the steel beams to prevent the impactor from moving during use. Using this apparatus, a weight of 25 pounds could be dropped from up to 7.56 feet, resulting in a maximum impact energy of 189 ft-lb. The weight was lifted to the required height (determined by the desired impact energy) and released. The apparatus contains no catch mechanism so a board was moved over the impact site during the rebound of the tup after the first impact to prevent additional impacts and additional damage to the cover panel. (Note that some of the DCDT's shown in the photographs were moved to allow positioning of the impact apparatus and are not shown in the same position as during testing)

Test Series

Four tests were conducted in which the test specimen was loaded in bending. In the first three tests, the load was increased until a specified load value was reached, then the load was slowly decreased until no load was applied. Load rates for increasing the load varied from 5,000 lb/min to 18,000 lb/min. Generally, the load rate was reduced as higher load levels were applied. The specimen was unloaded after each of the first three tests at a rate twice the maximum load rate for that test. For the last test, the load was increased until the test specimen failed. The load for the ordinates in subsequent figures of load-versus-displacement and load-versus-strain results is the load applied by the jack at the outboard end of the wing-tip extension structure. The applied load corresponding to Design Ultimate Load is 166,000 lb.

Test 1- System Checkout

The purpose of the first test was to verify the correct operation of the instrumentation and to determine that the load was being introduced into the structure as intended. The structure was to be loaded to no more than 50 percent of DLL, or approximately 55,300 lb. Strains and displacements were monitored as the structure was being loaded. Loading was stopped at 53,000 lb. The structure was then unloaded. This process left deformation in the structure so that it did not return to its initial position. The location of the point of load application was approximately 0.3 inches higher after this test than before it was started, indicating that permanent deformation occurred in

the structure. The most likely source of this deformation is deformation in the bolted joints.

Test 2- Undamaged Structure Loaded to Design Limit Load

The purpose of the second test was to verify that the initially undamaged structure could support DLL (110,600 lb of load application) without failure. Strains and displacements were monitored as the structure was being loaded. The structure was loaded to DLL and unloaded. This test left deformation in the structure so that it did not return to its initial position for this test. The displacement at the point of load application measured after the test was approximately 0.5 inches more than the initial value.

Test 3- Damaged Structure Loaded to Design Limit Load

The purpose of the third test was to verify that the impact-damaged structure could support DLL without failing. A dropped-weight impactor was used to inflict visible damage to the upper cover panel midbay between two stringers aft of the access door. The impact site, marked DET1, is shown in figure 5. For purposes of this test, "visible damage" was defined as a 0.1-inch-deep dent in the surface.

In order to limit the dent depth to 0.1 inches, the damage was inflicted by a series of impacts at the same location. Four impacts were required to inflict the required dent depth. After each impact, the dent depth was measured and the region of skin around the impact site was nondestructively evaluated by ultrasonic scanning to determine the area of the structure which had been damaged. The impact energies of the four impacts and their effects are shown in table 1. After the fourth impact, the dent was 0.093 inches deep and the damage area was defined by an oval with an axial dimension of 5.75 inches and a width dimension of 2.75 inches. No further impacts were made since further growth in the size of the damage area was not desired. The stringer flanges and blades of the upper cover panel were not damaged in the impact process. A photograph of the damaged region, with the region of damage outlined by white marks, is shown in figure 20. Damage was easily visible by eye.

8

Additional strain gages were added to the upper cover panel exterior surface in the vicinity of the impact damage prior to loading. The structure was loaded to DLL and unloaded in the same manner as in test 2. The displacement at the point of load application measured after the test was approximately 0.1 inches more than the initial value.

Test 4- Repaired Structure Loaded to Failure

The purposes of the fourth and final test were to determine whether the repaired structure could support Design Ultimate Load prior to failure, to evaluate the effects of nonvisible damage, and to activate one or more failure mechanisms.

A bolt-on metal patch was used to repair the upper cover panel. All materials for the patch were supplied by McDonnell Douglas Aerospace and personnel from American Airlines installed the patch. The structure was prepared for patch installation by cutting out the damaged section of skin, as shown in figure 21. The cutout was in the shape of an ellipse with dimensions 7.5 inches by 3.75 inches. The cutout was in the skin between stringers, as illustrated in figure 22. Bolt holes were drilled through the stringer flanges and skin. A 3/8-inch-thick aluminum plate was bolted to the external skin to cover the cutout. The plate dimensions were 11.7 inches by 7.28 inches. The completed repair is shown in figure 23.

A dropped-weight impactor was used to inflict nonvisible damage to the upper cover panel at two locations. An impact energy of 100 ft-lb was used to inflict the nonvisible damage. These impact sites are at a stiffener runout near the front spar and at the edge of a flange near the rear spar. The front and rear impact sites, labeled NDT1 and NDT2, respectively, are shown in figure 5. The damage area in the upper cover panel skin around each damage site was determined ultrasonically and that area was marked on the upper cover panel. Photographs of these damage regions prior to testing are shown in figure 24. The damage area at location NDT1 is an oval with dimensions of 4.0 inches by 3.0 inches. The damage area at location NDT2 is approximately "L" shaped with dimensions of 4.0 inches and 3.0 inches. The dent depth for the dent at location NDT1 is 0.014 inches. The dent depth at location NDT2 is 0.0134 inches.

No fiber breakage was visible on the outer surface of the structures and the dents were difficult to detect by eye. There was no way to gain access to the interior of the wing box at these locations to evaluate any possible damage to the interior structure, such as intercostals and stringers, prior to testing.

Results and Discussion

Results for strains and displacements and photographs of structural failures are presented in this section. Most of the strains and displacements measured during the first three tests were the same as those for the fourth test. As a result, data are only shown for the fourth test, except for the impact and repair regions. Strains are presented for the last three tests for the impact and repair regions. All results are presented prior to a discussion of the failure mode for the wing stub box.

Displacement Results

Displacement results are shown in figures 25-30. Displacement results for the lower surface of the test specimen, including the displacement at the loading point, are shown in figures 25 and 26. Displacement results for the upper surface of the test specimen are shown in figures 27-29. Displacement results for the vertical reaction structure are shown in figure 30.

The global behavior of the test specimen can be evaluated from the behavior of its lower surface. The displacement results shown in figure 25 indicate that the relationship between load and vertical displacement is approximately linear for the entire load range for all lower surface locations monitored. The relationship between the measured upward motion at each location and the distance from the wing root at the maximum load level applied is shown in figure 26. The displacement measured along the front edge and along the rear edge of the test specimen are shown in the figure. Measured displacements are shown as data points and a curve fit is used to connect the five data points on each of the front and rear edges. Since the structure is 15 inches wide at the load application point, the displacement measured at that point is assumed to apply to both front and rear edges. The measured upward deflection varies from 0.12 inches near the root to 14.1 inches at the point of load application.

At the rear and front edges just inboard of the splice between wing stub box and the wing-tip extension structure, the difference between the deformations is approximately 1.0 inch. The structure is approximately 5 feet wide at this splice. This difference indicates that there is a small amount of twist in the structure.

The local behavior of upper cover panel of the wing stub box can be evaluated from the behavior of DCDTs 7-12, shown in figure 27. The relationship between load and displacement measured in the upper cover panel is linear for loads less than approximately 70 kips. For loads greater than 70 kips, nonlinear behavior is apparent in all six upper surface DCDTs. The nonlinear behavior is most pronounced for the DCDTs measuring displacement along a line outboard from the access door. The stringer spacing in this region is 18 inches, rather than 7 inches as in all other parts of the upper cover panel. This wide spacing results in an unsupported region of the skin which exhibits local out-of-plane deformation at a lower load than any other part of the wing stub box.

There are two responses that affect the behavior of the upper cover panel. The first response is the global bending behavior and the second is the local behavior in the unsupported region of the cover panel. To evaluate the behavior of the upper cover panel, a comparison can be made between results from the three DCDTs measuring displacement in the unsupported region of the upper cover panel (DCDTs 7, 8 and 9) and the three DCDTs measuring displacements 15.875 inches aft of these DCDTs (DCDTs 10, 11, and 12). DCDTs 10, 11, and 12 represent far field deformations affected only by the global behavior of the upper cover panel. The differences between the displacements measured by DCDTs 7 and 10 (which are 18 inches outboard from the access-door cutout), DCDTs 8 and 11 (which are 33 inches outboard from the access-door cutout), and DCDTs 9 and 12 (which are 63 inches outboard from the access-door cutout) for the complete load range are shown in figure 28. The difference between the displacements in the unsupported region and the far field results is small for loads less than approximately 50 kips. However, this difference increases rapidly at locations 18 and 33 inches from the access-door for loads greater than approximately 100 kips. The difference increases

rapidly 63 inches from the access-door for loads greater than approximately 130 kips.

Ribs 5, 6, 7, and 8 support the cover panel outboard of the access-door cutout. By assuming that there is no difference between deformations in the unsupported region and the far field results at the locations of these ribs, and by considering the difference between displacement measurements in the unsupported region and the far field region, deformations caused by local behavior outboard of the access-door cutout edge to rib 8 can be determined. This deformation pattern is shown in figure 29 for a series of load levels. Measured differences are shown as symbols in figure. The curves shown in the figure are interpolations used to connect the assumed rib displacements and the measured data. Between ribs 5 and 6, the displacement increases monotonically as the load increases from zero to the maximum load. The location of the maximum displacement in this bay is half way between the ribs and the magnitude of the maximum displacement is approximately 0.33 inches. The skin deforms upward out of the wing stub box. Between ribs 6 and 7, the magnitude of the displacement also increases monotonically as the load increases from zero to the maximum load, however, the location of the maximum displacement is not half way between the ribs but is dependent upon the load level. The maximum displacement is 0.42 inches downward into the wing stub box between ribs 6 and 7. Between ribs 7 and 8, the magnitude of the displacement increases monotonically as the load increases from zero to 120 kips. However, the displacement reaches a maximum value of 0.07 inches downward into the wing stub box at a load of approximately 126 kips, then decreases in magnitude and changes sign at a load of approximately 144 kips. This reversal of direction of the displacement indicates that a change in the behavior of the upper cover panel skin has occurred. Nevertheless, the location of the maximum displacement in this bay is half way between the ribs for each load level whether the displacement is up or down. The maximum displacement between ribs 7 and 8 when the structure failed was 0.28 inches.

The displacements measured on the upper cover panel indicate that the skin between ribs 5 and 8 buckled well before the wing stub box failed. The reversal in direction of the displacement between ribs 7 and 8 indicate that a local phenomenon occurred, such as a local failure, in that region. This local

phenomenon led to large out-of-plane deformations which were not associated with the global bending behavior of the structure.

The displacement of the vertical reaction structure is shown for the last two tests in figure 30. The displacement of the vertical reaction structure never varied by more than 0.00015 inches during test 3, which had a maximum load of 110 kips. The displacement of the vertical reaction structure never varied by more than 0.00011 inches during the final test for loads less than 100 kips. However, for load levels greater than 100 kips in the last test, the displacement appeared to increase to almost 0.008 inches. Prior to each test, each DCDT was examined to verify that it would slide easily as the probe tip was moved. After the last test, examination of this DCDT revealed that the probe was jammed into its base and was not movable. No explanation for this damage could be found. Therefore, the data recorded from this DCDT during the last test must be considered suspect. There was no reason to believe that data recorded during the third test for this DCDT are in error.

Strain results

Data from all strain gages are presented in this section. Strains measured in the upper cover panel (away from the impact and repair locations) are shown in figures 31-43. Strains measured in the lower cover panel are shown in figures 44-47. Strains measured in the front and rear spars are shown in figures 48 and 49, respectively. Strains measured in the ribs are shown in figures 50-54. Strains measured in the load-transition structure are shown in figure 55. Strains measured in the wing-tip extension structure are shown in figure 56. Strains measured in the region of visible damage and repair are shown in figure 57 and 58. Strains measured in the region of nonvisible damage site 1 are shown in figure 59 and strains measured in the region of nonvisible damage site 2 are shown in figures 60 and 61.

A sketch of part of the test specimen is shown in each figure with a shaded region indicating the location of the strains shown in that figure. These sketches give a general location and are not meant to provide details of strain gage locations. Details of the strain gage locations are presented in figures 5-16. All strain gages are oriented axially (parallel to the rear spar and the

stringers), unless otherwise noted. Each curve shown is identified by the number of the strain gage it represents. In discussions of maximum values of strain, the magnitude of strain is discussed. All axial strain gages on the upper cover panel are in compression (negative strain) for load less than 50 kips. All axial strain gages on the lower cover panel are in tension (positive strain) for load less than 50 kips.

Strain gage results for the upper cover panel, in the form of strain versus load, are grouped together according to location for presentation in figures 31-42. A sketch of the upper cover panel is shown in each figure. All rib and stringer identification numbers are shown in figure 2 and all strain gage locations and numbers are shown in figure 5. The strains measured by rows of strain gages on the upper cover panel stringers halfway between ribs 6 and 7 and halfway between ribs 4 and 5 are shown in figures 31 and 32, respectively. Skin and lateral stiffeners are located in the unsupported region between ribs 6 and 7. The access door is located in the unsupported region between ribs 4 and 5. All strain gages in these rows are located on the external skin of the upper cover panel or on the side of the blade inside the wing stub box. The distance of each strain gage from the unsupported region (in terms of the number of bays or stiffeners away) is shown in the figures.

The strains measured between ribs 6 and 7 are shown in figure 31. The solid lines represent strains from strain gages 22, 23, 24, 607 and 608, which are on the stringer blades and skin at the edge of the unsupported region. The dashed lines represent strains from strain gages which are farther away from the unsupported region. Results from strain gages 23, 24 and 607, which are on the blades on the edge of the unsupported region, indicate the onset of nonlinear behavior at a load of approximately 100 kips and indicate pronounced nonlinear behavior starting at approximately 125 kips. Results from strain gages 18 and 19, which are the farthest from the unsupported region in this row, indicate nonlinear behavior away from the unsupported regions begins at a load of approximately 130 kips.

The strains measured between ribs 4 and 5 are shown in figure 32. The solid lines represent strain gages 75, 76, 81, 82 and 83 which are on the stringer blades and skin at the edge of the bay containing the access door. The dashed

14

lines represent strain gages which are farther away from the access door. Nonlinear behavior occurs at the stringers adjacent to the access door starting at approximately 50 kips of applied load. Four bays aft of the access door, at strain gage 8, the load-strain relationship is linear for the entire load range. Two bays away from the access door, nonlinear behavior is not evident for load less than 125 kips.

The strains measured in the region immediately around the access door are shown in figure 33. The strains in stringer 5 are shown as solid lines. The strains in stringer 7 and at the cutout edges are shown as dashed lines. Strain gages 78 and 612 are located at the corners of the access-door cutout on the external surface and record approximately linear strain for loads lower than 150 kips. The magnitude of the maximum strain recorded by these strain gages is approximately 0.007 in/in. Strain gages 79 and 80 are on the internal and external surfaces, respectively, at the side of the cutout. Strains at the side of the cutout are less than strains at the corners, and nonlinear behavior is evident at the sides but not at the corners. The nonlinearity in the behavior of the strain gages on the stringers is more dramatic than in the skin, although higher strains occur in the skin. The interaction between the access-door cutout edge and the bolt holes around the access door leads to high strains around the access-door cutout. The nonlinearity is caused by the large unstiffened region, i.e., the large cutout in the skin. The access-door carries little load and contributes little to the stiffness of the cover panel.

The strains measured in the unsupported skin between ribs 5 and 7 and in adjacent stringers 5 and 7 are shown in figure 34. Location "A" in the figure is half way between ribs 5 and 6. Location "B" in the figure is half way between ribs 6 and 7. The results from strain gages on the skin are shown as solid lines while the results from strain gage at the stringers are shown as dashed lines. All strain results in this region indicate nonlinear behavior. The most pronounced nonlinearity can be seen in the results from interior strain gages 23, 24 and 607, which are on the stringers surrounding the unsupported skin between ribs 6 and 7. Comparison of results from back-to-back strain gages 63 and 64, which are on the skin between ribs 6 and 7, suggest that an instability initiates at approximately 135 kips. Nonlinear behavior initiates prior to that load level. Similarly, results from strain gages 67 and 68, which are between

ribs 6 and 7, indicate that an instability initiates at approximately 135 kips. Strain gage 614, on the external surface at stringer 5, shows almost the same behavior as strain gage 613, on the external surface at stringer 7. No internal strain gages were located at these locations.

The strains measured on the runout of stringer 6 and at the intercostal at the intersection of rib 7 and stringer 6 are shown in figure 35. All strain gages are oriented axially except for strain gage 34, which is oriented 45 degrees to the stringers, and for strain gage 35, which is oriented 90 degrees to the stringers. All strain gage results indicate linear behavior with no pronounced discontinuities in slope for loads less than 120 kips. Nonlinearity in the load-strain behavior in the runout at stringer 6, indicated by strain gages 55, 56 and 58, begins at a load of approximately 120 kips. Nonlinear behavior initiates between 130 and 140 kips for strain gages 57, 35, 49 and 50. A strain reversal occurs at a load of 140 to 145 kips at strain gages 33, 34, and 35 on the intercostal at rib 7 and at strain gages 55, 56, 57, and 58 on the stringer at the runout. This reversal also occurs on stringer 6 away from the runout at strain gages 49 and 50, though no pronounced discontinuities in slope occur at strain gages 49 and 50. Discontinuities in slope occur in strain gages 55, 56, 57, and 58 at 145 kips. Discontinuities in slope occur at strain gages 33 and 34 at 140 kips, 145 kips and at 150 kips. A series of local failures would explain this behavior.

The strains measured in the upper cover panel at the front spar are shown in figure 36. The solid lines in the figure represent strains at the inboard splice between the load-transition structure and the composite stub box. The dashed lines represent strains further outboard on the stub box. Strain gages 48, 74, 77, 609, 610 are parallel to the front spar (-13 degrees to the stringers). Strain gage 47 is perpendicular to the front spar (-103 degrees to the stringers). Strain gages 69, 70, and 71 form a rosette measuring strain in the 0, 45, and 90 degree directions, respectively. The magnitude of the strain measured by these strain gages were less than 0.005 in/in. All strain gages along the front spar indicate linear behavior for load less than approximately 110 kips. Strains at the inboard splice and at rib 8 remain linear throughout the entire load range. However, nonlinear behavior initiates and a discontinuity in the slope of the load-strain relationship occurs in the 45 and 90 degree components of the rosette at rib 5 at a load of 100 kips. Nonlinear behavior

initiates between ribs 4 and 5 and the outboard splice between the composite wing stub box and the wing-tip extension structure at a load of approximately 125 kips.

The strains measured in and around the stiffener runouts which terminate at ribs 7 and 8 by the front spar are shown in figure 37. Strain gages 43 through 46 are on the stiffener runout which terminates at rib 7. Strain gages 59 through 62 are on the stiffener runout which terminates at rib 8. Strains measured at the center of the stringer flange are shown as solid lines. Strains measured at the edge of the stringer flange are shown as long dashed lines. Strains measured on the intercostal flange are shown as medium dashed lines, and strains on the external surface of the skin are shown as short dashed lines. For loads less than 100 kips, the stiffener runouts behave the same way, except at the flange edge, gages 44 and 60. Impact damage was inflicted at the stiffener runout which terminates at rib 8 prior to the final test. All strain gages shown in figure 37 are in compression except strain gage 44. Unlike the other strain gages, the behavior of strain gage 44, which is close to the impact site, is not the same in the final test as in the preliminary tests. A comparison between the strain gages at the impact site for the tests with and without impact damage is presented in a subsequent section. Strain gages at the stiffener runout which terminates at rib 7 indicate linear behavior for loads less than approximately 130 kips. For load greater than 130 kips, a slight deviation from linear behavior can be seen. Nonlinear behavior can be seen for the strain gages at the stiffener runout which terminates at rib 8 for a load of approximately 110 kips. Pronounced nonlinearities and discontinuities indicating failures and load redistribution can be seen in the results for strain gages 43 and 45 for loads greater than approximately 110 kips.

The strains measured in the upper cover panel near the rear spar are shown in figure 38. All strain gages are oriented axially except strain gages 6, 7 and 30. Strain gages 7 and 30 are oriented 90 degrees to the rear spar. Strain gage 6 is oriented 45 degrees to the rear spar. All strain gages indicate linear behavior for the entire load range. The magnitude of the maximum strain recorded in this region is approximately 0.004 in/in.

The strains measured in the upper cover panel in the aft outboard corner are shown in figure 39. Strain gages 25 and 26 are oriented axially. Strain gages 28 and 30 are oriented 90 degrees to the stringers. Strain gage 27 is oriented 45 degrees to the stringers. Except for strain gage 29, the strain gages in this region indicate linear behavior for the entire load range. Strain gage 29 is on the blade of stringer 1 and indicates nonlinear behavior for loads greater than 100 kips, however, no discontinuities in the slope of the load-strain curve occur. Strains in this region do not exceed 0.005 in/in.

The strains measured on the blade of stringer 3 and on the external skin at stringer 3 are shown in figure 40. All strain gages are halfway between the ribs, with strain gages 84 and 85 between ribs 4 and 5, strain gage 17 between ribs 5 and 6, strain gages 20 and 21 between ribs 6 and 7, and strain gage 615 between ribs 7 and 8. Stringer 3 is away from the access door and the unsupported region, and can be considered a far field region. Strains on the external skin are shown as solid lines in the figure, and strains on the stringer blade are shown as dashed lines. The magnitudes of the strains do not exceed 0.005 in/in. However, nonlinearity is evident in the data from strain gages 20, 21, 84 and 85. This nonlinearity and the difference between blade and skin strain gages at the same axial location is caused primarily by the global bending of the test specimen.

The strains measured at the composite-to-metal splice joints are shown in figures 41 and 42. Data from splices between the load-transition structure and the wing stub box and between the wing stub box and the wing-tip extension structure are shown in the figures (see figures 5-17 for the details of the strain gage locations). Strains in the composite skin are shown in figure 41 and strains in the metal splice components are shown in figure 42. Strains in the composite skin exterior and interior surfaces are shown as solid curves and dashed curves, respectively, in figure 41. Interior strain gages are placed on the skin at the base of the stiffener where the blade ends. Exterior gages are placed at the same location as interior gages, but on the external surface. Strains on the external surface at inboard and outboard splices do not exceed -0.005 in/in. and remain linear for almost the entire load range. However, strains on the internal surface at the base of the stiffener record unusually high strains at the outboard splices. The strains recorded at the base of the

stiffeners in the outboard splices are linear for loads less than 120 kips, then indicate nonlinear behavior for subsequent loads up to failure. At 120 kips, the strains are approximately -0.0011 in/in. for strain gage 32 at stringer 1, -0.02 in/in. for strain gage 36 at stringer 5, and -0.009 in/in. for strain gage 38 at stringer 6. For loads up to 110 kips, these curves were the same for each load applica-tion. At a load of 150 kips, the strain measured at stringer 5 is -0.025 in/in.

Strains measured on the splice plates and fittings are shown in figure 42. Strains for the exterior metal splice plates are shown in solid lines. Strains for the interior metal splice plates are shown as short dashed lines and strains for the splice angle fittings are shown as long dashed lines. The strain gages on the splice plates recorded linear strain for the entire load range with maximums ranging from -0.001 to -0.0025. However, the strain gages on the splice angle fittings recorded nonlinear behavior. The strain gages on the inboard splice angle fittings, strain gages 89 and 90, recorded strains which are linear for load less than approximately 110 kips and then the strains increase nonlinearly to a maximum of 0.005 and 0.0058 for stringers 1 and 3, respectively. The strain gages on the outboard splice angle fittings, strain gages 86 and 88, recorded strains which are compressive initially and approximately half the magnitude of the strain for the angle fittings of the inboard splice. However, at a load of approximately 125 kips, the curves in the figure reverse and the strains become tensile and grow rapidly, though they do not exceed 0.002 in/in. at failure of the structure.

Since the strains measured by gages 36 and 38 were unusually high, the strain gage locations and wire connections were verified by tracing wires to the splice locations, examining photographs of the strain gages taken prior to final assembly of the structure, and examining the strain gages themselves after testing was completed and the structure was disassembled. The measurements were verified by disconnecting the gages from the data recording system and checking the signals individually during the application of a small load after the first test to 50 percent DLL was completed. Despite these high strains, no evidence of failure could be seen at these strain gage locations during testing or after the structure was disassembled. These strain gages were smaller than most strain gages used on the structure and

were intentionally placed at a strain concentration to measure a very local strain. Strain gages placed on the inboard splices at the base of the stiffeners were damaged during assembly of the test specimen, so there is no information about strains on the internal surface at the base of any stiffeners on the inboard splices. After the load-transition structure and the wing-tip extension structure were disconnected from the wing stub box and all metal splice pieces were removed, several stiffener terminations were cut from the stub box for more extensive examination. Post-test nondestructive evaluation (NDE) and sectioning revealed a separation between the skin and the flange at the end of stringer 5, which is the location of strain gages 36 and 37. Results of a C-scan of this region are shown in figure 43. Similar separations were found after testing in the outboard end of stringer 2 and the inboard end of stringer 3. NDE performed before assembly of the wing stub box revealed no separations at these locations. No further NDE was performed until the stub box was disassembled. Such separations would be expected to move the strain concentration away from the location of the strain gage rather than increase the strain at this location. The cause of the separations and their effect is unknown. However, the wing stub box failed well away from the splice locations and the separations apparently only had a local affect on the behavior of the upper cover panel.

Strains measured on the lower cover panel are shown in figures 44 through 47. Strains on the external surface parallel to the rear spar are shown as solid lines in the figures. Strains on the stiffeners parallel to the rear spar and on the skin oriented -45 and 90 degrees to the rear spar are shown as dashed lines. Strains inboard of rib 5 are shown in figure 44. Strains halfway between ribs 6 and 7 are shown in figure 45. Strains outboard of rib 7 are shown in figure 46. Strains near the front spar are shown in figure 47. All strains inboard of rib 5 are linear for the entire load range and none of these strains exceed 0.003 in/in. Strains on the skin and blade of each stiffener halfway between ribs 6 and 7 also show little nonlinearity and the magnitude of these strains are between 0.0021 and 0.0032 in/in. for the maximum load of 154 kips.

Strains outboard of rib 7 are linear for the entire load range except for the strain gages at stringer 7 on the external surface (strain gages 131, 132, and 133) and at the termination of stringer 8 at the front spar (strain gage 135), as

shown in figure 46. Strain gages 131, 132 and 133 form a rosette that measures strains in the 0, -45, and 90 degree directions, respectively, at stringer 7 halfway between ribs 7 and 8. Each of these strain gages shows a significant discontinuity in the load-strain relationship for a load of approximately 120 kips. This discontinuity represents a load redistribution, but, since there were no comparable strain gages on stringers 6 or 8, little additional information can be determined from this redistribution of load. No visible failure could be seen in this region of the structure.

Results from strain gages on the top of the blades which terminate by tapering as they approach the front spar are shown in figure 47. Strain gages 122, 124 and 137 are parallel to the front spar (oriented -13 degrees to the rear spar). All other strain gages are parallel to the rear spar. Nonlinear behavior for loads greater than 110 kips is evident. The strain measured by strain gage 123 at stringer 11 suddenly decreases in magnitude at a load of approximately 125 kips. The strain measured by strain gage 125 at stringer 10 is 0.0011 in/in. for a load of 110 kips and does not increase significantly as the load is increased greater than 110 kips. The strain measured by strain gage 128 at stringer 9 does not increase significantly for loads greater than 120 kips. The strain measured by strain gage 135 at stringer 8 is 0.0016 for a load of 120 kips and does not increase significantly for loads greater than 120 kips. Other strain gages at the front spar, such as those on the external skin surface, indicate slightly nonlinear behavior.

Strain gage results for the front and rear spars are shown in figures 48 and 49, respectively, for strain gages positioned in midbay locations and on the cutout edges. Results for axial midbay strain gages are shown in the figure as solid curves. Results for strain gages oriented 90 degrees to the upper cover panel (out-of-plane to the cover panels), oriented at a 45 degree angle to the upper cover panel, and at the cutout edges are shown as dashed curves. The plots of strains in the front and rear spars are shown to the same scale. Strains measured on the front spar are linear for the entire load range except for strain gages 213, 214, 215 and 216. These four strain gages have a linear behavior for loads less than approximately 120 kips, then have a nonlinear behavior. They are located on the upper edges of cutouts in the front spar, with the more outboard strain gages recording the higher strains. The

magnitude of the maximum strain recorded on the front spar is less than 0.005 in/in. Strain gages located away from the cutouts record less than 0.001 in/in.

Only strain gage 313 on the rear spar recorded nonlinear strains, as shown in figure 49. There was one cutout in the rear spar and strain gage 313 was located on the upper edge of that cutout. No strains with magnitudes greater than 0.002 in/in. were recorded on the rear spar.

The strains measured on ribs 4 through 8 are shown in figures 50 through 54, respectively. Results from all ribs are shown to the same scale. Results from midbay strain gages are shown as solid curves. Results from cutout edges are shown as short dashed curves. Results from stiffeners on the ribs are shown as long dashed curves. Most strain gages on the ribs recorded nonlinear strains.

The magnitudes of the strains for the most inboard rib, rib 4, do not exceed 0.002 in/in. and these strains do not reverse. The magnitudes of the strains for rib 5 do not exceed 0.001 in/in., but these strains do reverse at approximately 125 kips of load. Rib 5 is located at the inboard edge of the unsupported region of the skin and the strain gages which show strain reversal are located near the region of unsupported skin. The magnitudes of the strains for rib 6 do not exceed 0.002 in/in. and all strains recorded for rib 6 are linear for loads less than approximately 120 kips. Strain gages on the edge of the cutout show strain at approximately 140 kips of load. The magnitude of the strains for rib 7 do not exceed 0.003 in/in., but some strains gages show strain reversal at approximately 120 kips of load while others have a significant amount of nonlinearity. Rib 7 is located at the outboard edge of the unsupported region of the skin, and the strain gages which show strain reversal are located below the region of unsupported skin. Strain gage 480 is located on the skin of the rib at the end of a rib stiffener where the intercostal meets the rib and recorded a strain of approximately 0.00035 in/in. for a load of 115 kips, and a strain of 0.002 in/in. for a load of 153 kips. The magnitudes of the strains for the most outboard rib, rib 8, do not exceed 0.001 in/in. and have a nonlinear behavior and strain reversal for loads greater than approximately 125 kips. The change in the direction of bending in the upper cover panel skin effects the strain measured in rigs 7 and 8.

The strains measured for the load-transition structure are shown in figure 55. The strains measured for the wing-tip extension structure are shown in figure 56. Results for strain gages between stiffeners are shown as solid lines. Results for strain gages on stiffeners are shown as dashed lines. All strain gages are parallel to the rear spar, except those which are part of back-to-back rosettes on the front spar web of the wing-tip extension structure (strain gages 502, 503, 505 and 506). The magnitudes of the strains measured for the load-transition structure are linear to failure and do not exceed 0.002 in/in. The strains measured for the wing-tip extension structure are linear to failure and do not exceed 0.003 in/in.

The strains in the impact-damaged regions are presented in figures 57-61. The strains recorded for the upper cover panel skin in the region of detectable impact damage during three tests of the structure are shown in figure 57. Results are shown for the structure loaded to DLL prior to inflicting damage, the structure loaded to DLL after inflicting damage and the structure loaded to failure after the repair was installed. The strains for the skin and the repair for the final test only are shown in figure 58.

During the loading prior to inflicting damage, the strains in the skin are linear and reach a maximum magnitude of approximately 0.003 in/in. All strain gages in the region to be repaired recorded approximately the same strain. In the loading after visible damage was inflicted, the strains in the skin closest to the damage site were nonlinear in behavior for the entire load range. The maximum strain recorded in the region of visible impact damage is approximately 0.0073 in/in. in a strain gage which is 0.6 inches away from the impact site (strain gage 97). Interior strain gages 1.2 inches away from the impact site (strain gages 9 and 10) recorded the same strains with and without impact damage and with repair. The repair of the structure required the removal of the exterior strain gages closest to the impact site (strain gages 11, 12, 96 and 97). Axial strains measured during the final loading in the repaired bay and the bay adjacent to the repaired bay are shown in figure 58. Strain gages 5, 8, 9 and 10 on the skin recorded approximately the same strain. Strains recorded in the metallic repair are less than half the strains recorded

by the strain gages on the composite structure. No strains in the repair region exceed a magnitude of 0.0045 in/in. after the repair was completed.

Two locations on the upper cover panel were subjected to nonvisible impact damage prior to the final test. The strains recorded during the last three tests near the location labeled NDT1 in figure 5 are shown in figure 59 and the strains around the location labeled NDT2 in figure 5 are shown in figures 60 and 61. Impact site NDT1 is located at the edge of an intercostal flange half way between the rear spar and stringer 1. Strain gages 13, 14, 15 and 16 are located 1.2 inches from impact site NDT1 and strain gages 94 and 95 are located 0.6 inches from site NDT1. Prior to impact, the strains 1.2 inches from NDT1 are linear and all strain gages recorded approximately the same values. The strain 1.2 inches from NDT1 at DLL is -0.003 in/in. After impact, the strains on the interior surface of the skin 1.2 inches from the NDT1 show the same linear behavior as they did prior to impact and remain linear to failure. A small amount of nonlinearity can be seen in the exterior strain gages 1.2 inches from the impact site and significant nonlinearity can be seen 0.6 inches from the impact site. At the maximum load of 154 kips, the largest compressive strain recorded in this region is -0.009 in/in. There were no failures detected in this region, and post-test evaluation of the site indicated no growth in the size of the damaged skin region.

Impact site NDT2 is located at the edge of an intercostal flange and at the edge of the flange of a stringer runout. Strain gages were placed on the skin, on the stringer, and on the intercostal. Results from strain gages on the skin, the intercostal flange and the stringer flange for the last three tests are shown in figure 60. Results from these strain gages and from strain gages farther away from the impact site on the intercostal and on the stringer runout for the last test are shown in figure 61. The most obvious difference between the strains for the last test and the strains for the previous tests is in strain gage 44. Strain gage 44 is located on the stringer flange slightly inboard of the impact site. During the first tests this location was in compression. During the last test, this location was in tension. However, strain gages on the external surface (strain gages 46 and 617) are in compression for all of the tests. The most likely explanation for this difference is that the impact caused separation between the skin and stringer flange, allowing the stringer flange and skin to deform independently at that location. At a short distance from the impact site

on the intercostal flange, strain gage 45 recorded compression, but not precisely the same values for the final test as for the previous tests. Similarly, strain gage 43, which is on the stringer flange approximately 1.0 inch away from the impact site, recorded compression, but not precisely the same values for the final test as for the previous tests.

For load less than 110 kips, all strain gages in this impact damaged region, except strain gage 44, recorded linear strains which are not significantly different for the first to the final tests. For load greater than 110 kips, strain gages 44 and 45 recorded an erratic strain response. Response caused by damage growth results in such data. Strain gages 43, 46, and 617 show a small amount of nonlinearity for loads greater than approximately 130 kips. A discontinuity in the slope of the load-strain curve is seen for strain gage 43 for a load of approximately 140 kips, indicating a sudden local failure or load redistribution. Another discontinuity in strain is seen for approximately 153 kips of load. Further separation of the skin and the stringer flange would explain this behavior. The maximum recorded compressive strain in this region is -0.0075 in/in. for strain gage 43 immediately prior to failure of the test specimen. This strain is well below the allowable strain of -0.0093 in/in. for this material system and would not have caused failure in an undamaged structure.

Results from strain gages closest to the impact damage site NDT2, (strain gages 43, 44, 45, 46 and 617), and back-to-back strain gages in the unsupported skin region, (strain gages 63 and 64), are shown in figure 62. C-scans of the damaged region made immediately after impact indicate the presence of damage at strain gages 44 and 45, so the structure may not perform as an undamaged structure at these locations. Nonlinear material behavior caused by the impact damage would explain the behavior of gage 45. Strain gages 43 and 46 at the impact damage site show linear behavior at higher loads than strain gages in the unsupported skin region which show linear behavior. The fact that the strain in the unsupported skin region becomes nonlinear before the strain at the impact damage site become nonlinear indicates that the behavior at the impact damage site was not influenced significantly by the buckling of the unsupported skin region.

Failure

The maximum load supported by the structure at failure was 154 kips. A view of the entire structure after failure is shown in figure 63. Failure occurred across the entire width of the upper cover panel and into both spars. The lower cover panel skin remained intact. Photographs of the failures in the upper cover panel, and in the stringers between ribs 7 and 8 are shown in figures 64 and 65, respectively. Two independent failures occurred in the wing stub box. The first failure was in the unsupported region at the runout of stringer 6 where it terminates at rib 7 at a load of approximately 140 kips. During the test, the flanges and web of the stringer failed and the skin remained intact. This stringer has extensive damage in the form of delaminations between the skin and flange, broken stitches, bolts pulled through the flange, and cracking of the blade, as shown in figure 65b. The second failure was catastrophic and initiated at the nondetectable impact damage site at the runout of stringer 7. This failure began at a load of approximately 145 kips. This failure resulted in a crack that runs across the upper cover panel through impact damage site NDT2, as shown in figure 66, and across the upper cover panel into the spars. Failed stringers aft of the impact site are shown in figure 65a.

Delamination between the flange of stringer 5 and the upper cover panel skin inboard and outboard of rib 7 were also found, although the stitches between the flange and skin remained largely intact. Stringer 5 is on one edge of the unsupported skin region. This type of damage was not found in stringer 7, which is on the other edge of the unsupported skin region.

Other damage was found in post-test evaluation of the wing stub box, but is believed to have occurred after the failure of the upper cover panel. One rib stiffener from each of ribs 6, 7, and 8 separated completely from the ribs. The stiffeners on the ribs prevented rib buckling prior to failure of the upper cover panel, but were only attached to the ribs by secondary bonding and two mechanical fasteners at each end of the stiffeners. Intercostals were damaged where the bolts attached the intercostals to ribs 5, 6, 7 and 8. The damage to the intercostals occurred only between stringers 1 and 2 at rib 5, but occurred between other stringers as well for ribs 6, 7, and 8. The intercostals are

approximately 0.12 inches thick and would have been subjected to severe loading during failure of the upper cover panel. Small cracks were found in the angle pieces connecting the rear spar of the load-transition structure to the upper and lower covers of the load-transition structure.

Concluding Remarks

A series of tests were conducted on a McDonnell Douglas all-graphite-epoxy wing stub box to evaluate its structural performance. The structure supported Design Limit Load with no damage and with visible damage in the form of a 0.1-inch-deep dent to the upper cover panel skin. The structure supported 140% of Design Limit Load with nonvisible damage in the form of damage from 100 ft-lb of impact energy at two locations on the upper cover panel, and a repair of the visible damage. The failure of the structure involved large out-of-plane deformations in the wide upper cover skin bay outboard of the access door. These deformations caused failures in the stiffener terminating in that region. Final failure of the upper cover panel initiated at the nondetectable impact damage site and consisted of a large crack that propagated across the width of the panel through the impact damage site and into both spars.

References

1. Markus, Alan; Thrash, Patrick; and Grossheim, Brian: Manufacturing Development and Requirements for Stitched/RTM Wing Structure. Proceedings of the Fourth NASA/DoD Advanced Composites Technology Conference, NASA CP 3229, 1993, pp. 503-523.

2. Hinrichs, Steve: ICAPS Stub Box Structural Analysis. McDonnell Douglas Aerospace Transport Aircraft-West, Report Number MDC94k9101, March 1995.

3. Anon.: ICAPS Composite Wing Stub Box Test. McDonnell Douglas Aerospace Transport Aircraft-West, Task Assignment Drawing Z7944503. Final Version, February 1995.

Acknowledgment

Table 1   Impacts resulting in visible damage

Impact	energy (ft-lb)	dent depth (inches)	damage area (length x width, inches)
1	150	.032	3.75x2.25
2	100	.038	3.75x2.25
3	150	.043	5.0x2.5
4	189	.091	5.75x2.75
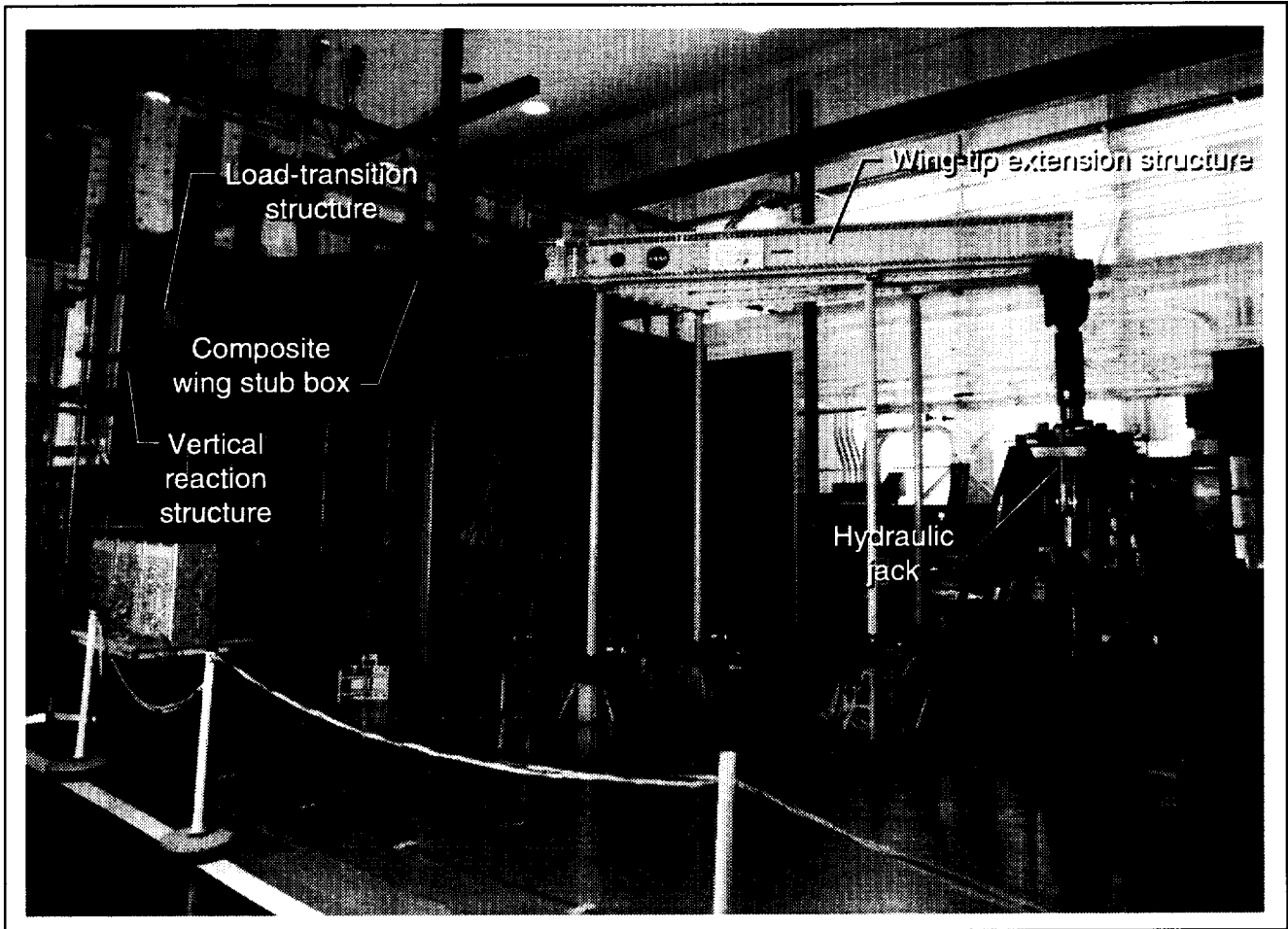
a) Test specimen

Figure 1. Test specimen and test setup.

Load reaction plate

Swivel (2)

Load cell

Steel wing-tip extension structure

Supports(4)

300 kip jack assembly and support truss

Aircraft jacks (4)

Floor

Vertical reaction structure

Aluminum load-transition structure

Composite Wing Stub Box

146.9

163.1

133.4
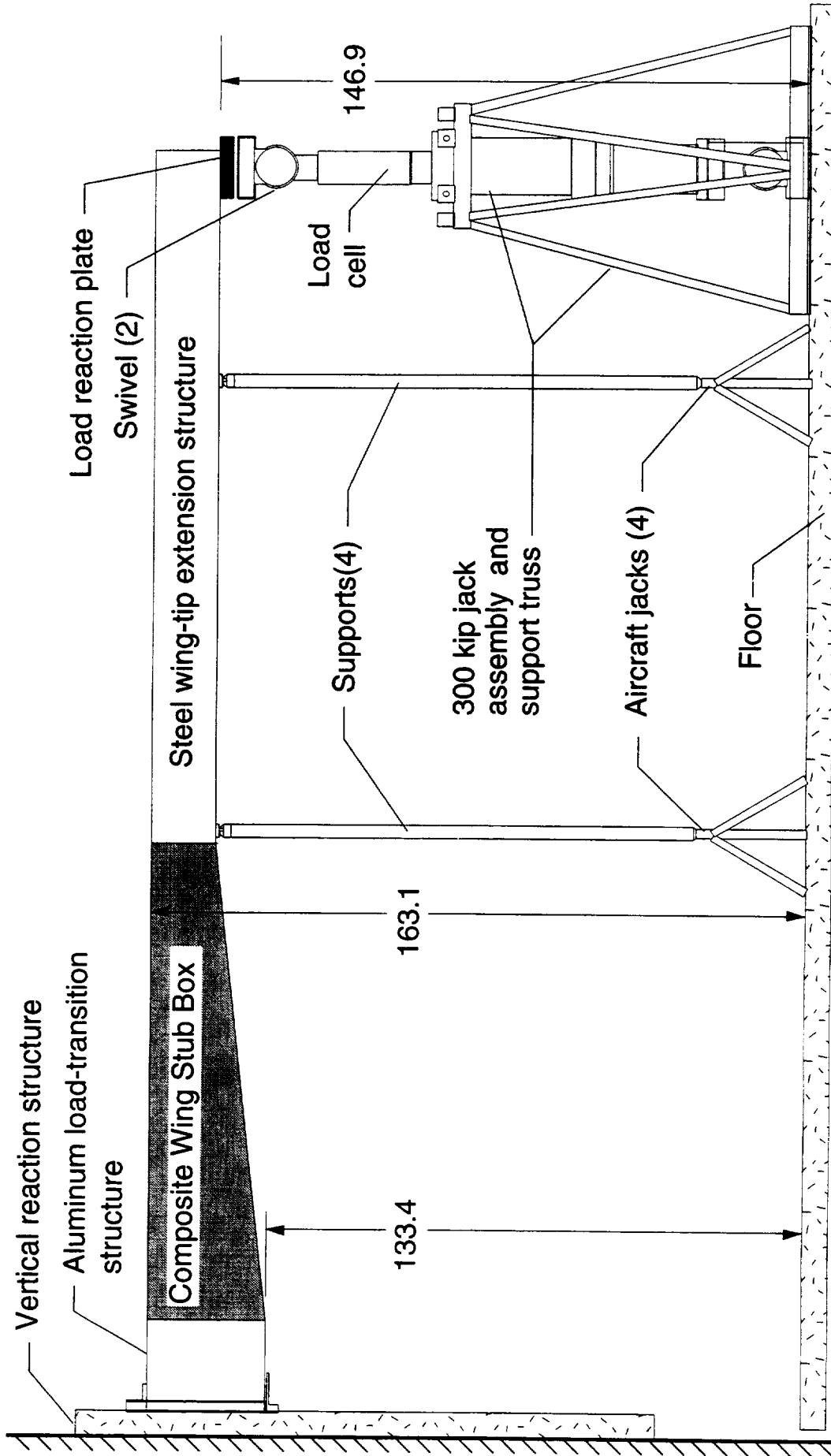
b) Test setup. All dimensions are in inches.

Figure 1. Concluded.

30

Figure 2. Geometry of upper and lower cover panels of stub box.
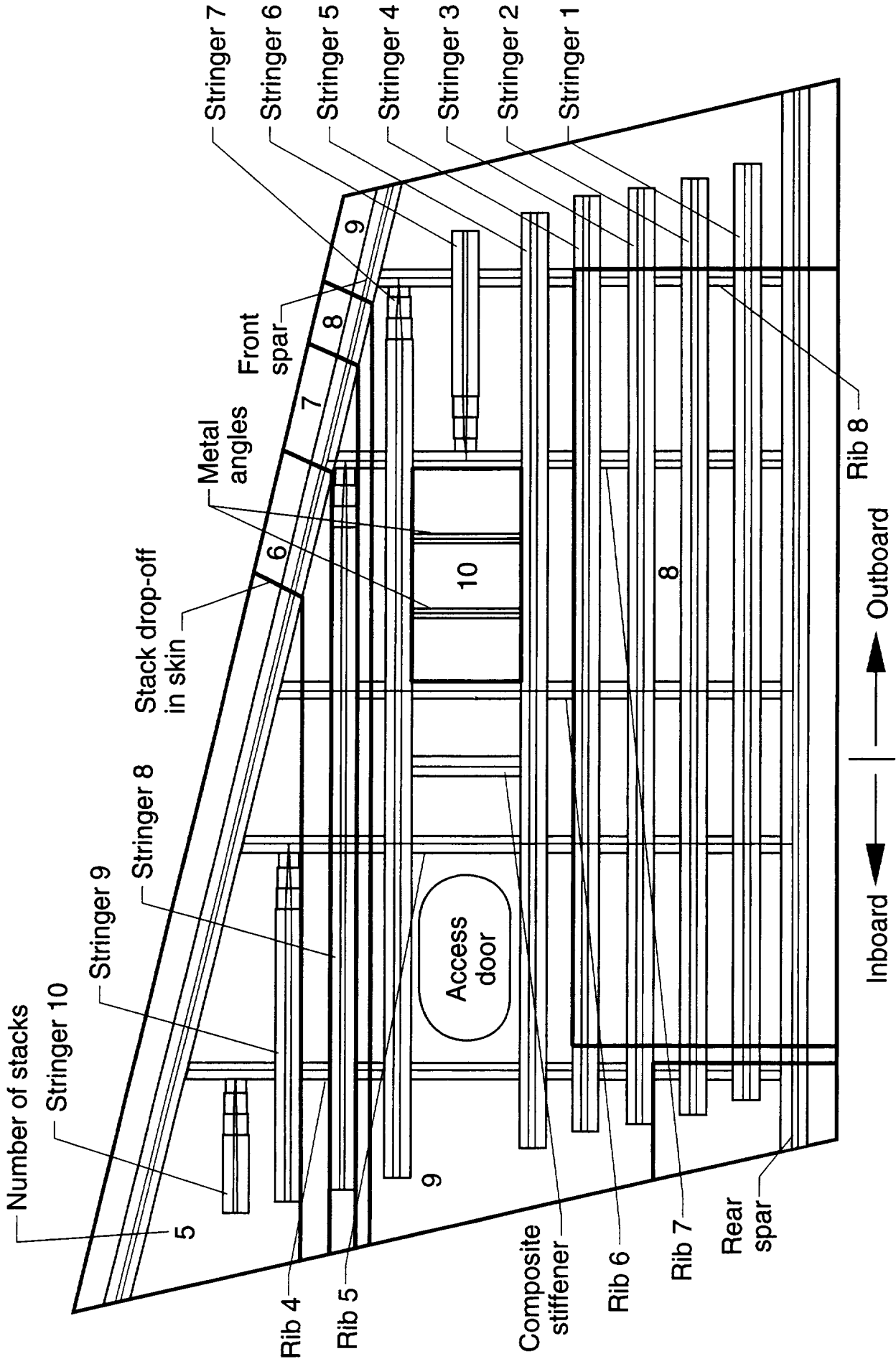
a) Geometry of upper cover panel

31

Front spar

Stringer 11
Stringer 10
Stringer 9

Stringer 8
Stringer 7
Stringer 6
Stringer 5
Stringer 4
Stringer 3
Stringer 2
Stringer 1

Rib 4
Rib 5

Stack drop-off in skin

Number of stacks

Rib 8
Rib 7
Rib 6
Rear spar

15
6
9
12
15
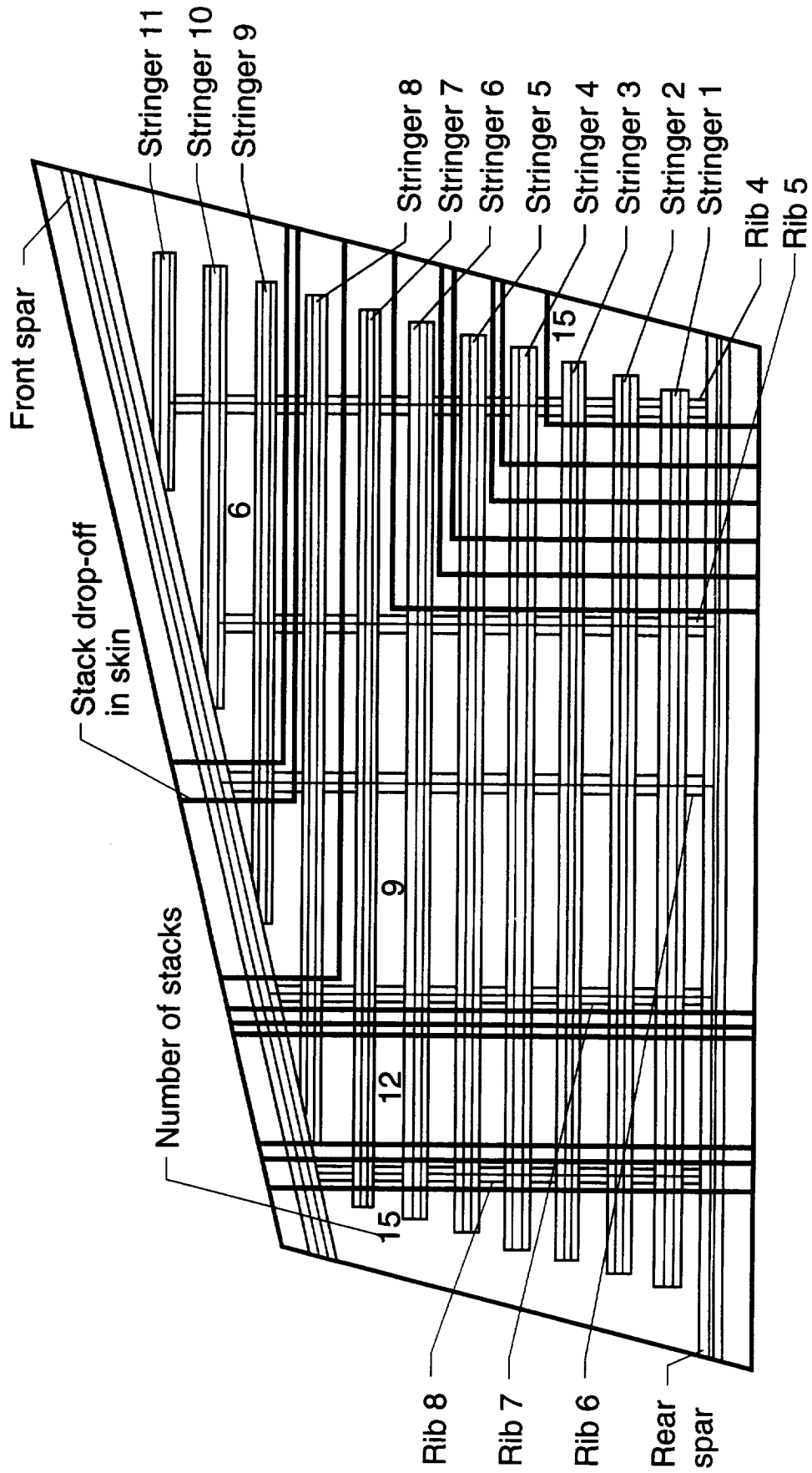
b) Geometry of lower cover panel

Figure 2. Concluded.
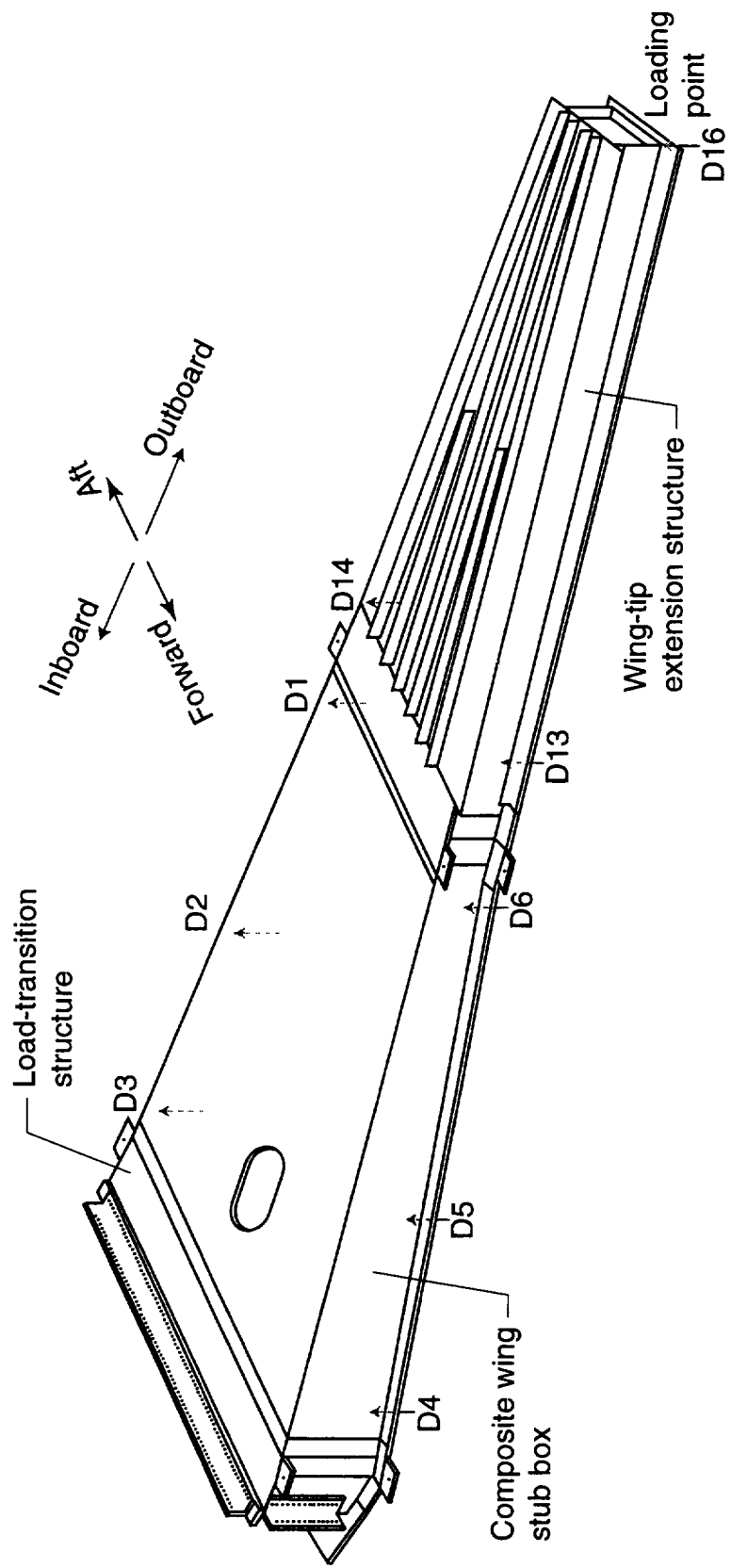
Figure 3. Displacement measurement locations on lower surface of test specimen.
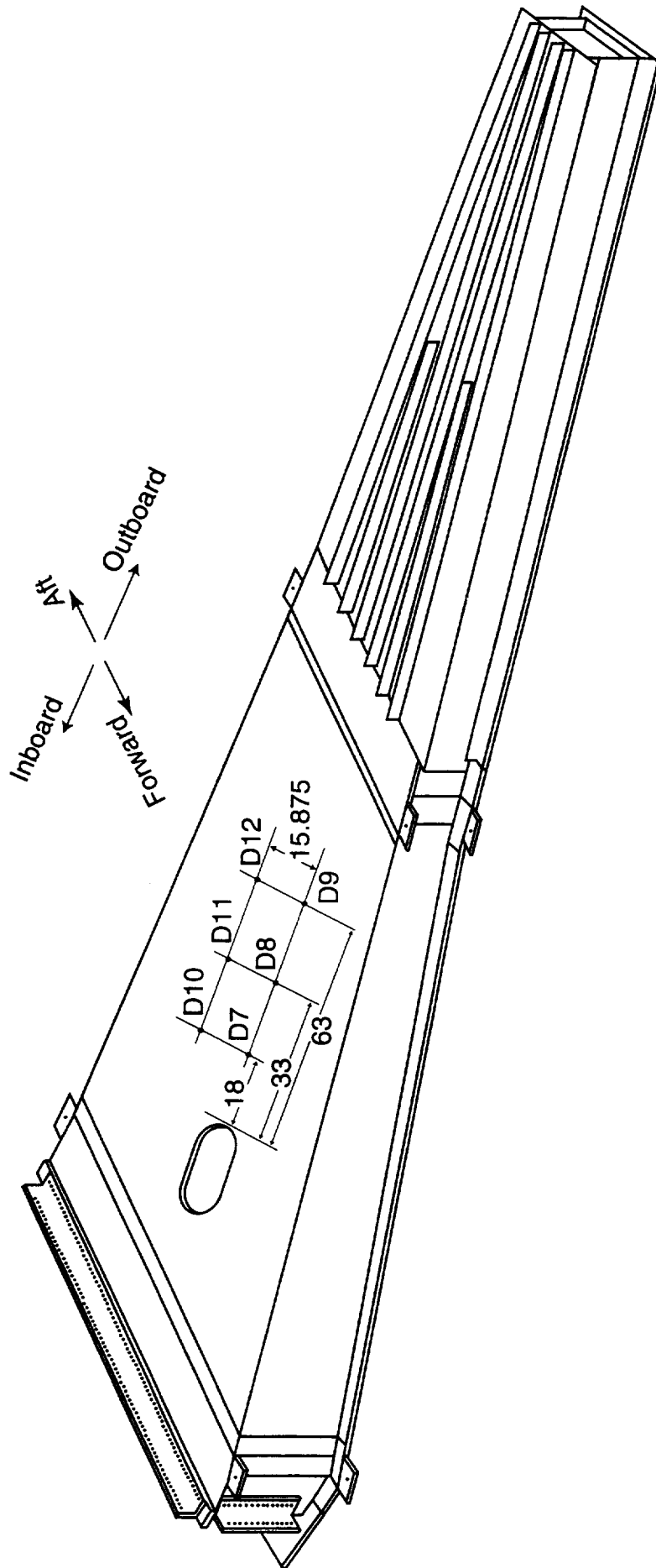
Figure 4. Displacement measurement locations on upper cover panel. All dimensions are in inches.

Figure 5. Strain gage locations on upper cover panel.

Legend:
- ⬜ External, skin
- ▨ Internal, flange
- ▯ Internal, both sides of blade and external, skin
- ▮ Back-to-back gages on skin
- ◪ Internal, side of blade and external, skin rosette
- ▬ Internal, side of blade and external, skin

Legend (top):
- ▤ External skin and internal flange
- ⓌM Rosette on intercostal
- ▲ Splice region gages
- △▷ Runout region gages
- ✳ Impact site

Labels: 77, 610; 75, 76; 72, 73; 74; 79, 70, 71; 59, 60, 61, 62; 55, 56, 57, 58; 51, 52, 53, 54; NDT2, 43, 44, 45, 46, 617; 48, 609; 40, 41, 42; 38, 39; 36, 37; 86, 87, 93; 26, 27, 28, 29; 31, 32; 30; 25; 47; 49, 50; 88; 33, 34, 35; 65, 66; 607, 608; 63, 64; 22, 23, 24; 605, 606; 20, 21; 603, 604; 18, 19; 601, 602; 616; 615; 67, 68; 613; 614; 17; 612; 79, 80; 78; 81, 82, 83; 84, 85; 8; 5, 6, 7; 2; 4; 89; 611; 90, 91, 92; DET1, 11, 12, 96, 97, 9, 10; NDT1, 13, 14, 15, 16, 94, 95

35

Figure 6. Strain gage locations on lower cover panel.

Legend:
- External, skin
- Internal, flange
- Internal, side of blade and external, skin rosette
- Internal, side of blade and external, skin
- External, skin and internal, flange
- Internal, side of blade

Outboard ◄──── | ────► Inboard
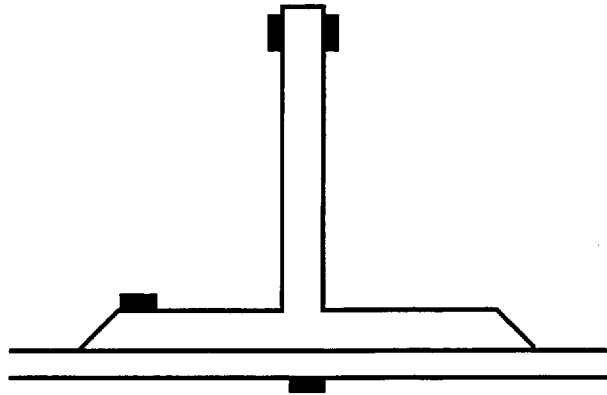
Figure 7. Location of strain gages on blades, flanges and skin of upper and lower cover panels. All gages measure axial strain.
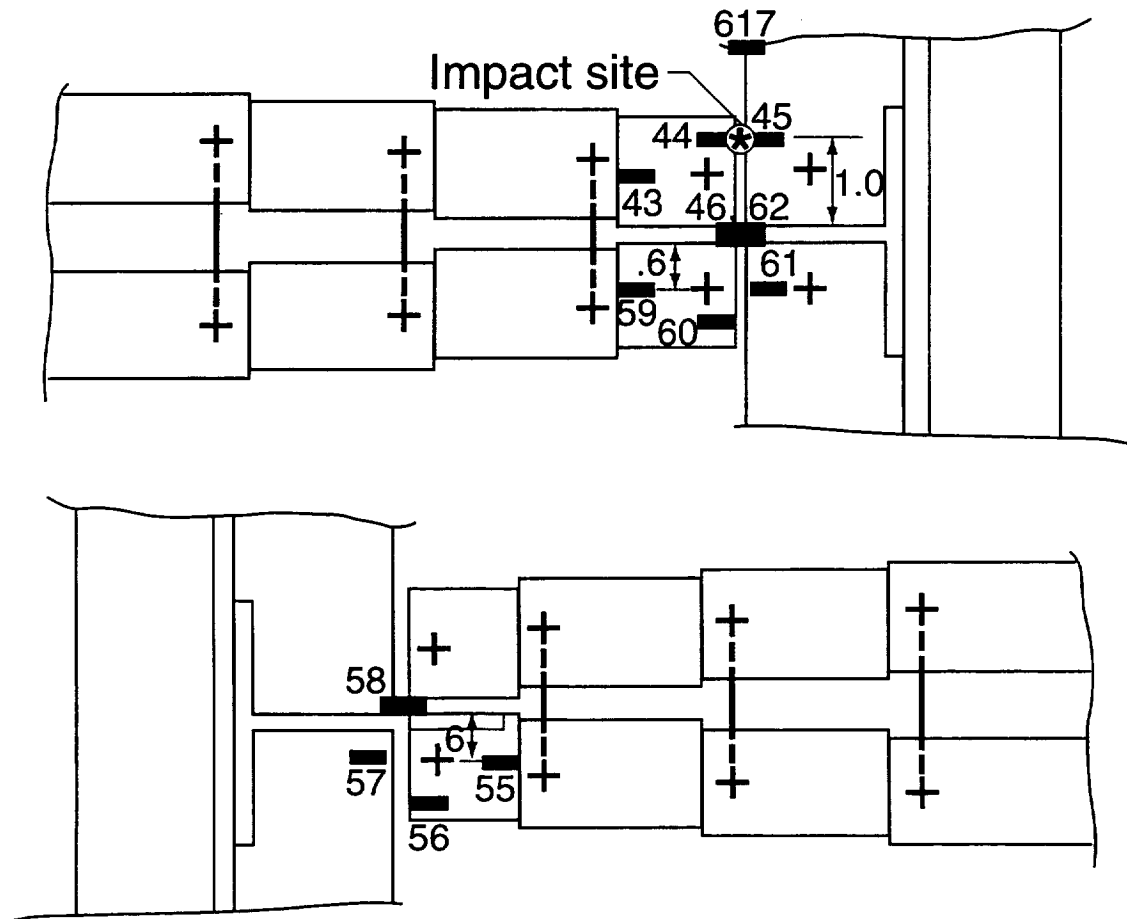
Figure 8. Location of strain gages on stiffener runouts in the upper cover panel. All gages measure axial strain.

| Metal parts are shaded |
| + Bolt |

Identification in figure	Strain gage number
A	31, 36, 38
B	88, 89, 90
C	91
D	2, 4, 32, 37, 39, 616
E	92, 93

Composite skin

Composite blade

Composite skin
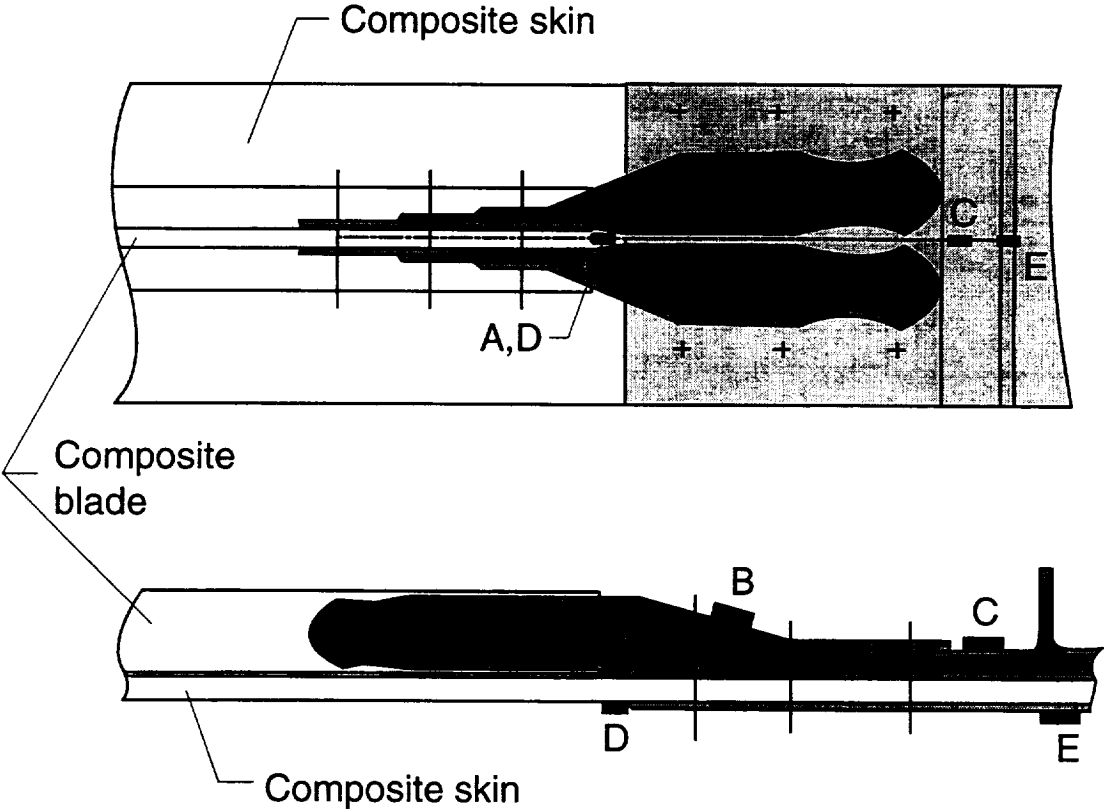
Figure 9. Location of strain gages at splice between the upper cover panel and the wing-tip extension and load transition structures.
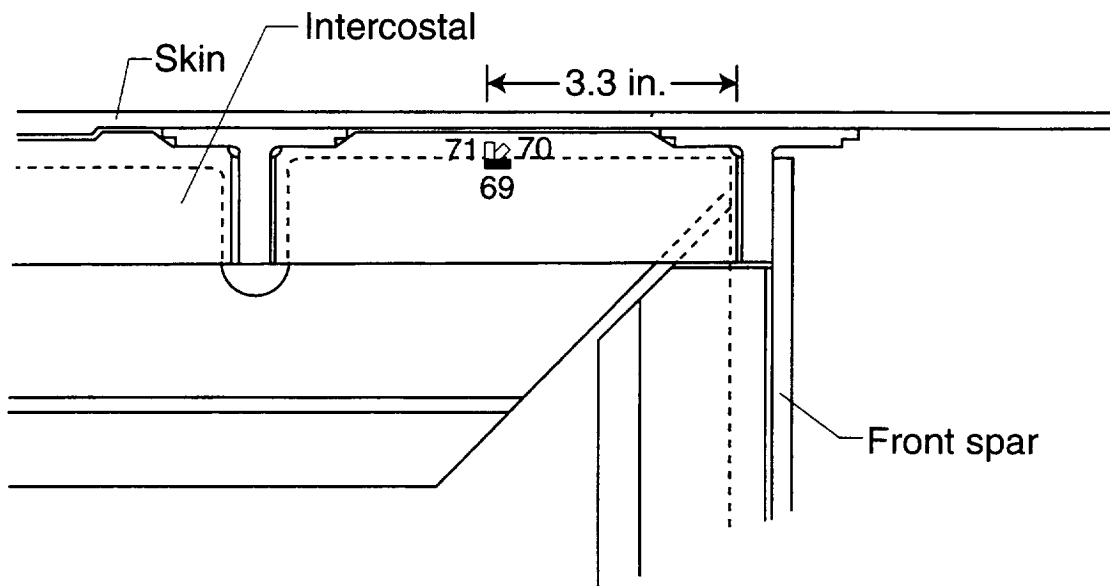
a) Strain gage locations on intercostal of rib 5. (Inboard side shown)

Figure 10. Strain gage location on ribs.

Skin — ⌐ Intercostal

35 ⊠ 34
33

◄—3.1 in.—►|

□480
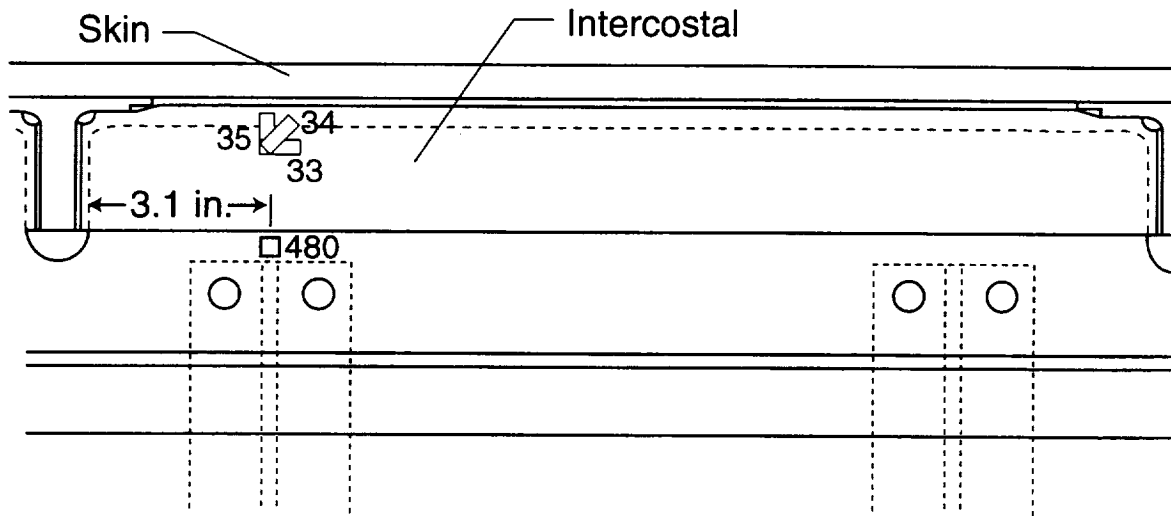
b) Strain gage locations at intercostal of rib 7

Figure 10. Continued.

|◄—————— 5.7 in. ——————►| Skin —

42 ⊠ 41
40
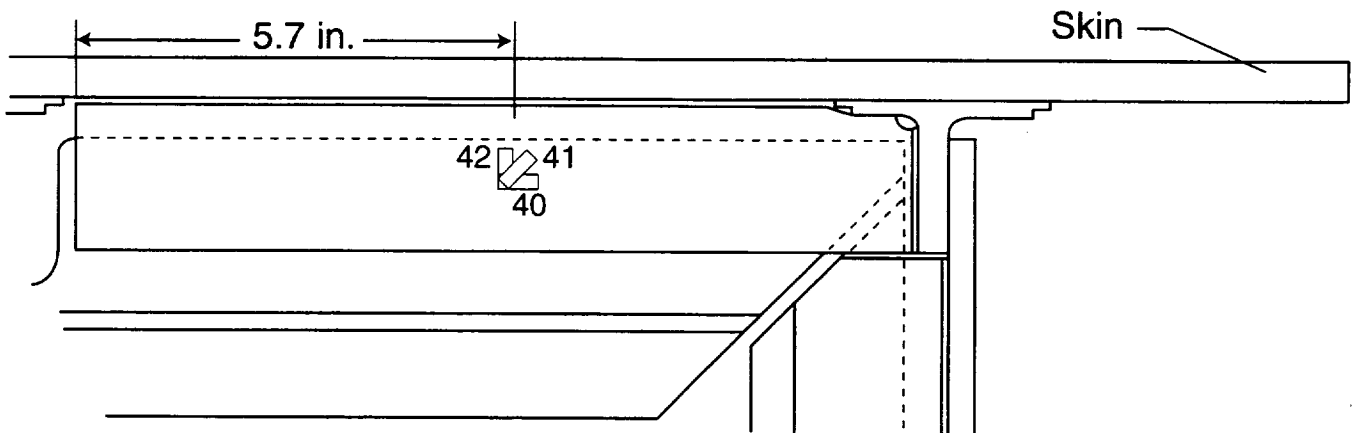
c) Strain gage locations at intercostal of rib 8

Figure 10. Concluded.

Identification in figure	Strain gage number
A	9, 13
B	11, 15
C	94, 96
D	10, 14
E	12, 16
F	95, 97
G	5, 6, 7 rosette 0°, 45°, 90°
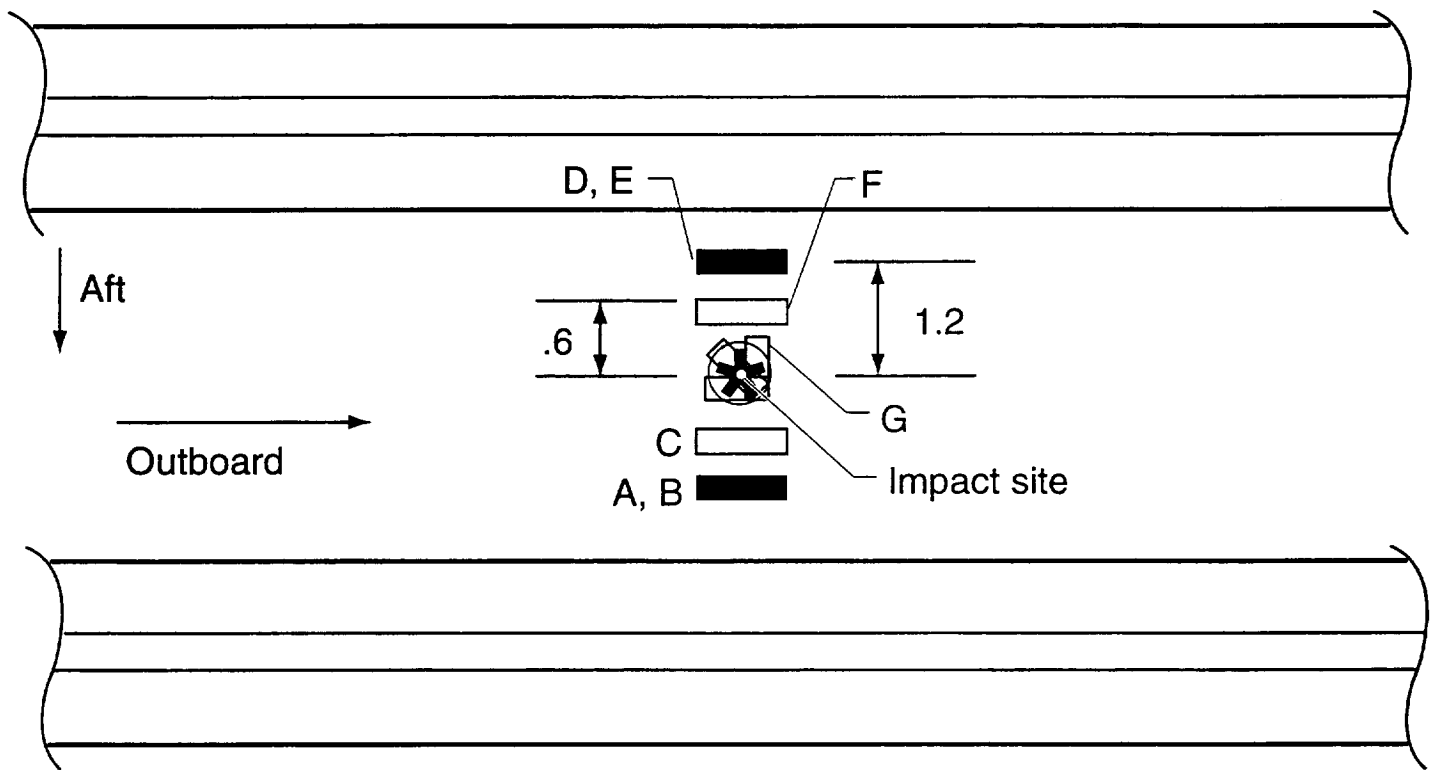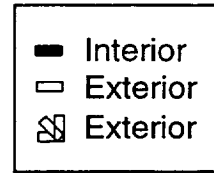
Figure 11. Strain gage locations near impact sites. All dimensions are in inches.

Rosette and 45° strain gage

Single strain gage
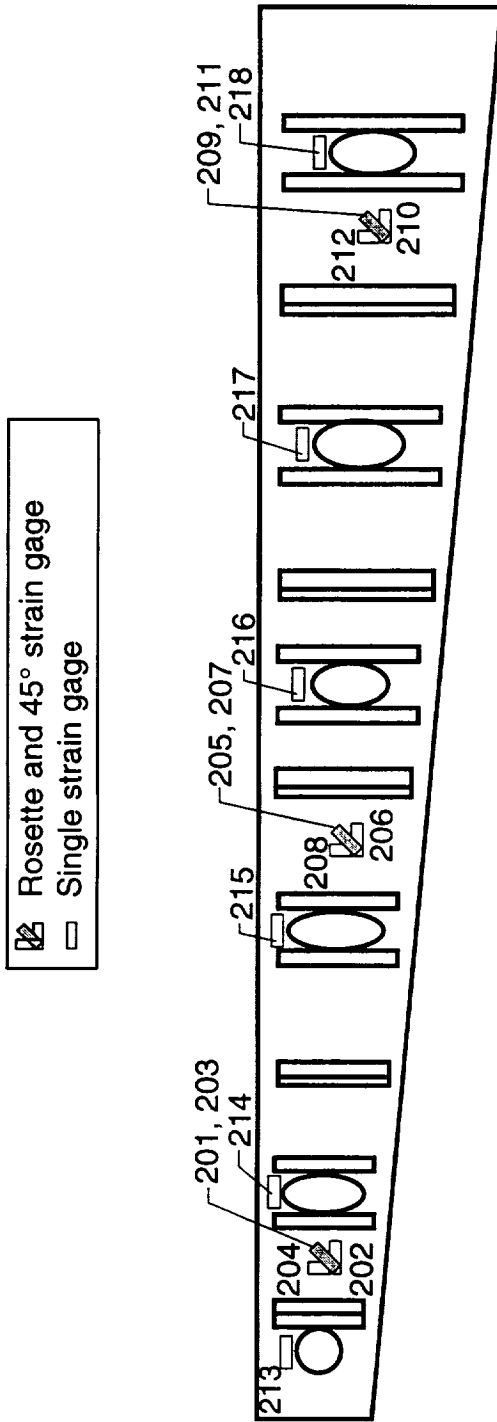
Figure 12. Strain gage locations for front spar.

42
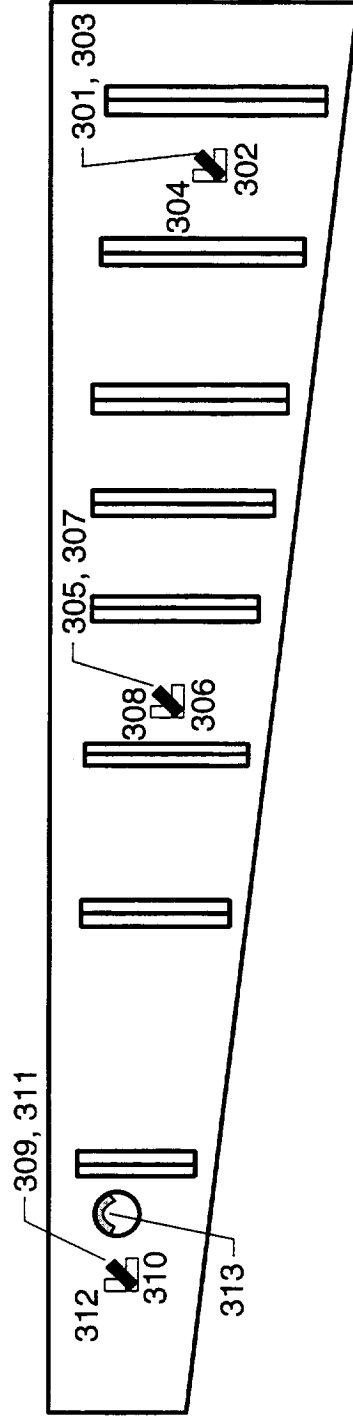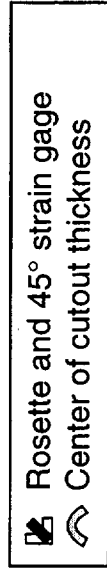
Figure 13. Strain gage locatons for rear spar.
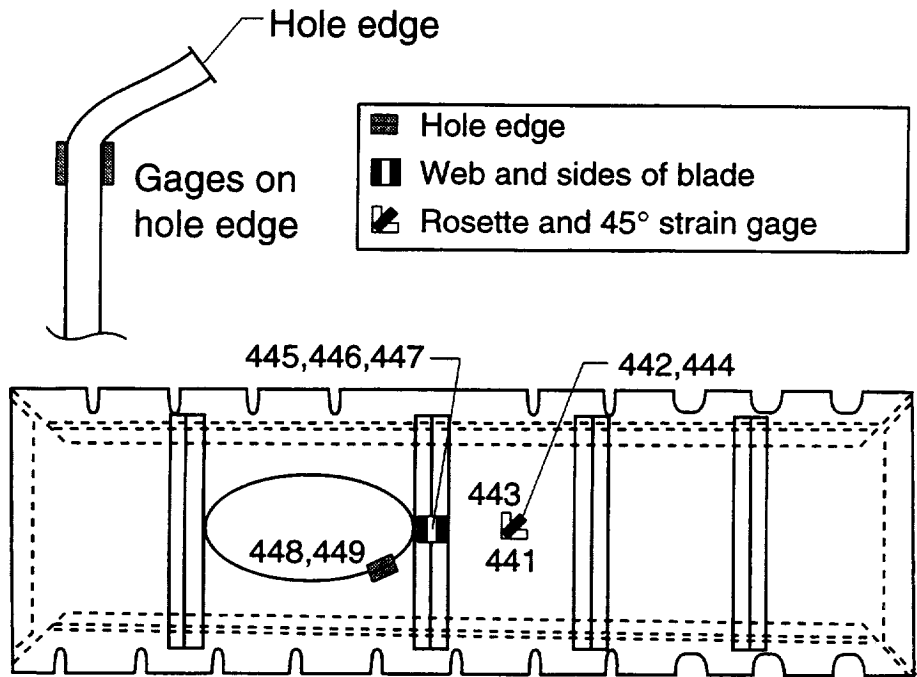
a) Strain gage locations for rib 4

Figure 14. Strain gage locations on ribs.
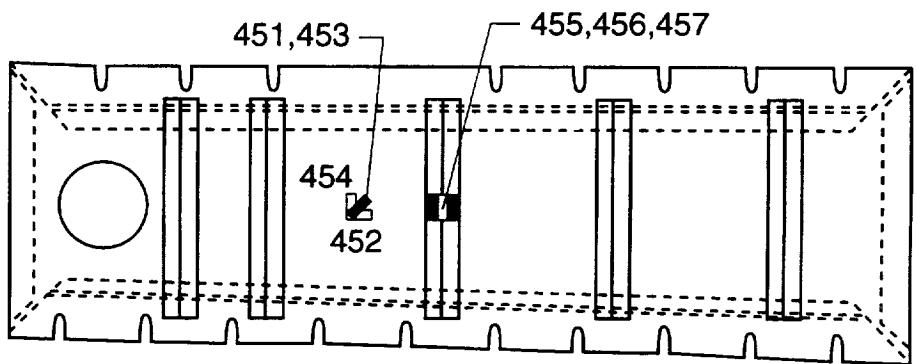
b) Strain gage locations for rib 5

Figure 14. Continued.

Rosette and 45° strain gage
Web and sides of blade
Hole edge
Web at end of stiffener

462, 464

463
461

468, 469

465, 466, 467
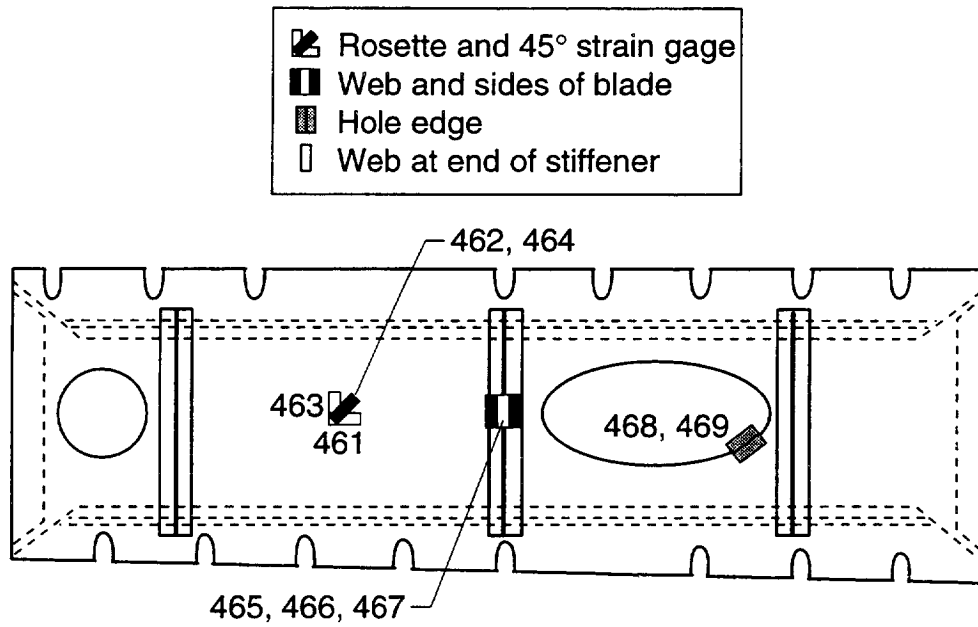
c) Strain gage locations for rib 6

Figure 14. Continued.

472, 474

480

473
471

478, 479

475, 476, 477
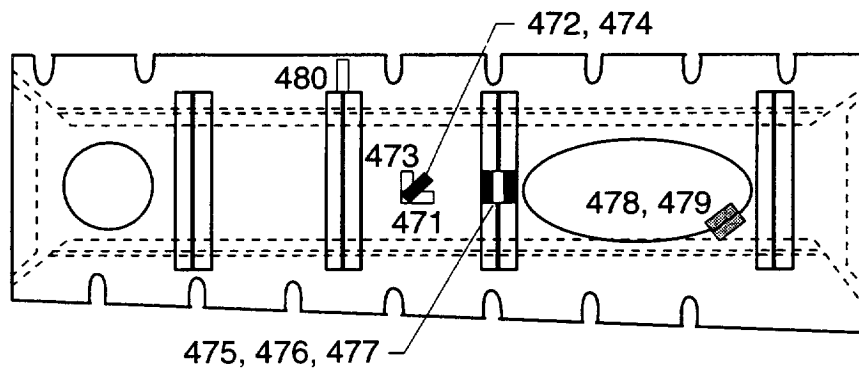
d) Strain gage locations for rib 7

Figure 14. Continued.
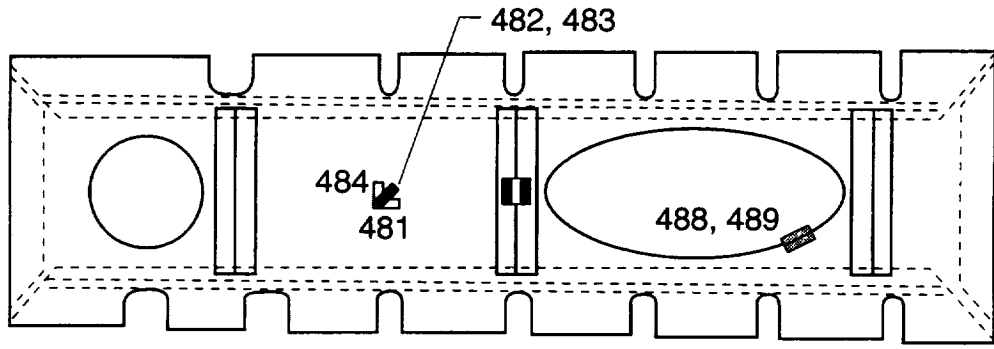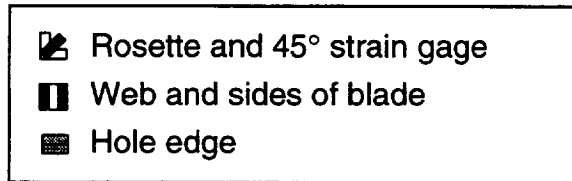
e) Strain gage locations for rib 8

Figure 14. Concluded.
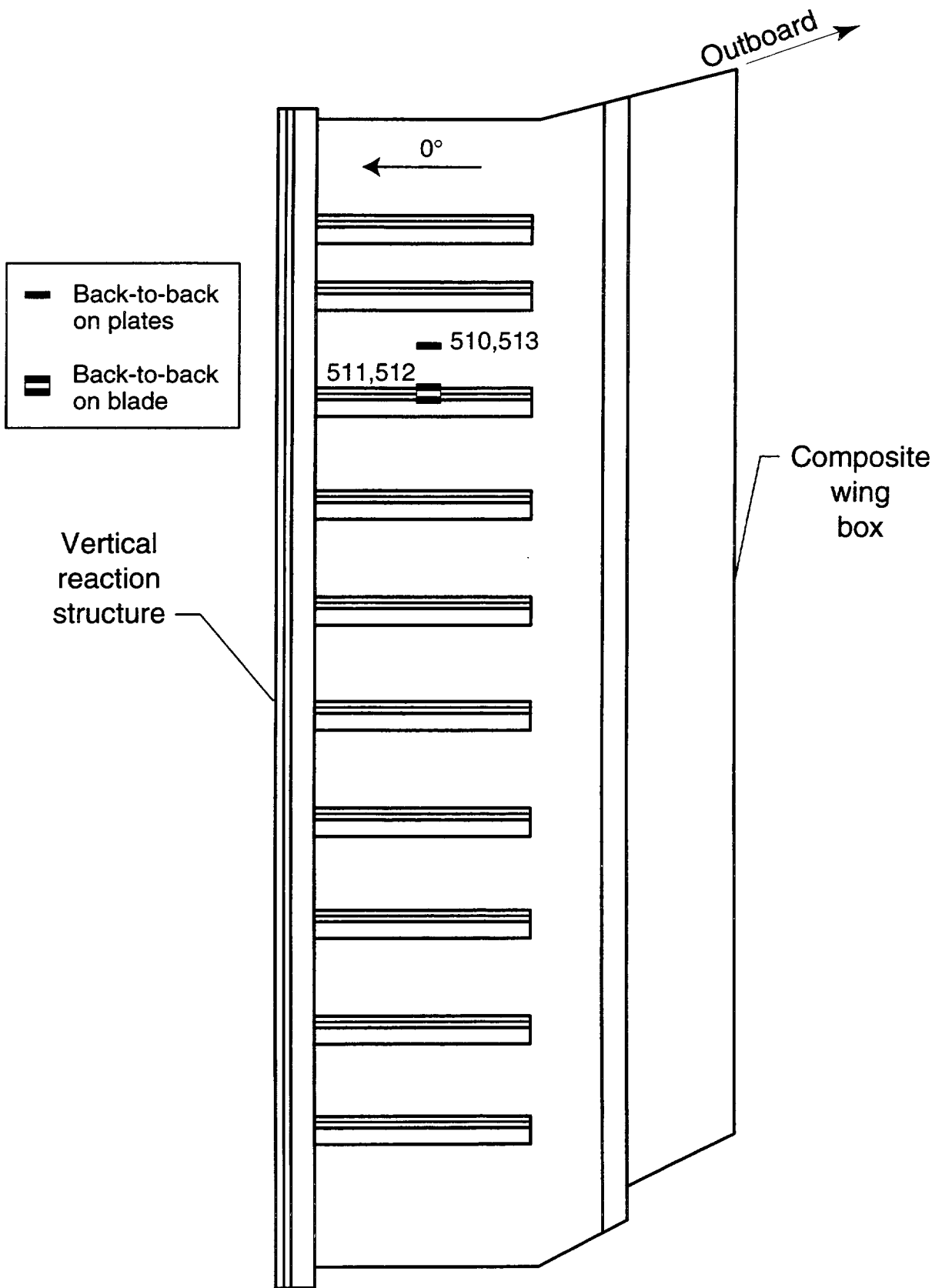
Figure 15. Strain gage locations on load-transition structure.
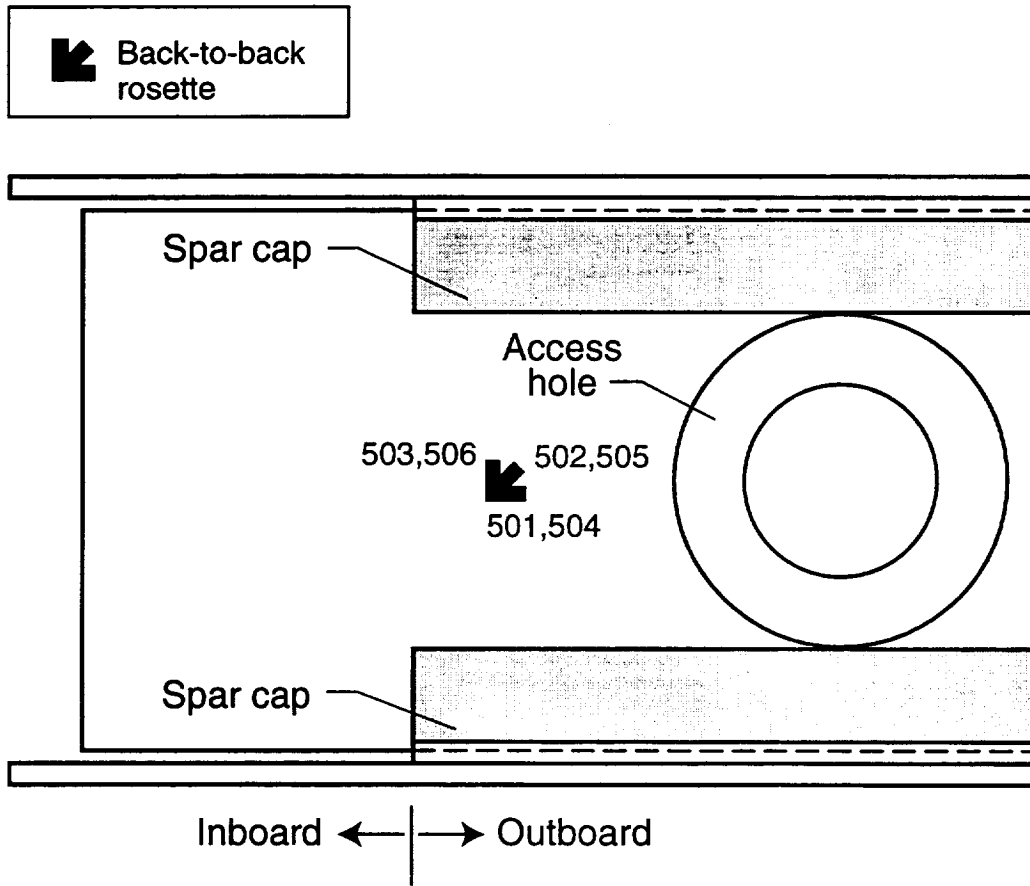
Figure 16. Strain gage locations on front spar web of wing-tip extension structure.
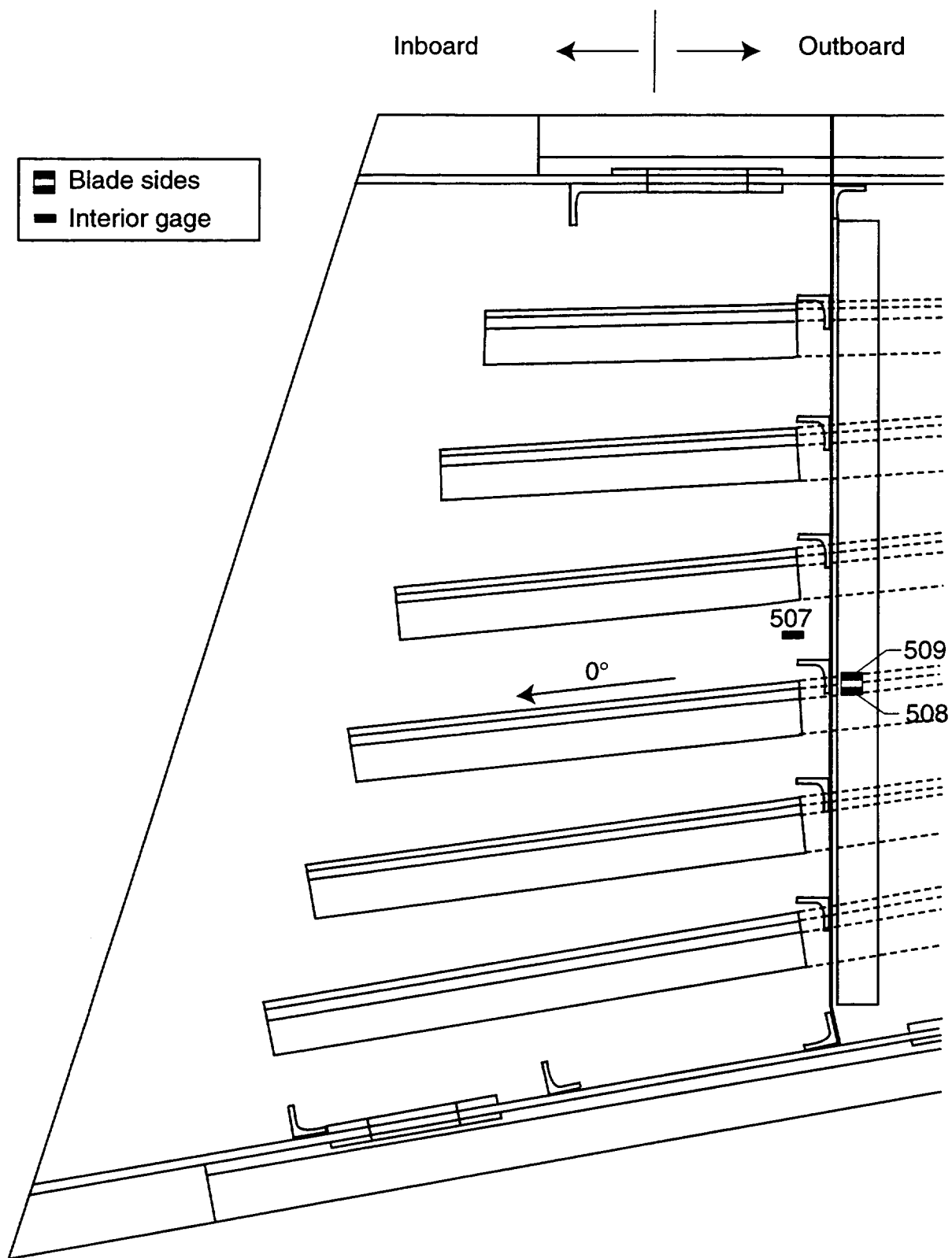
Figure 17. Strain gage locations on upper skin of wing-tip extension structure.
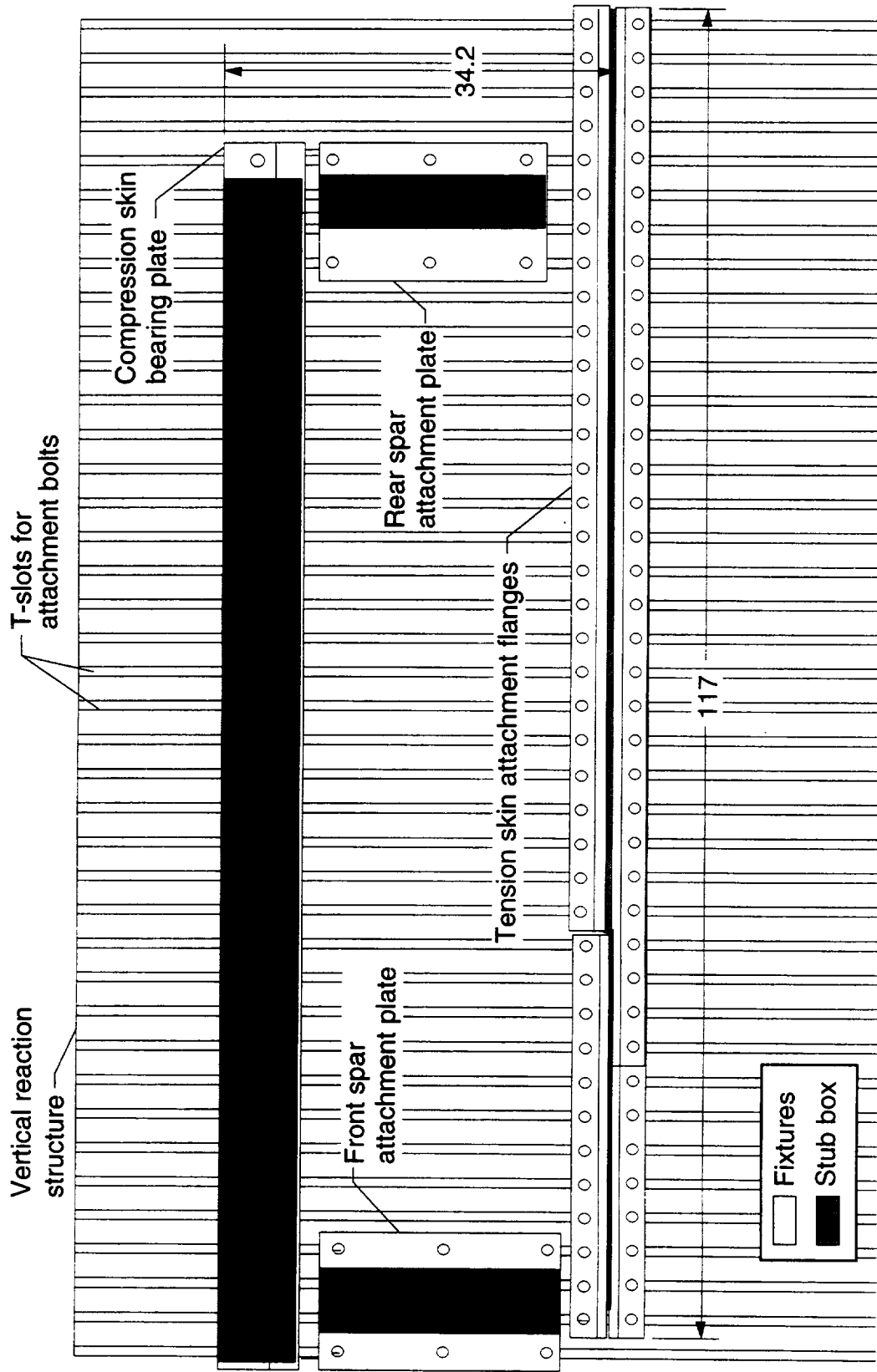
Figure 18. Vertical reaction structure mounting arrangement. All dimensions are in inches.
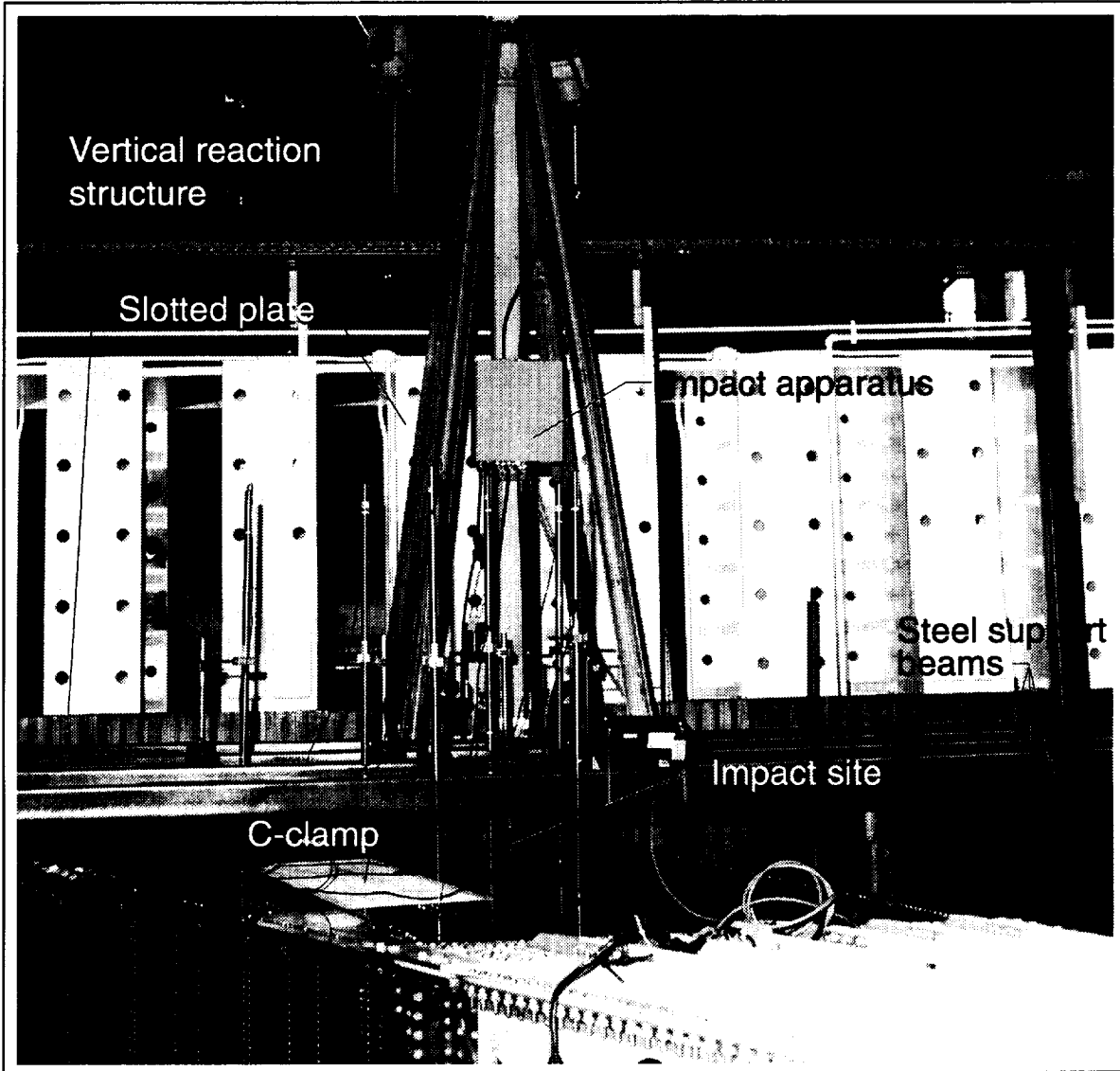
Figure 19. Dropped-weight impact apparatus.
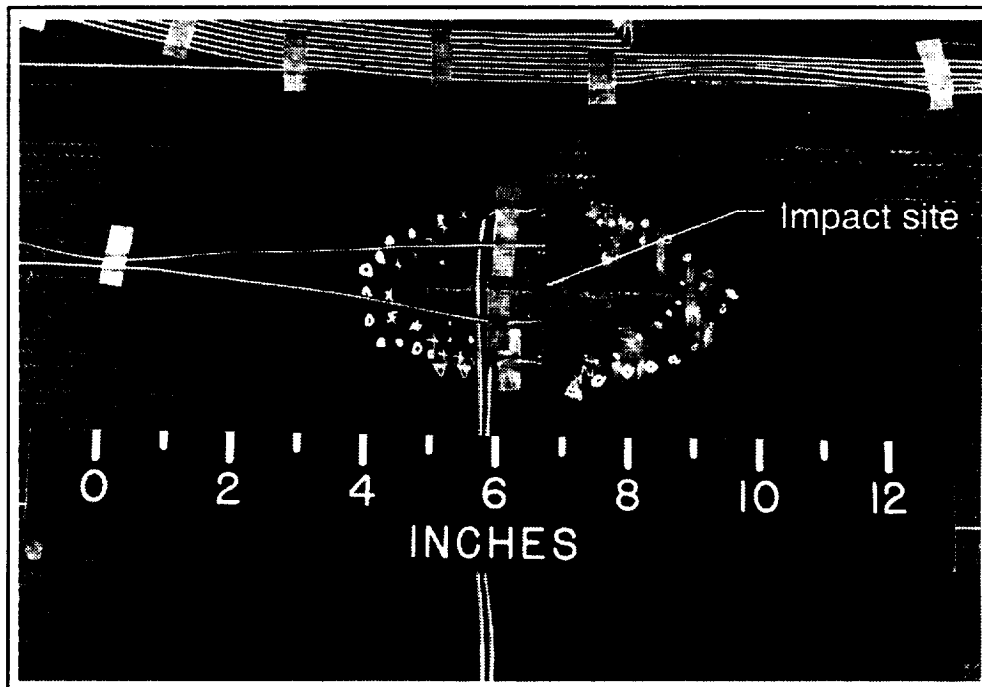
Figure 20. Visible impact damage region DET1.
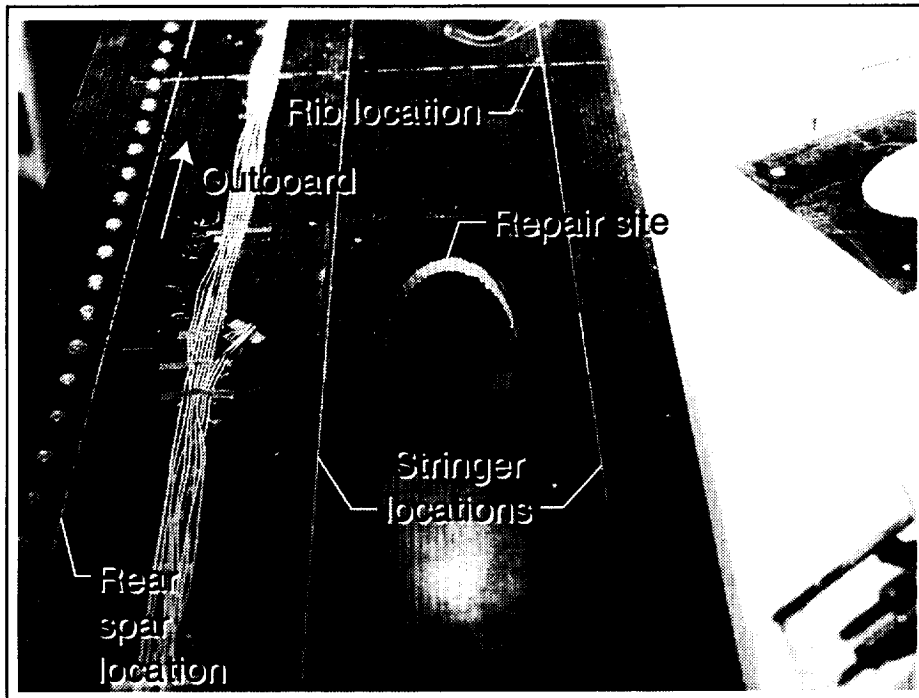
Figure 21. Upper cover panel prior to installation of repair.
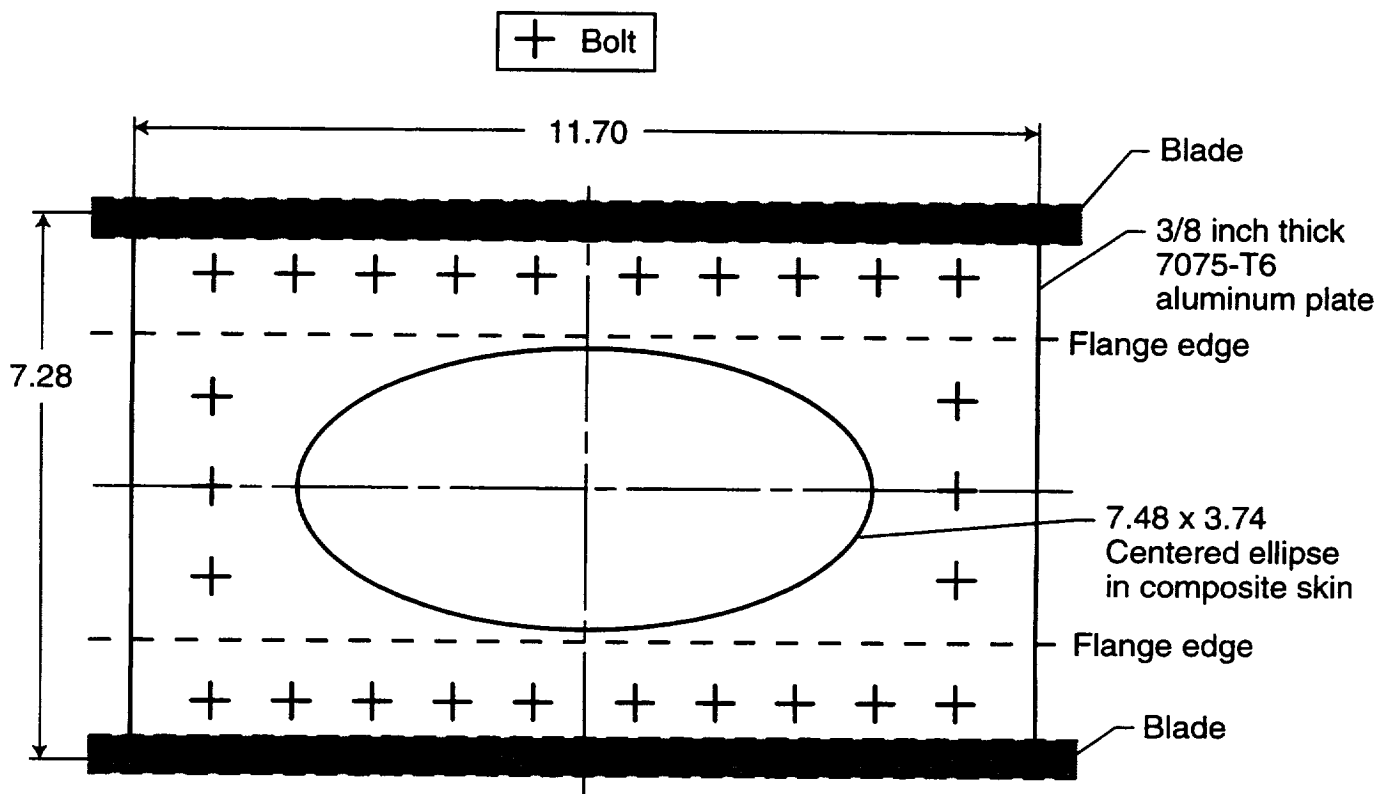
Figure 22. Repair configuration. All dimensions are in inches.
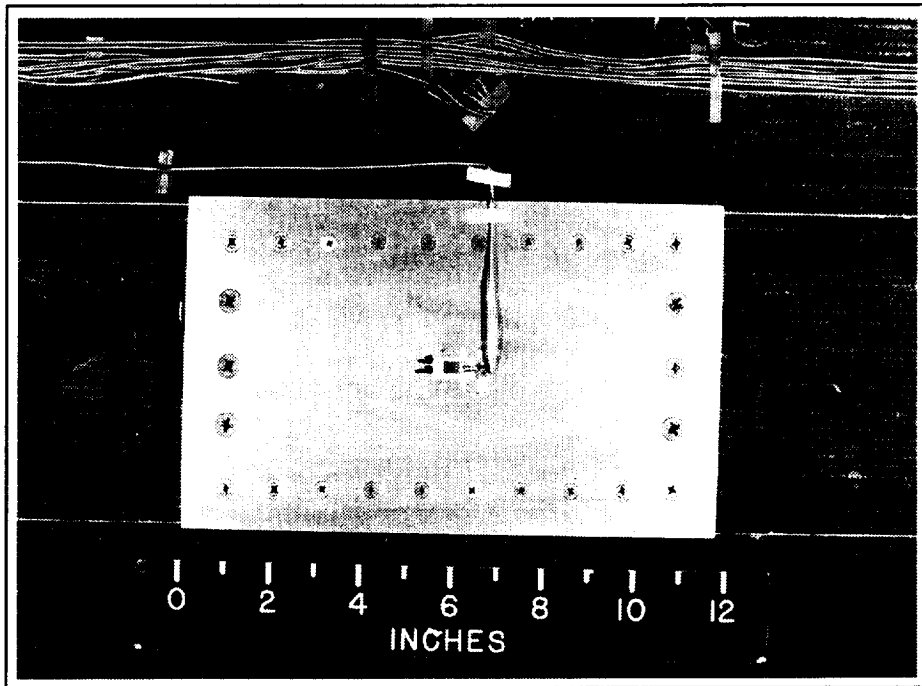
Figure 23. Completed repair.
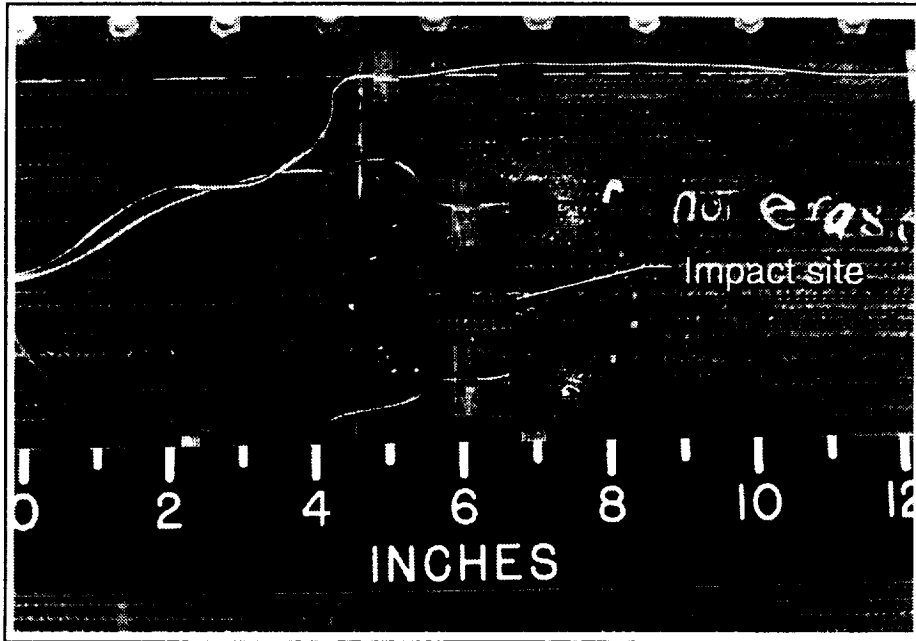
a) Impact region NDT1

Figure 24. Nonvisible impact damage sites.
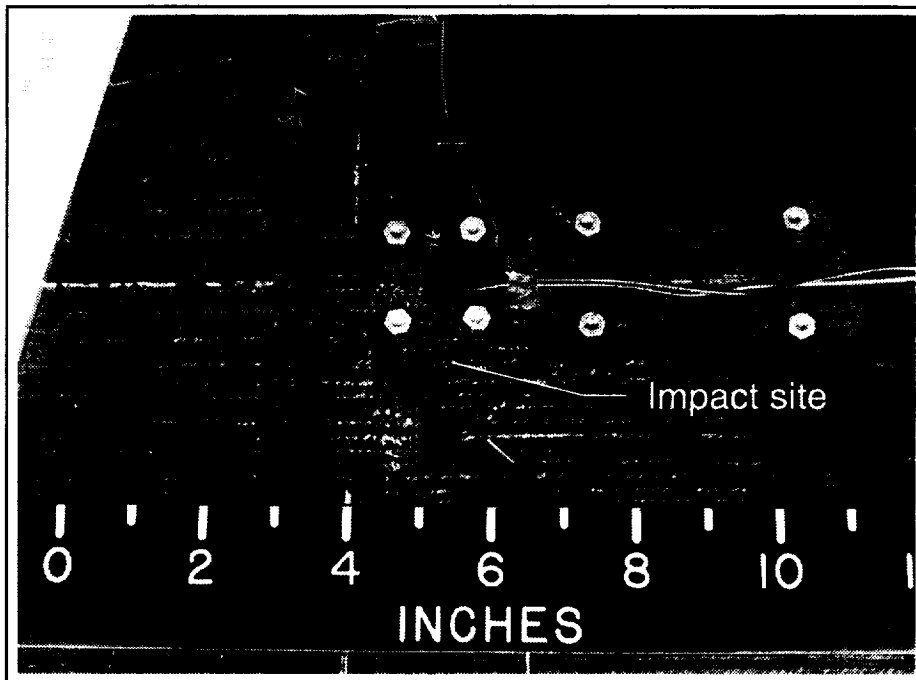
b) Impact region NDT2

Figure 24. Concluded.

56
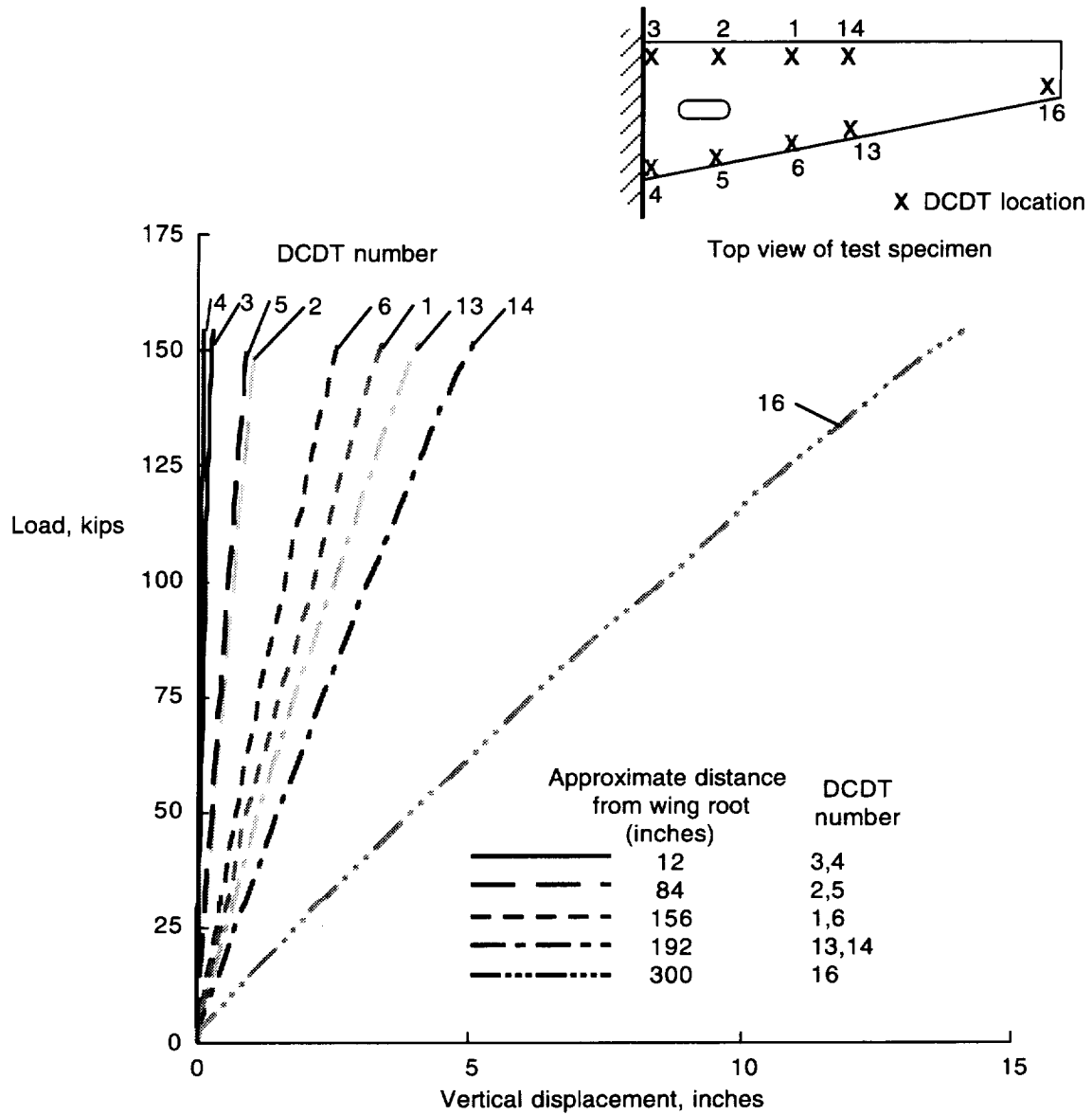
Figure 25. Displacements of test specimen lower surface.
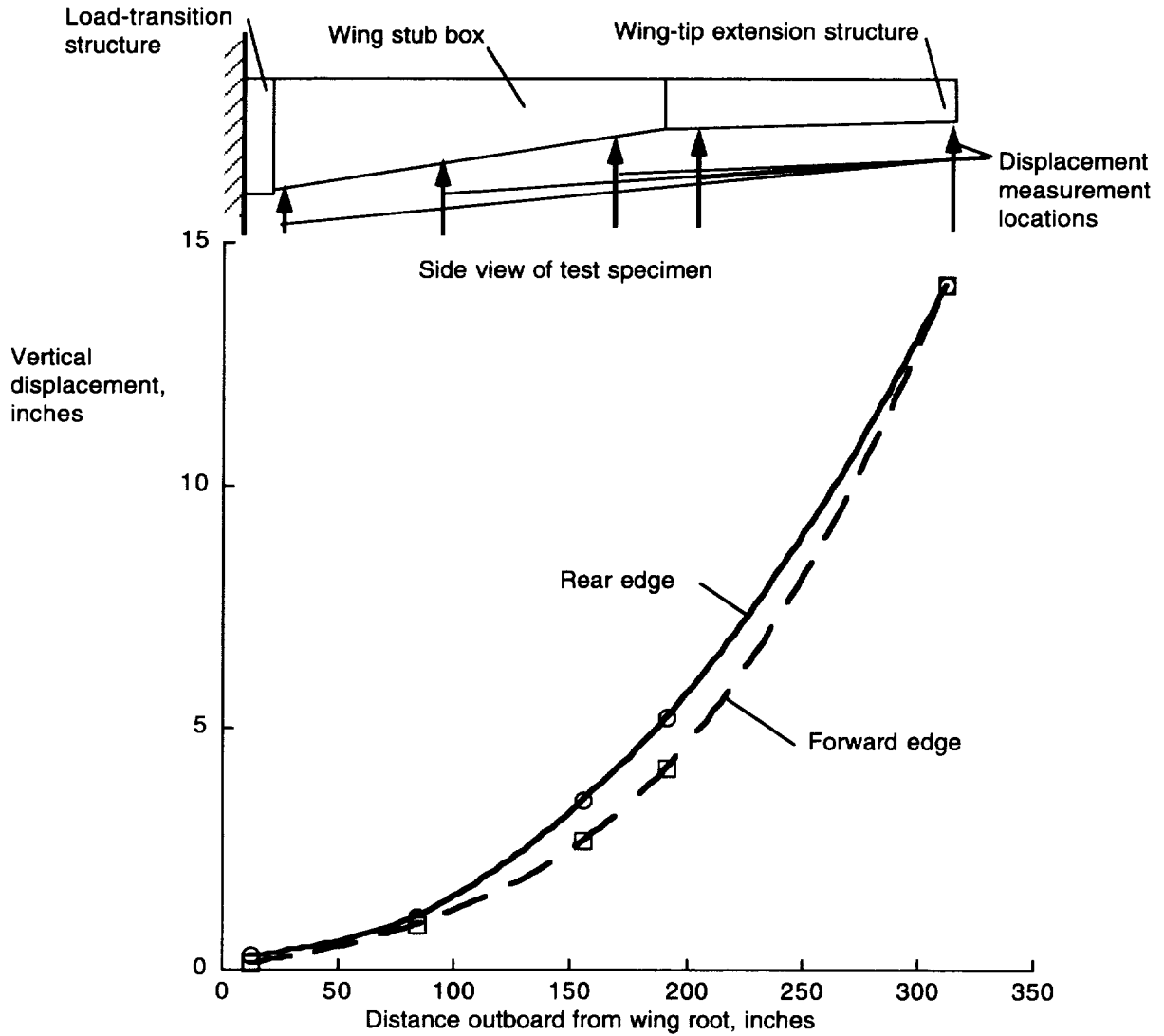
Figure 26. Lower surface displacements at maximum applied load.
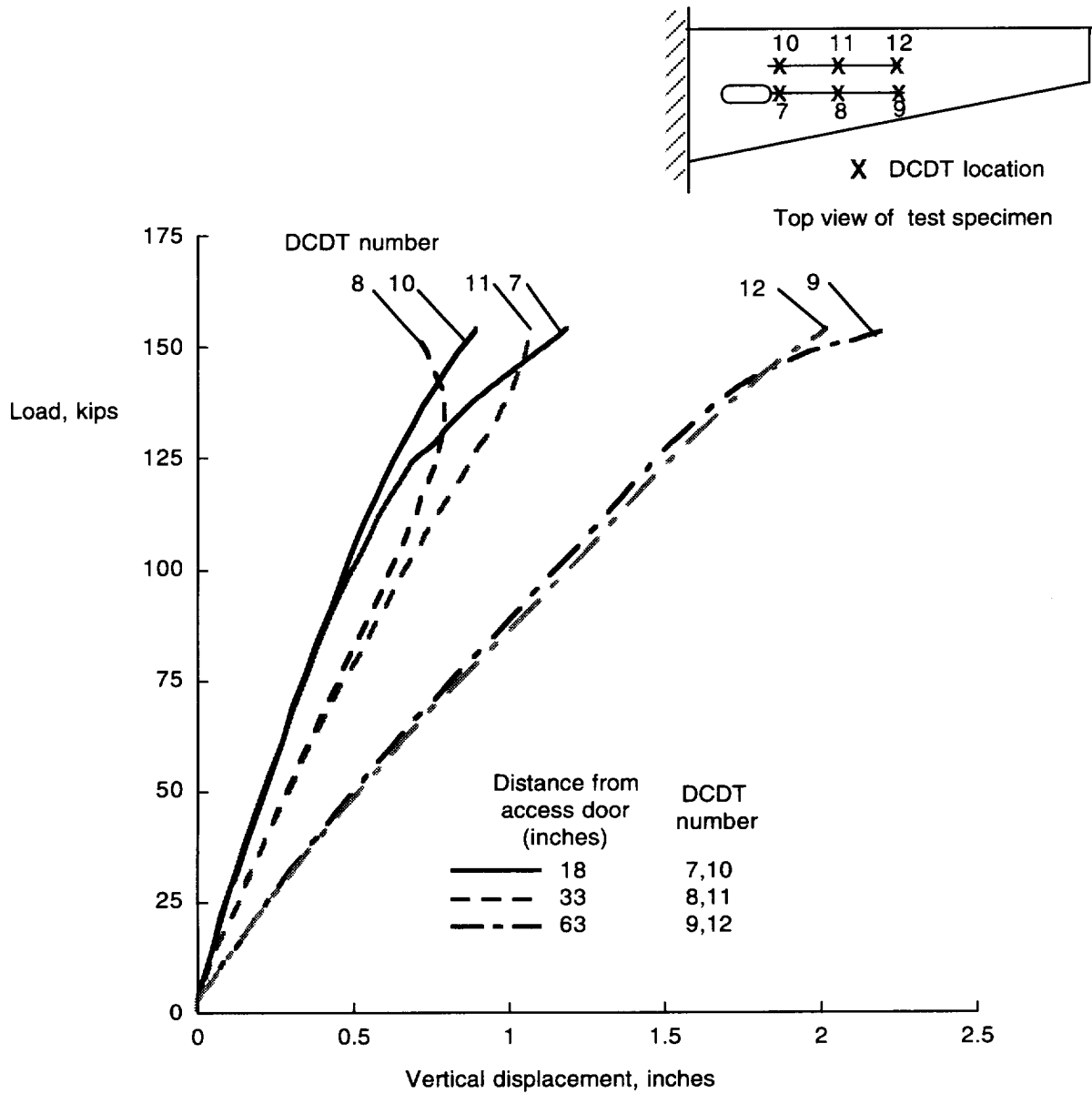
Figure 27. Displacements on the upper surface of the wing stub box.
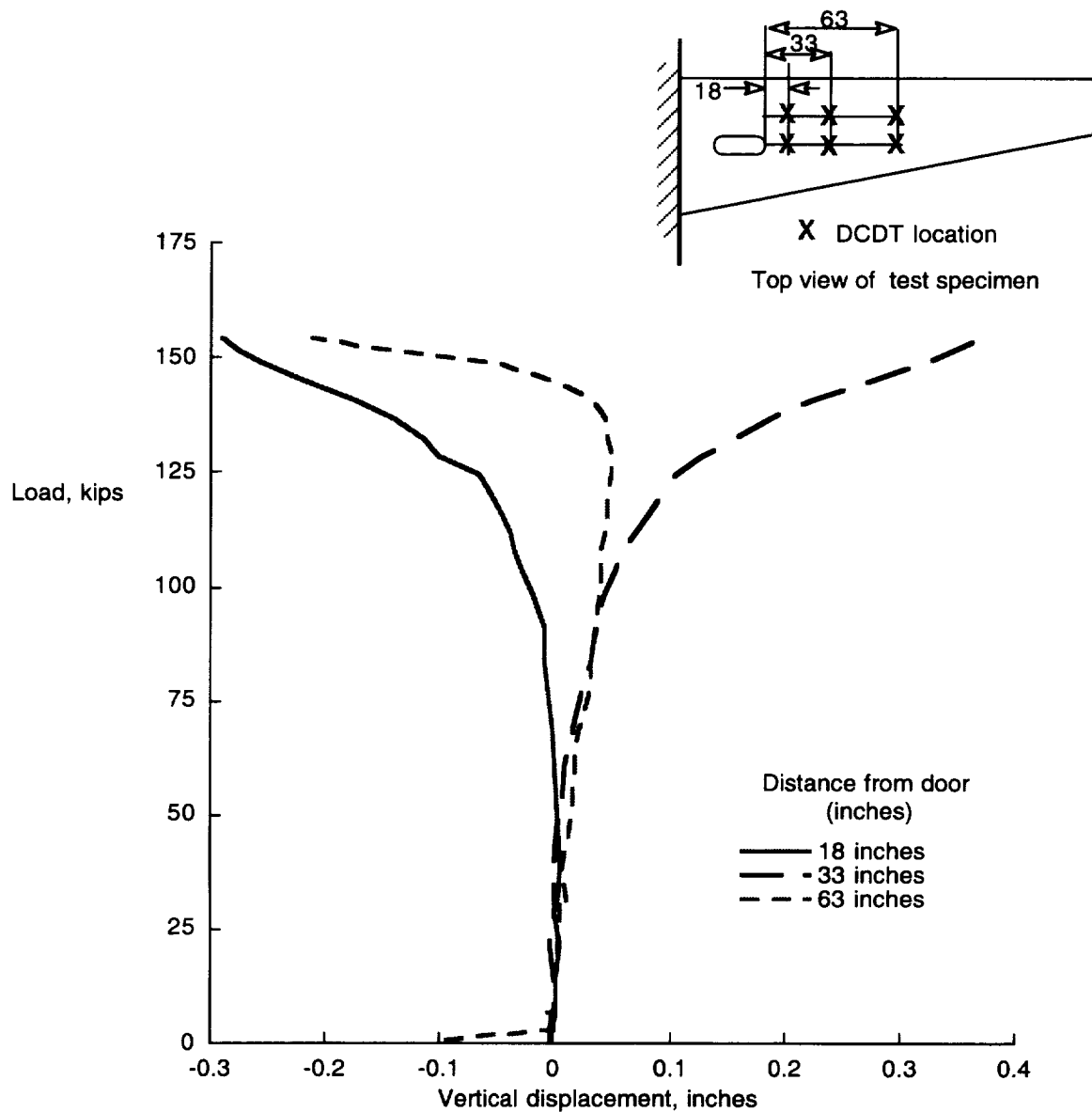
Figure 28. Difference between displacements in the unsupported skin region and a far-field location. Dimensions are in inches.
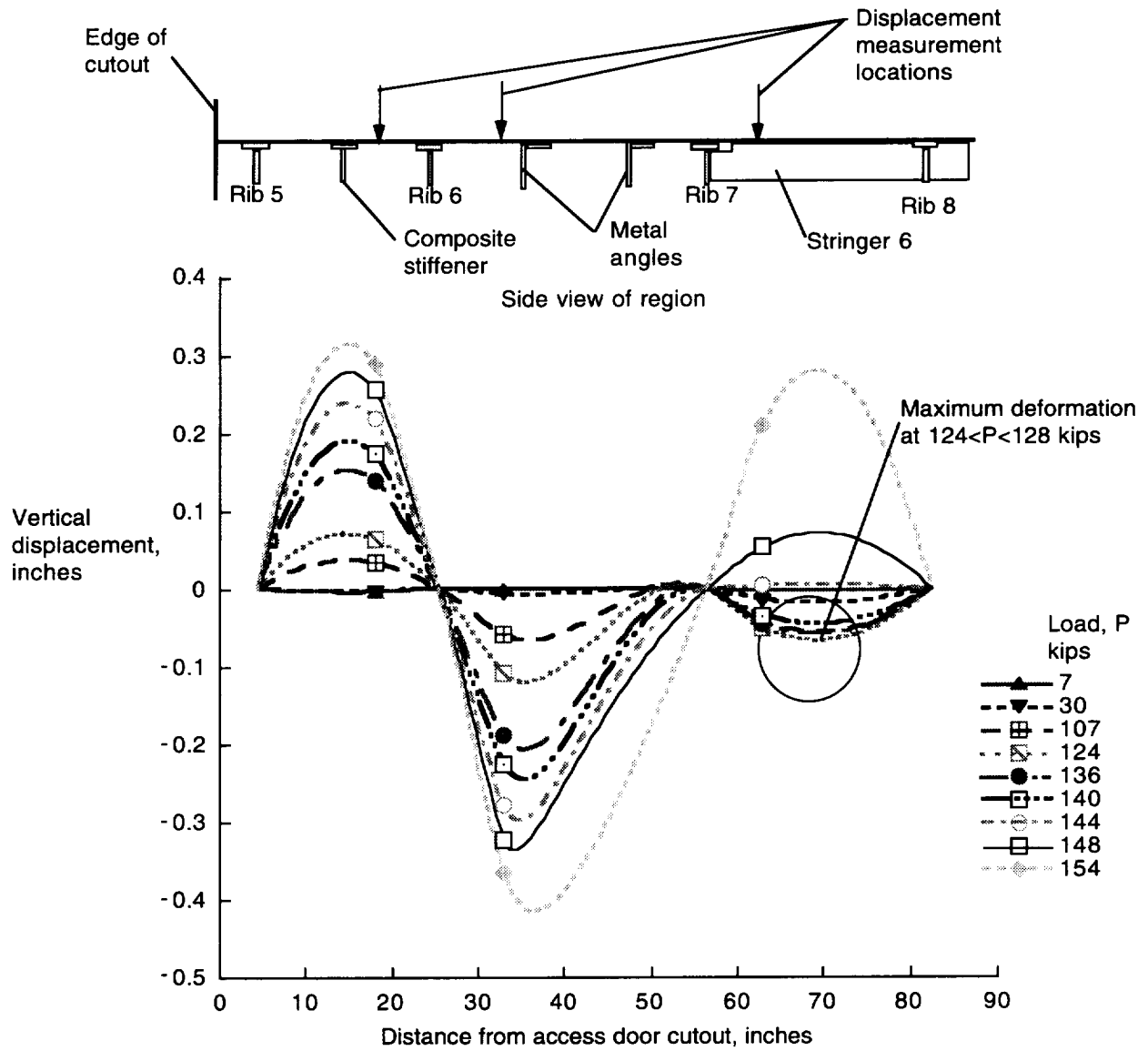
Figure 29. Relative vertical displacements outboard of access door cutout.

intei
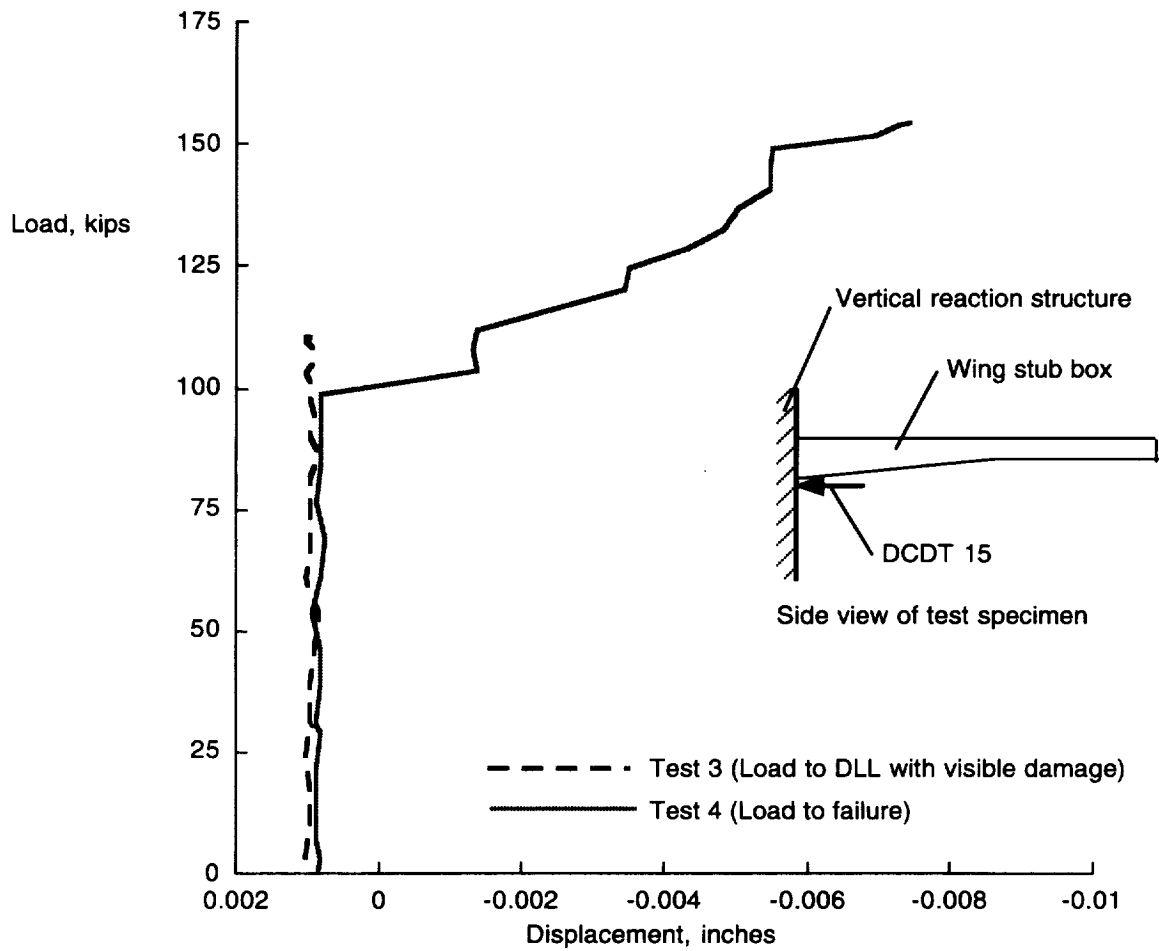
Figure 30. Displacement of vertical reaction structure slotted plate near the rear spar.
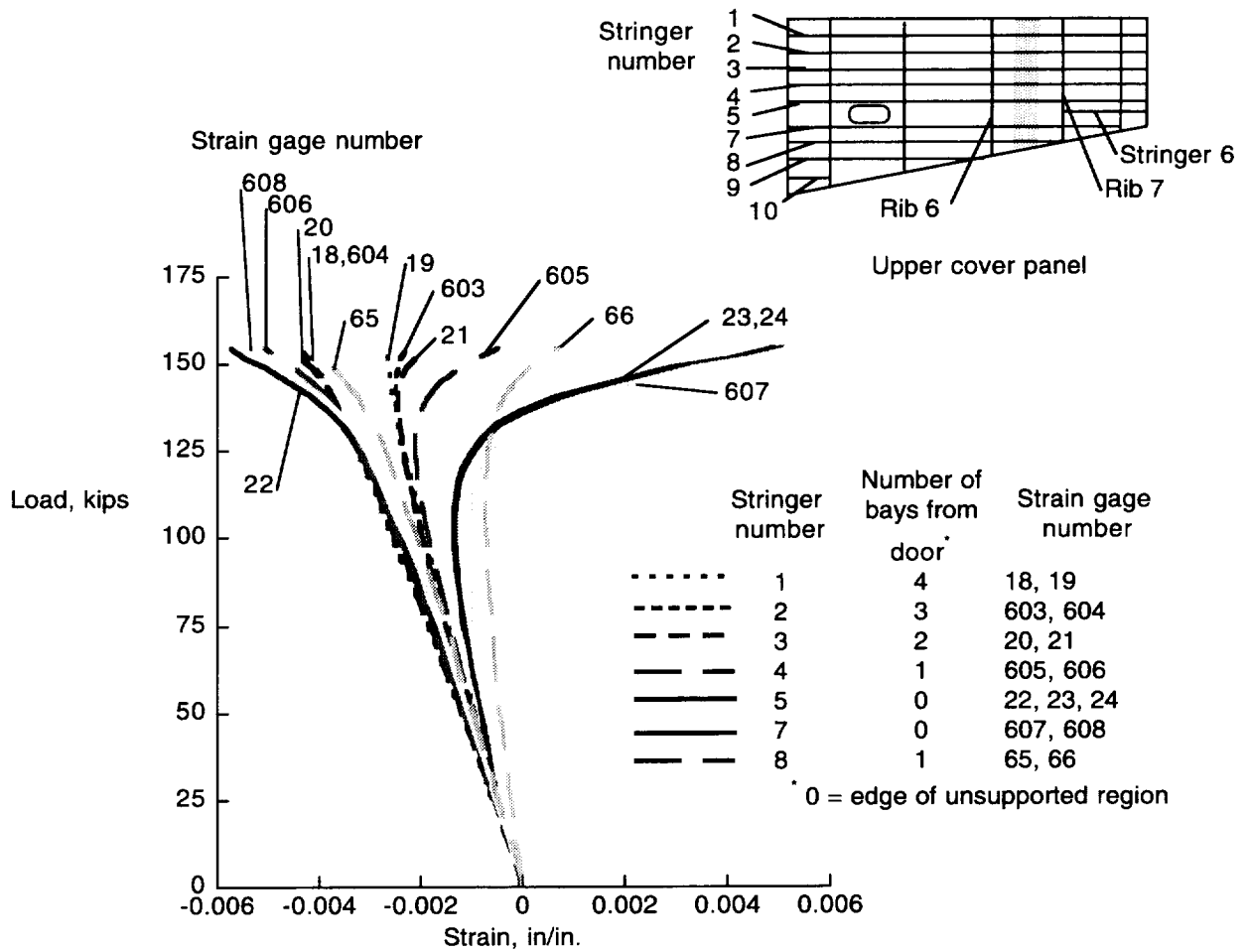
Figure 31. Strains for stringers in upper cover panel between ribs 6 and 7.
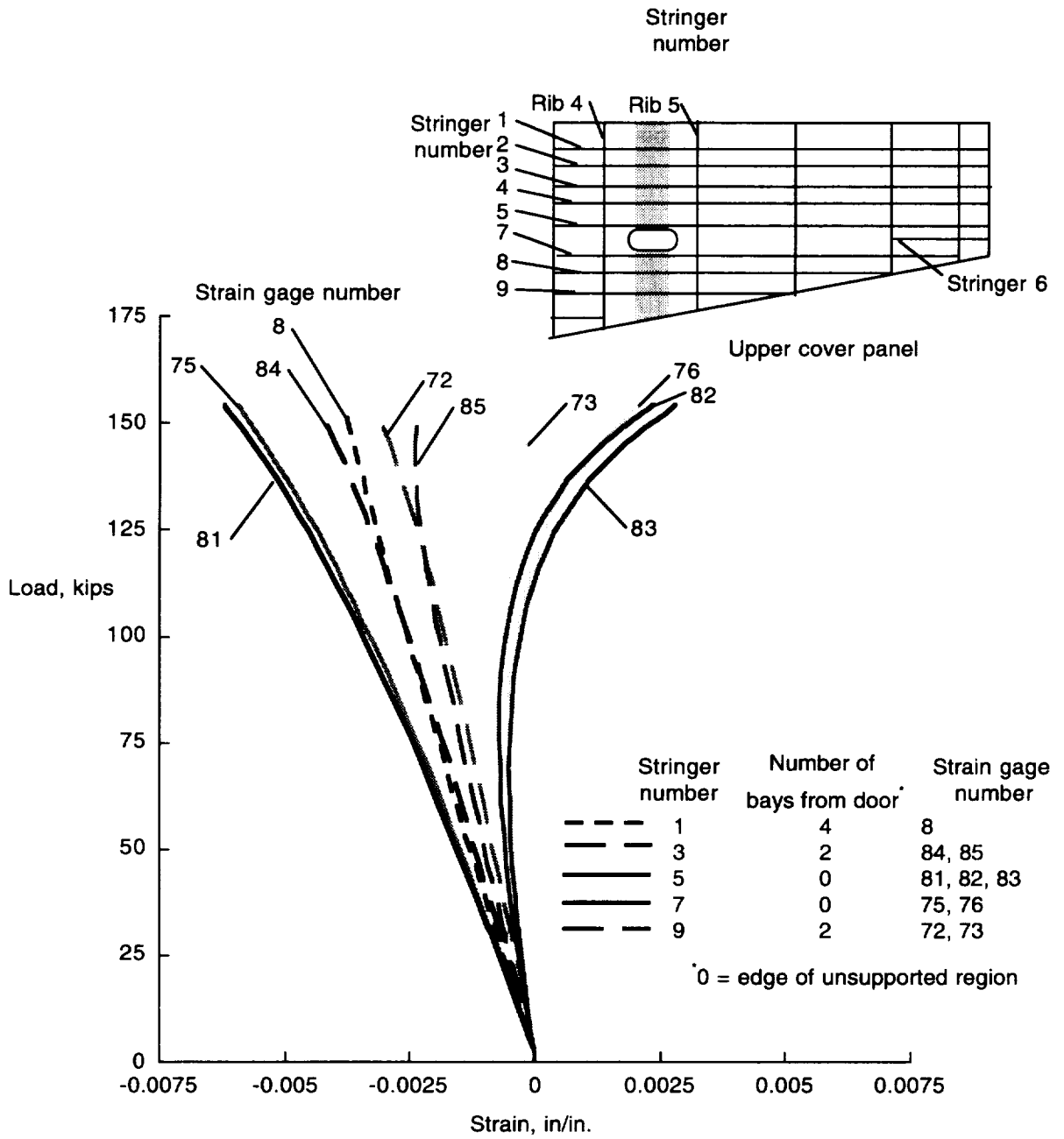
Figure 32. Strains at stringers for upper cover panel between ribs 4 and 5.
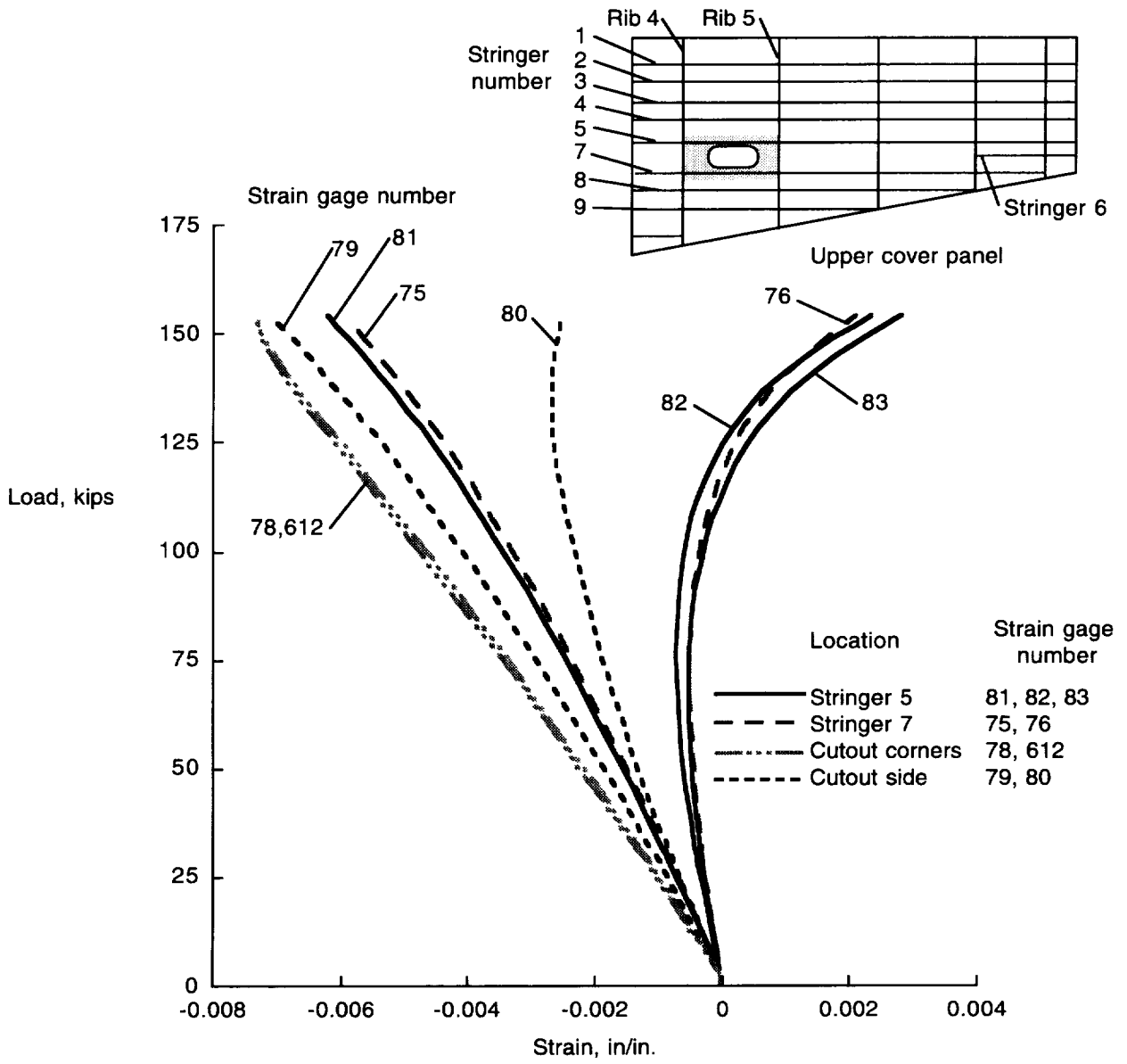
Figure 33. Strains for the region around the access door.
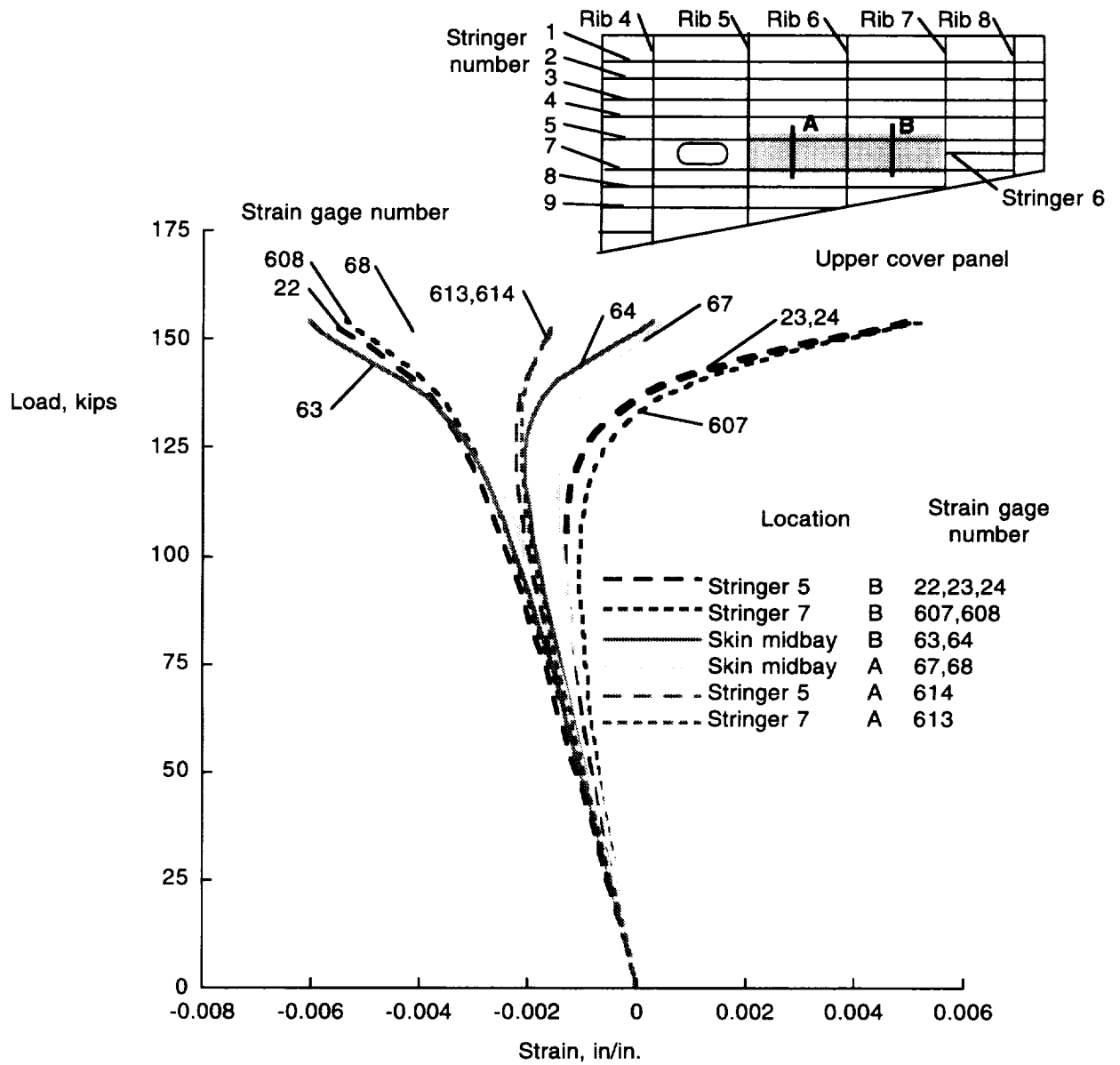
Figure 34. Strains in and around unsupported skin region between ribs 5 and 7.
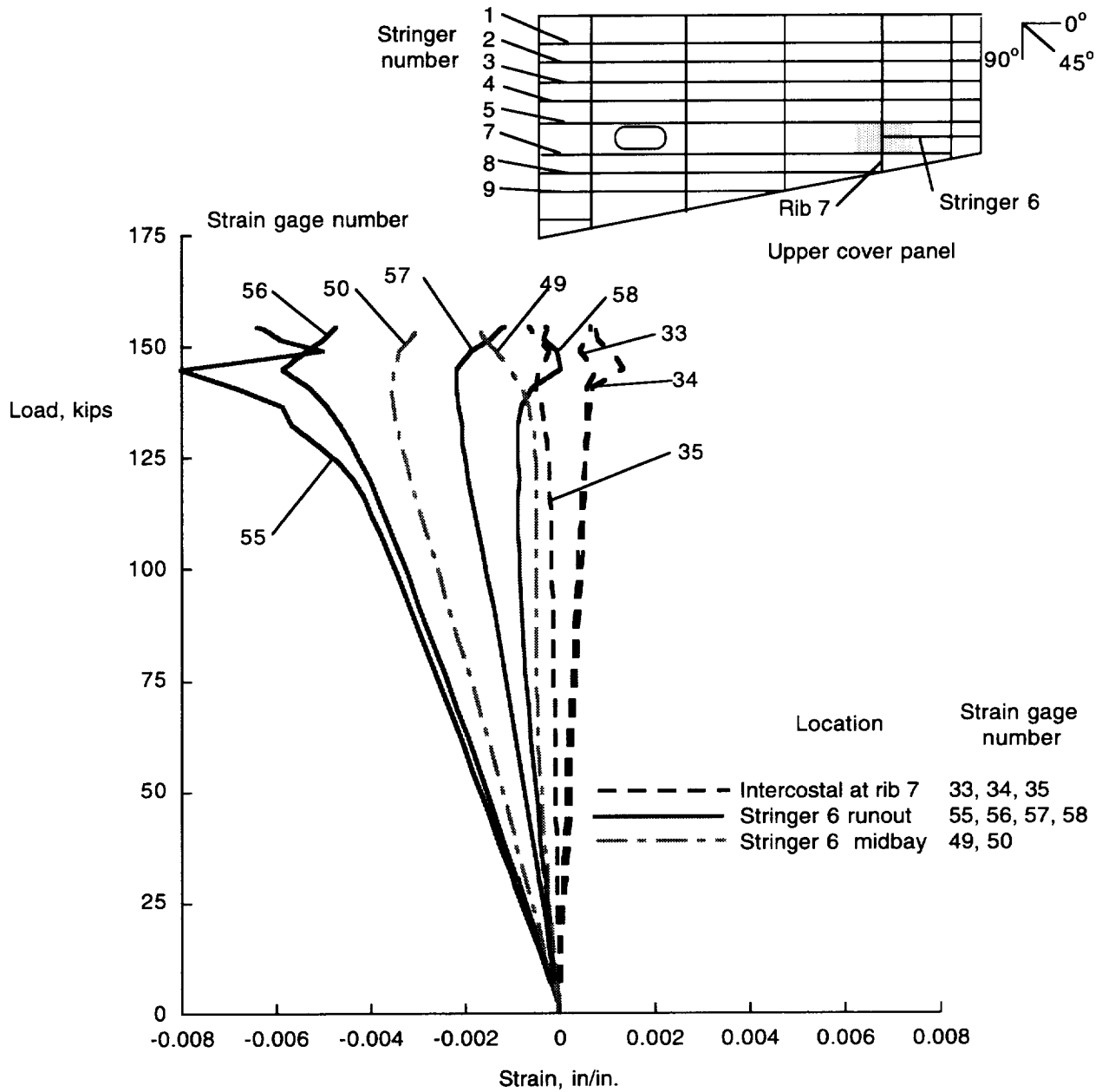
Figure 35. Strains for stringer 6 runout and intercostal at rib 7.
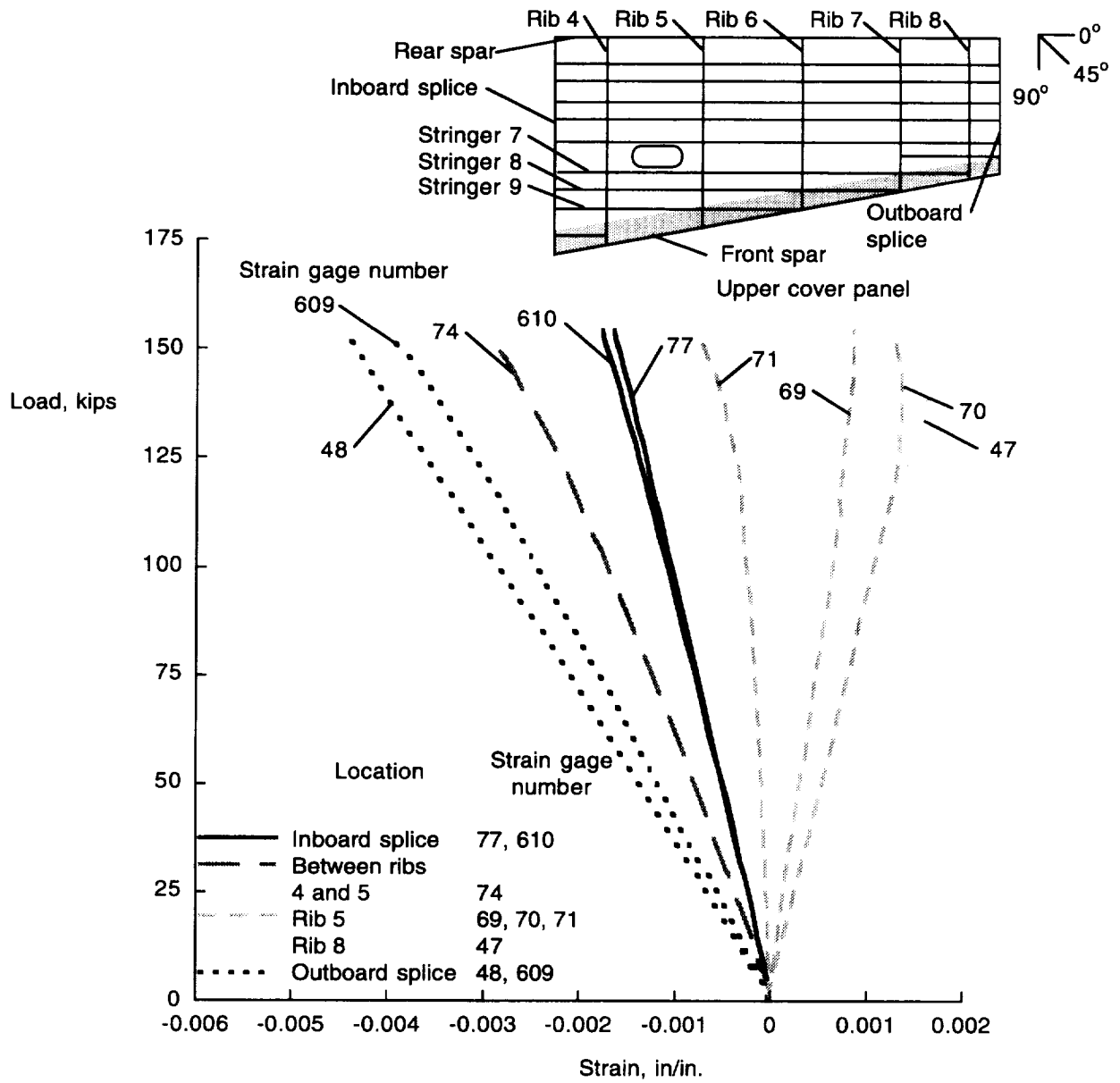
Figure 36. Strains for upper cover panel at the front spar.
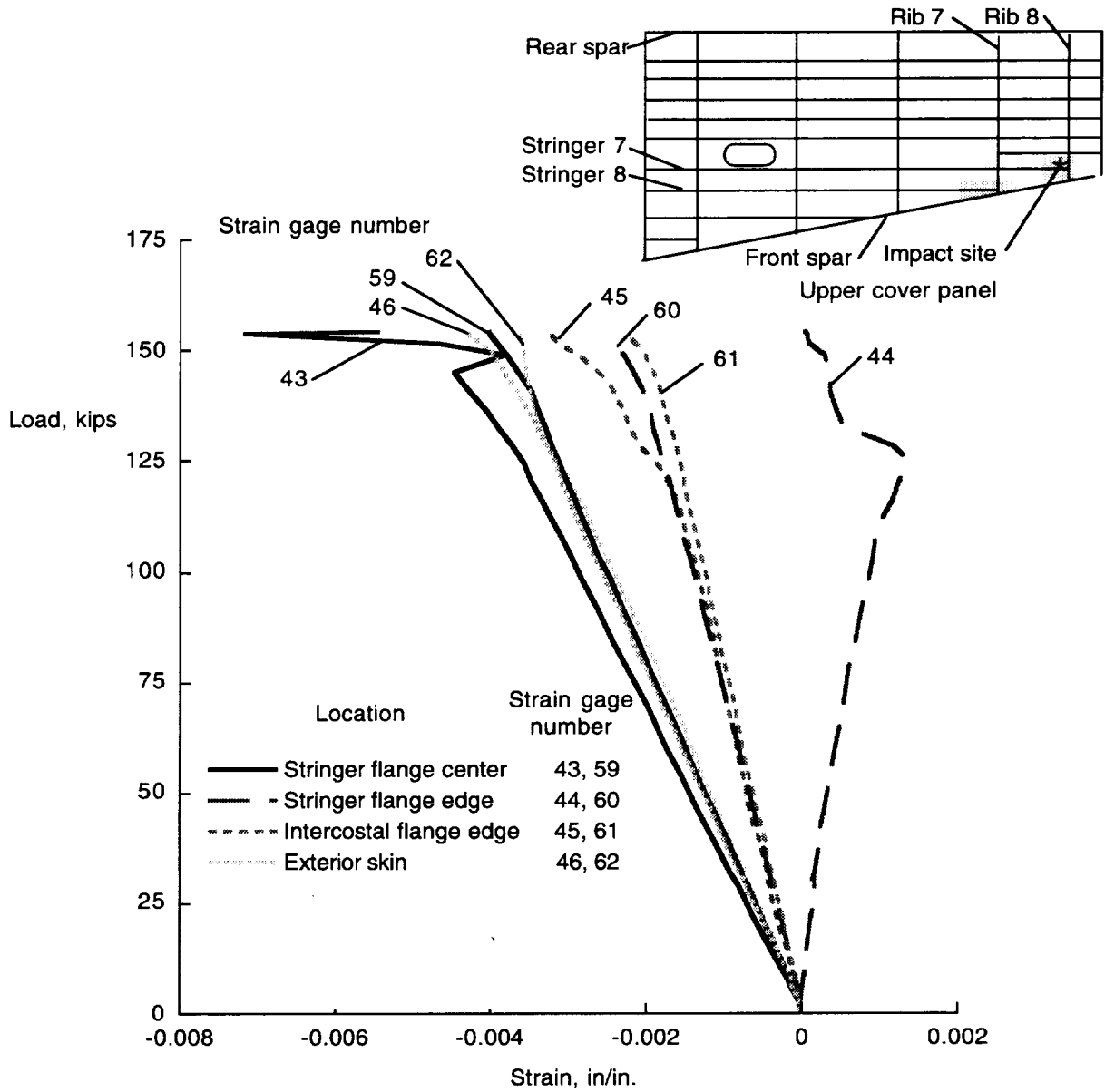
Figure 37. Strains for stiffener runouts which terminate at ribs 7 and 8 near the front spar.
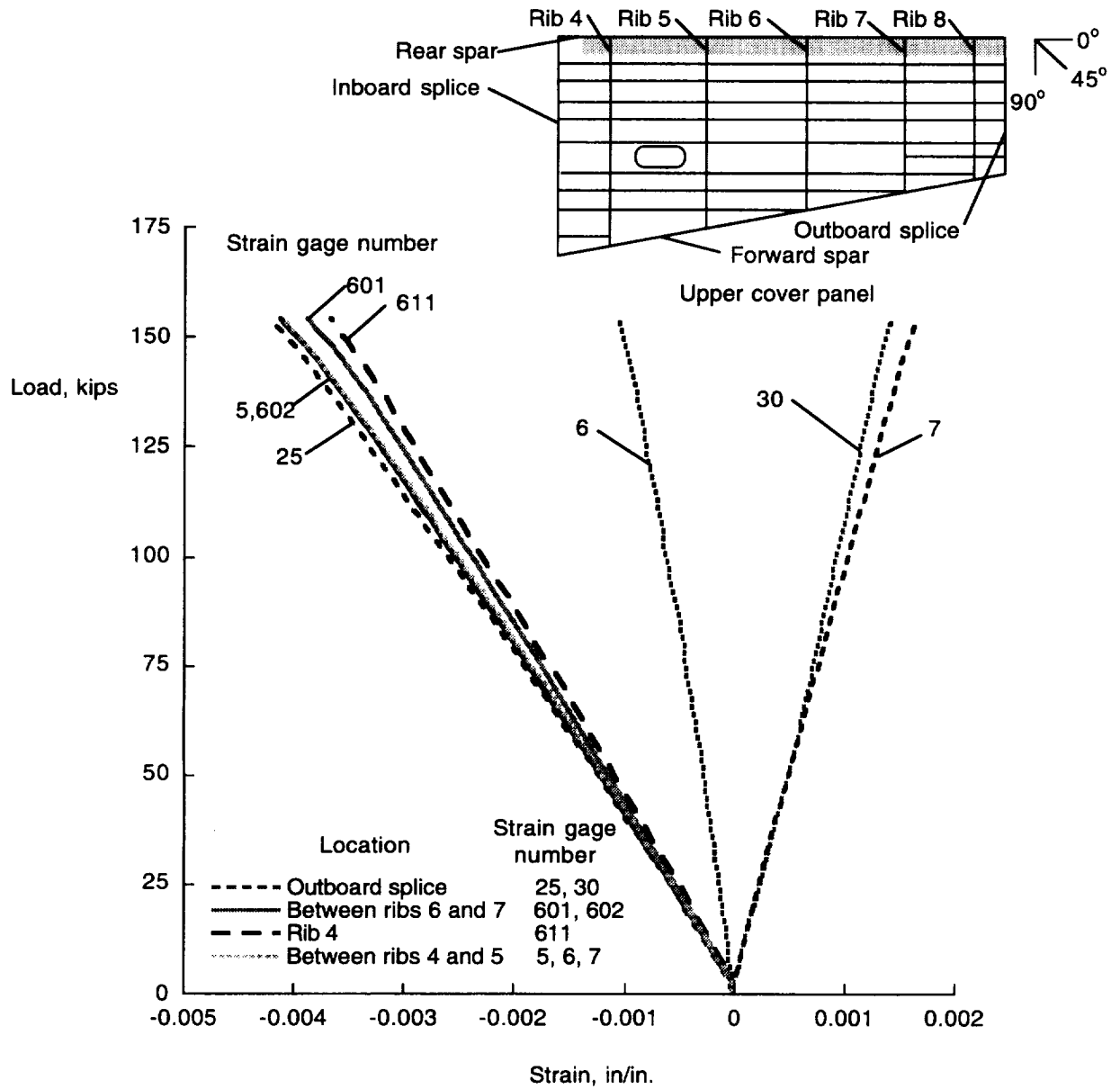
Figure 38. Strains for upper cover panel at rear spar.
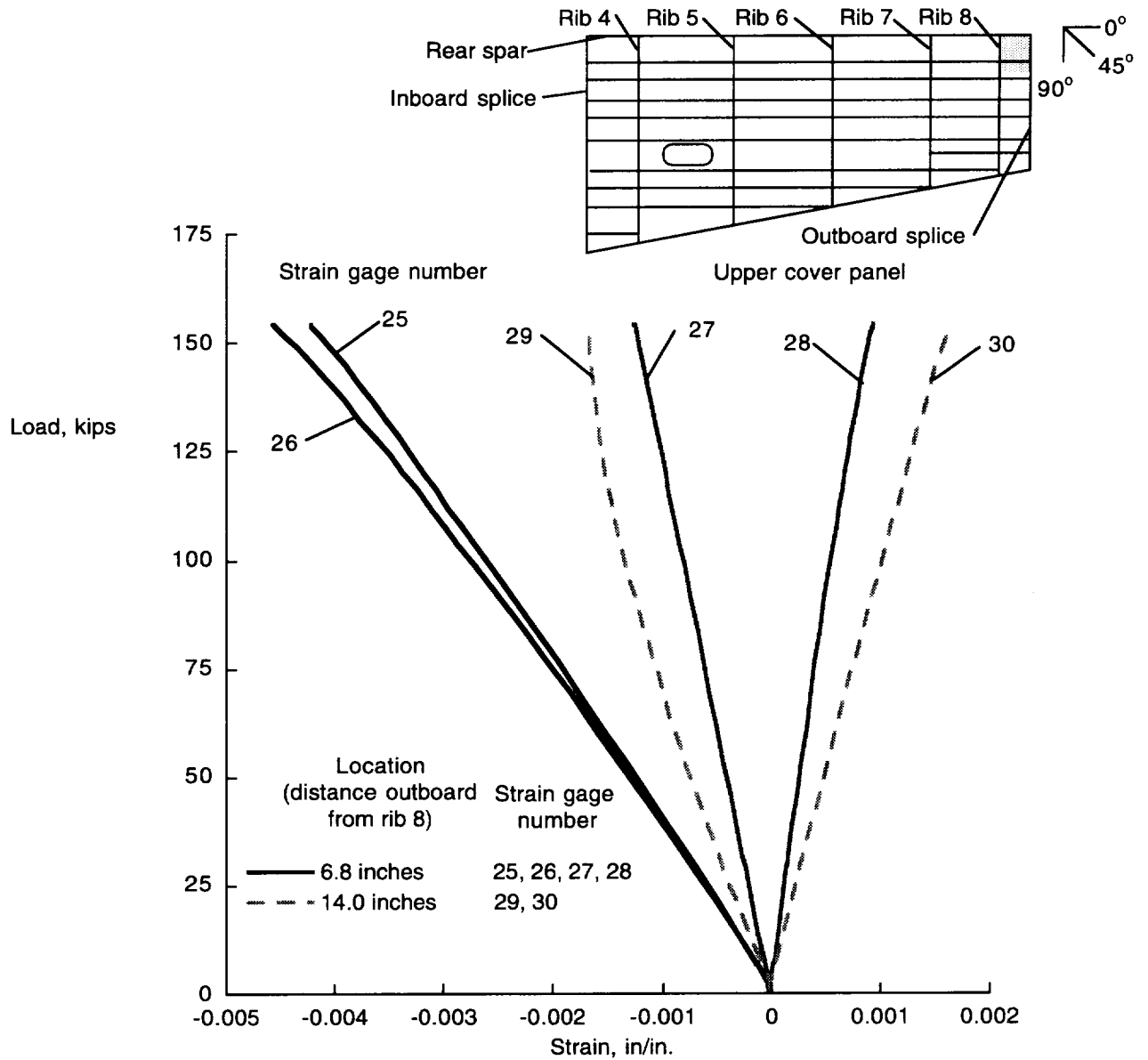
Figure 39. Strains for upper cover panel at the outboard aft corner.
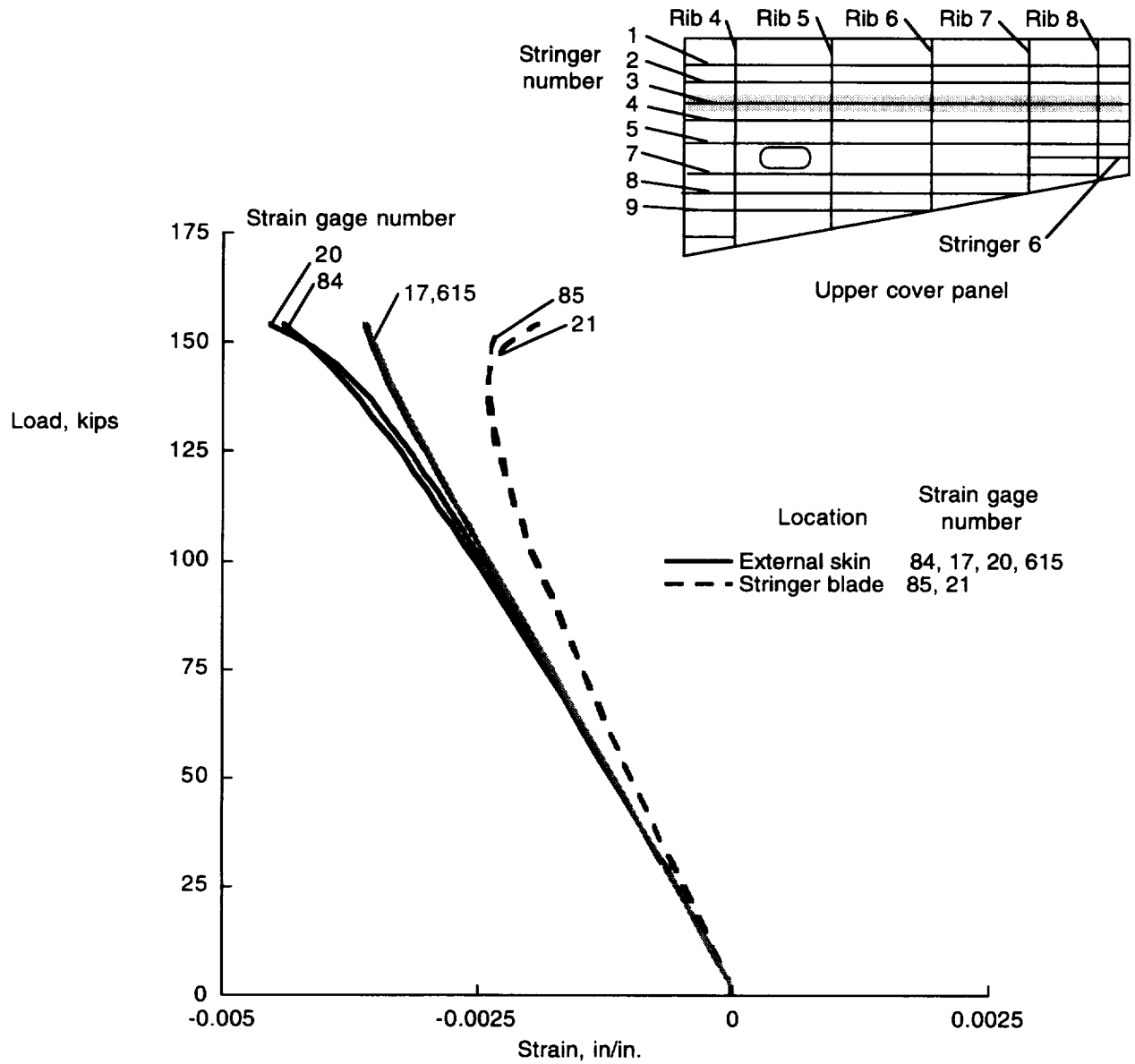
Figure 40. Strain along third stringer from rear spar on the upper cover panel.
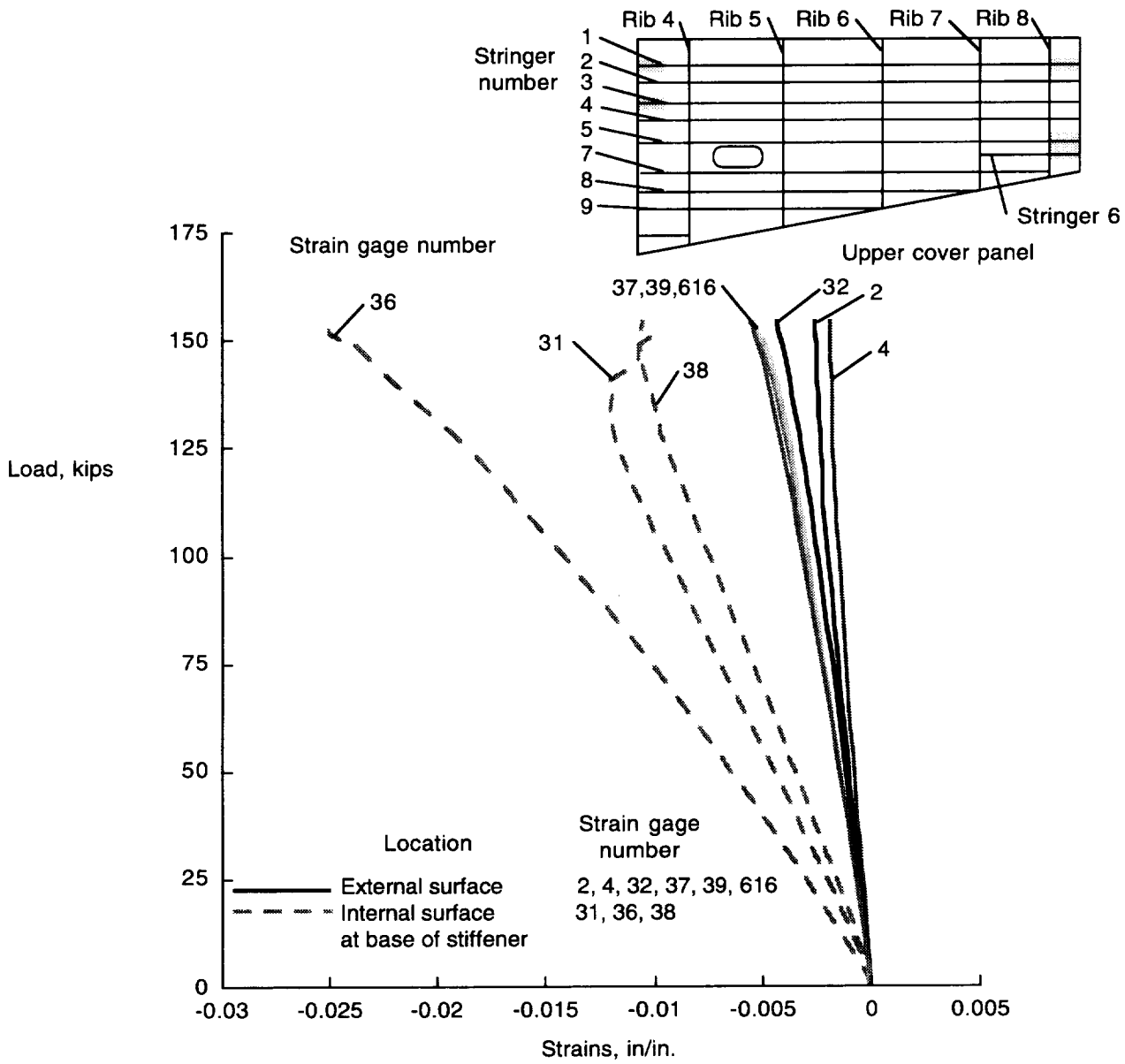
Figure 41. Strains in composite parts of splices.
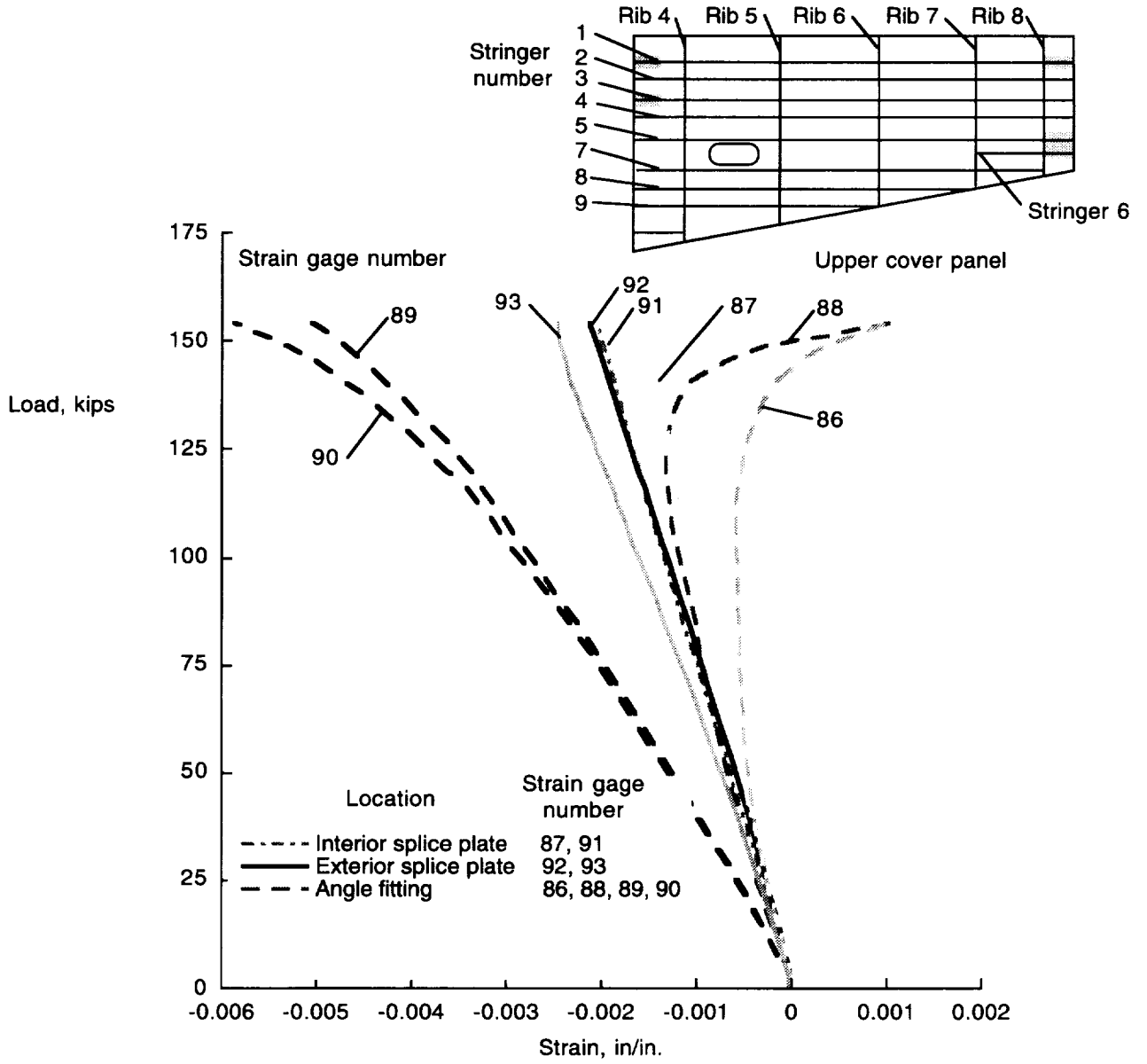
Figure 42. Strain for metal splice components.
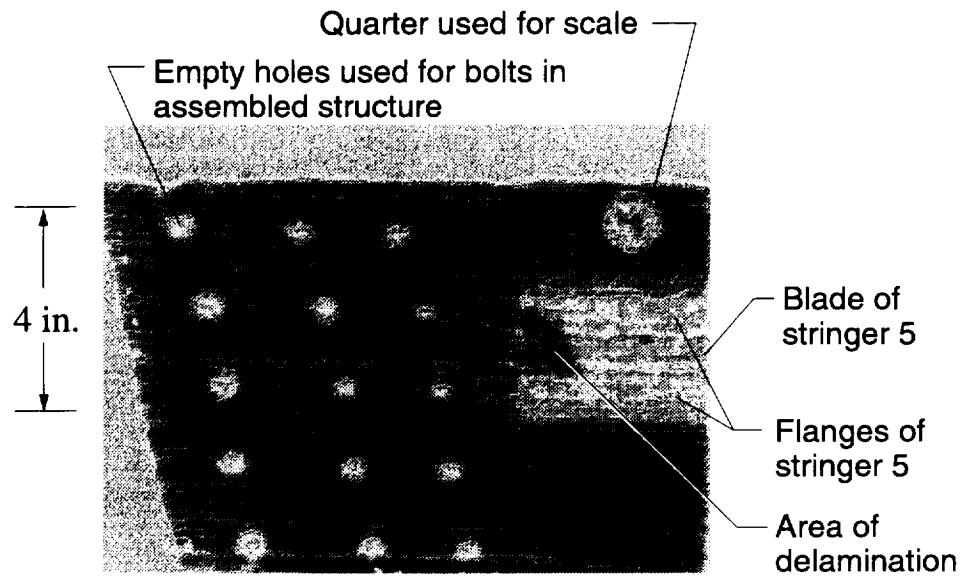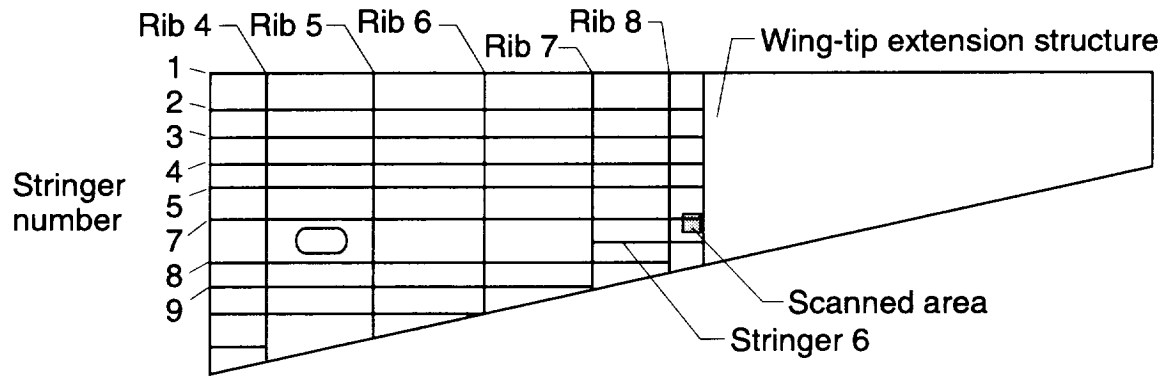
Figure 43. Damage area for upper cover splice on stringer 5.
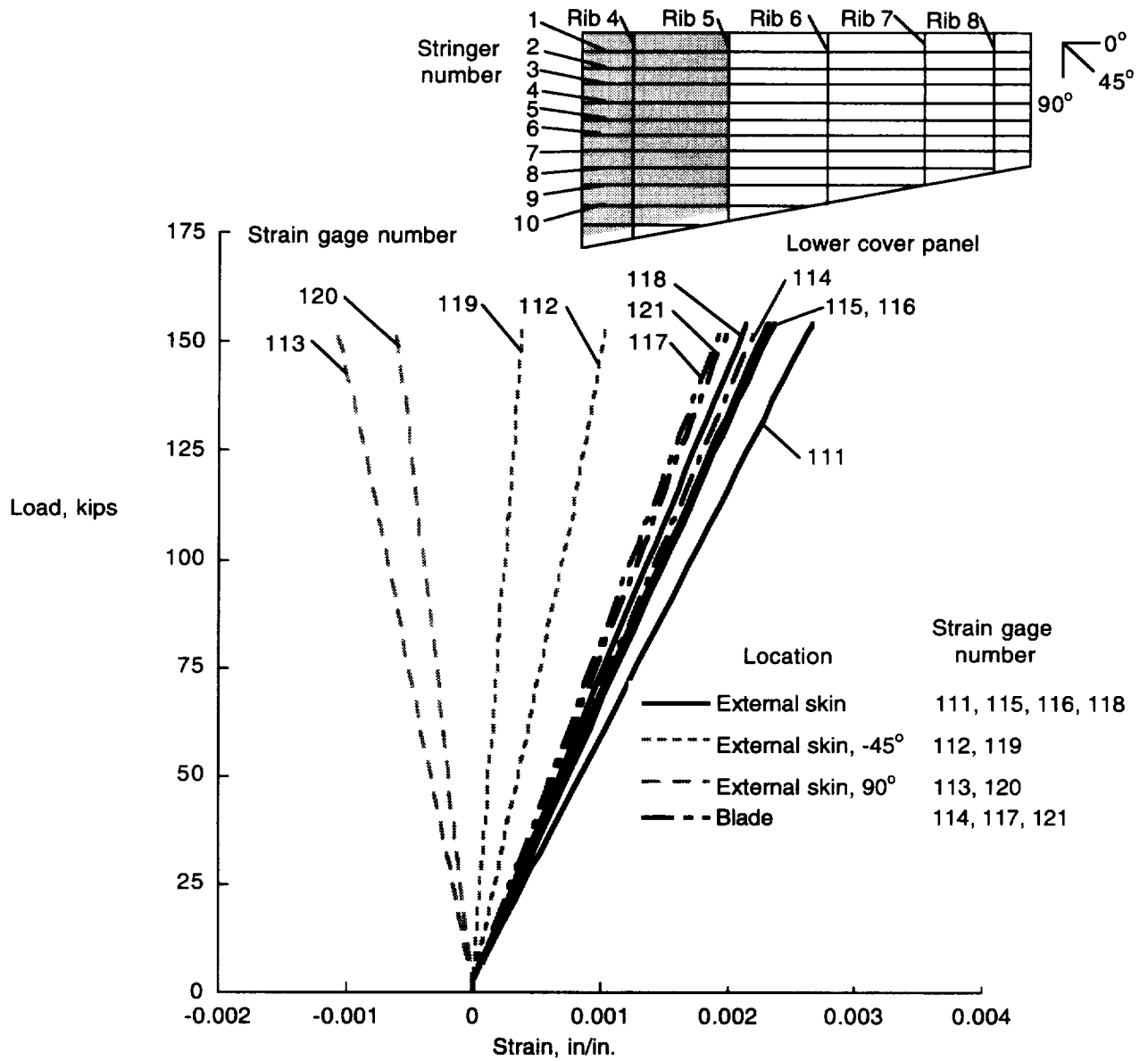
Figure 44. Strains for lower cover panel stringers and rear spar inboard of rib 5.
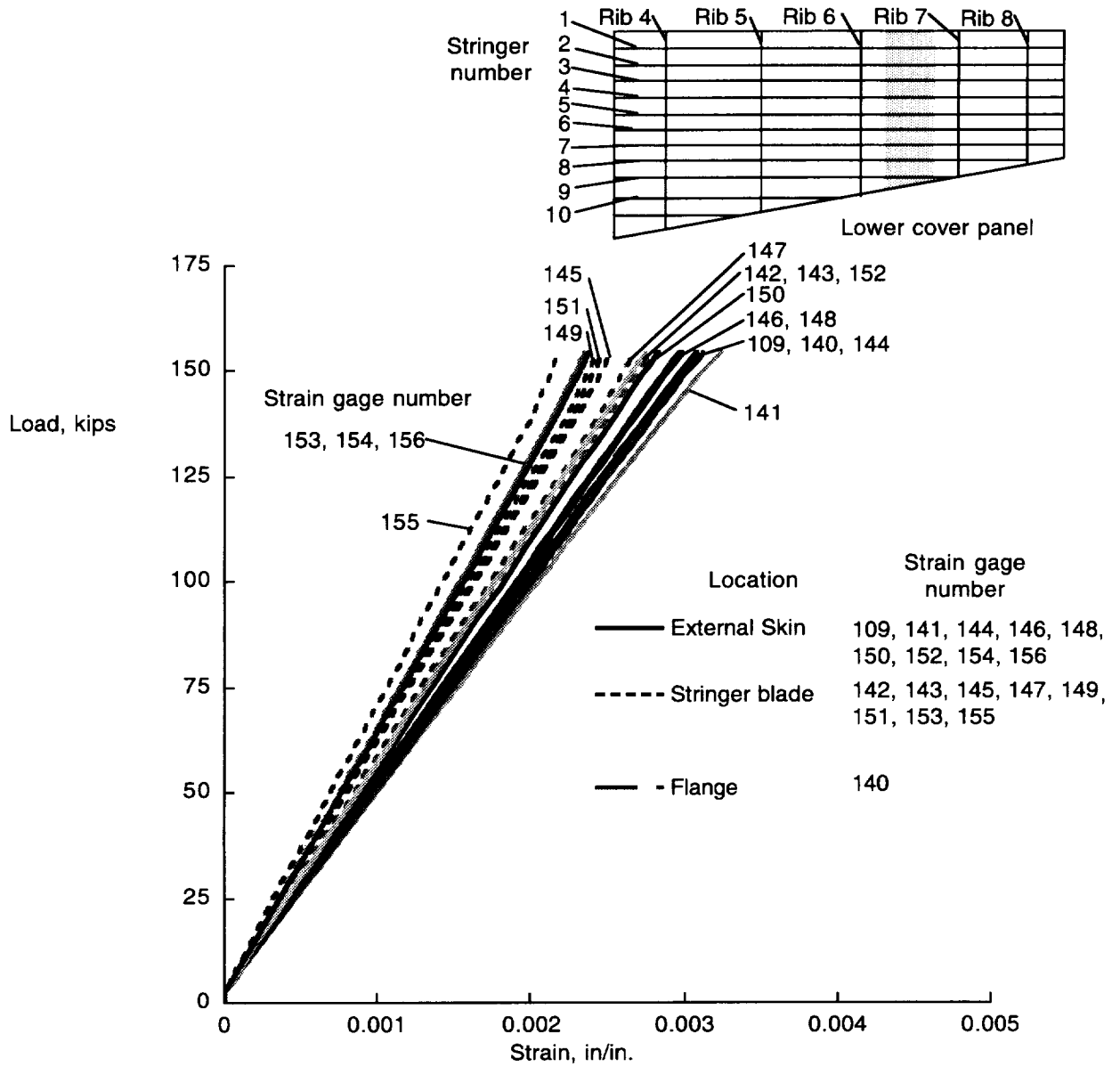
Figure 45. Strains for lower cover halfway between ribs 6 and 7.
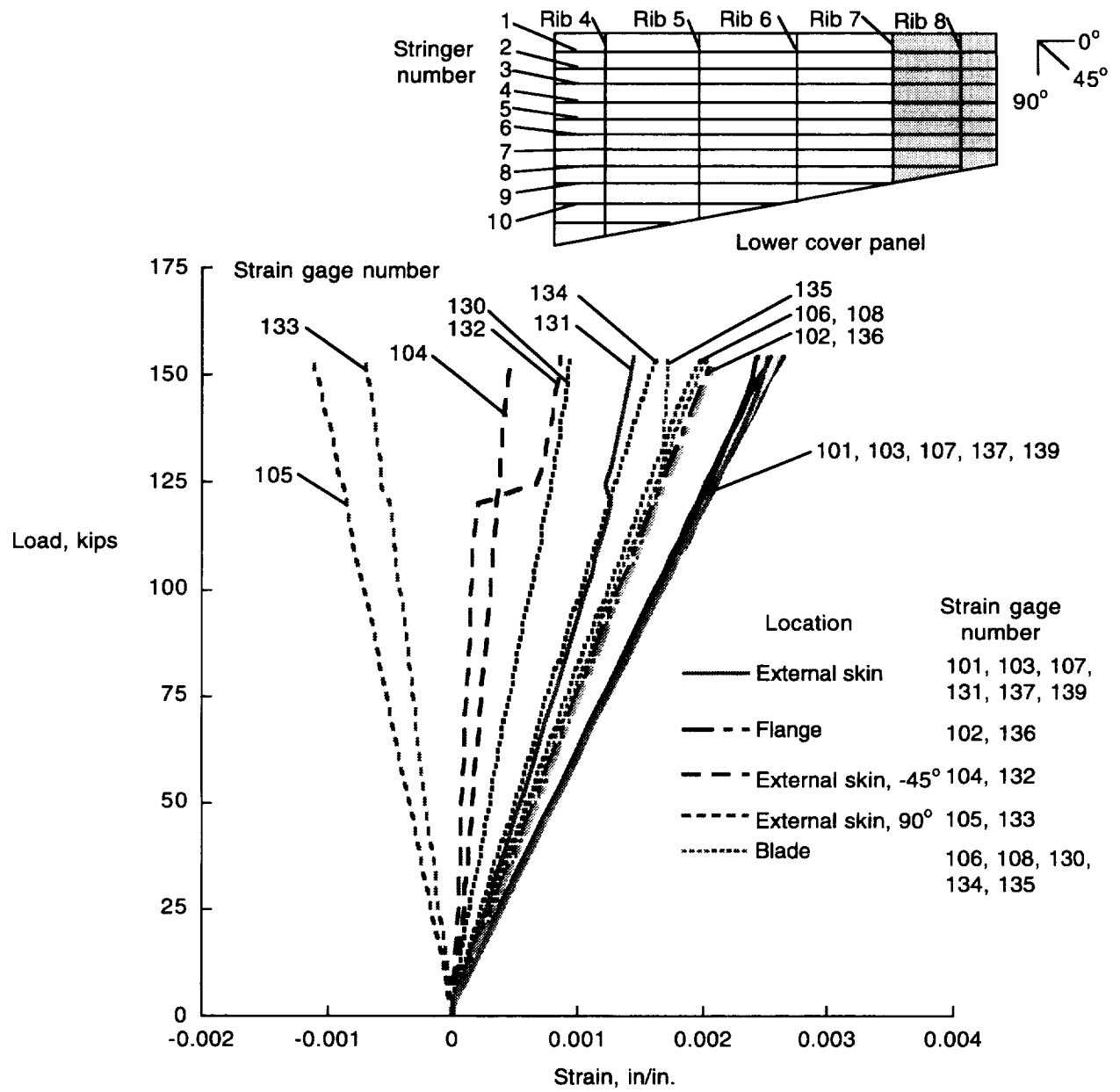
Figure 46. Strains for lower cover panel outboard of rib 7.
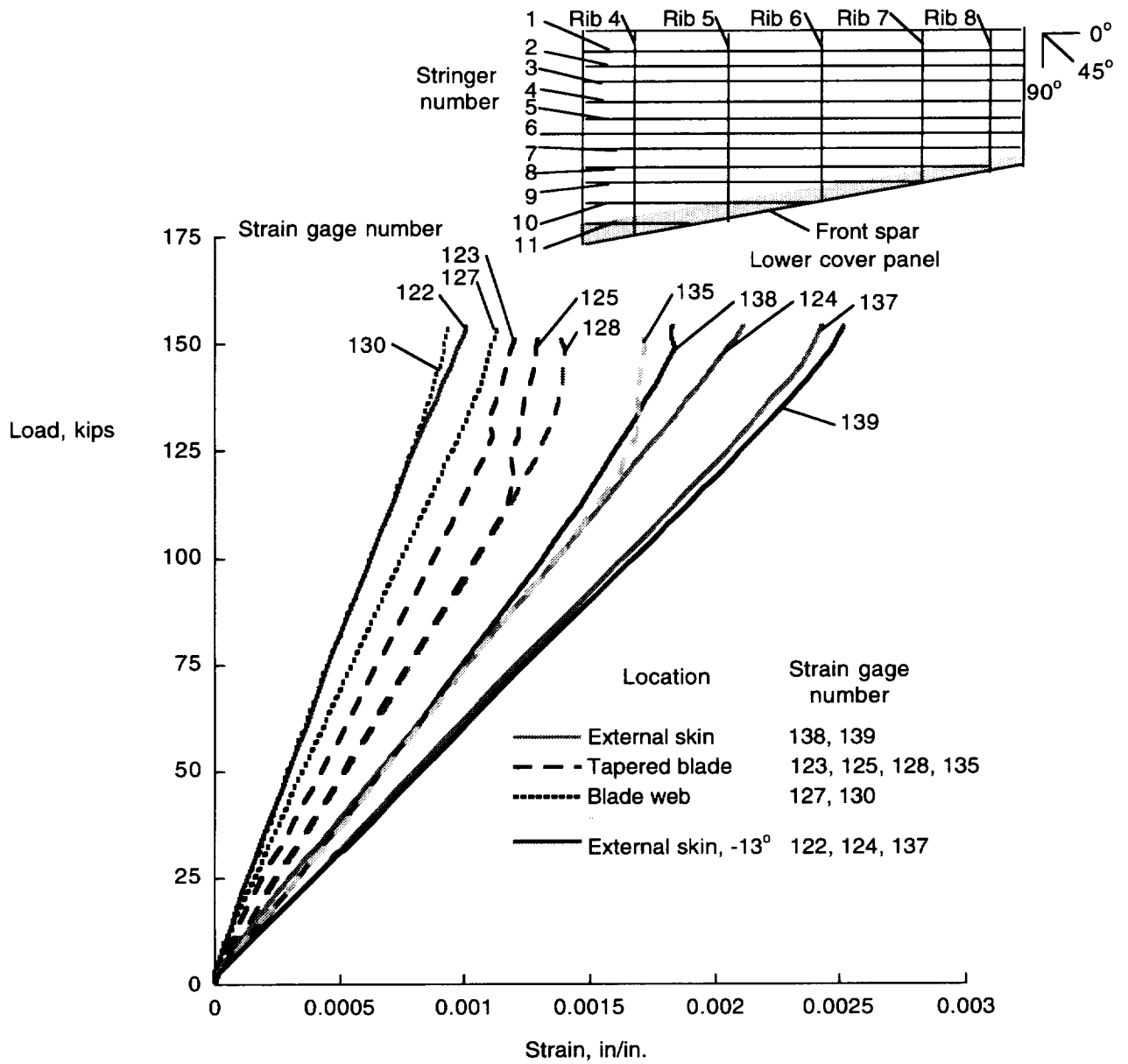
Figure 47. Strains for lower cover panel near front spar.
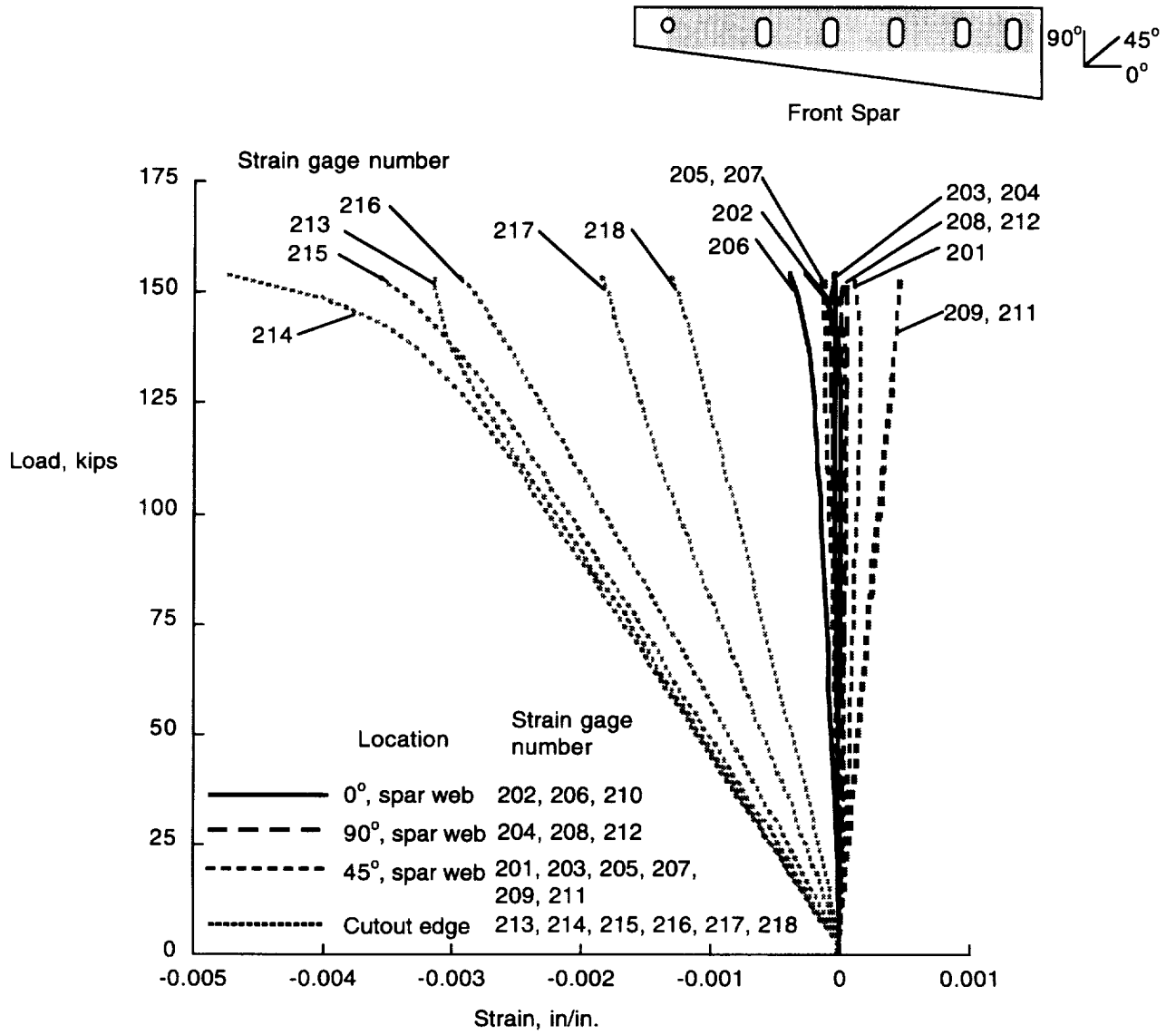
Figure 48. Strains for front spar.

Rear Spar
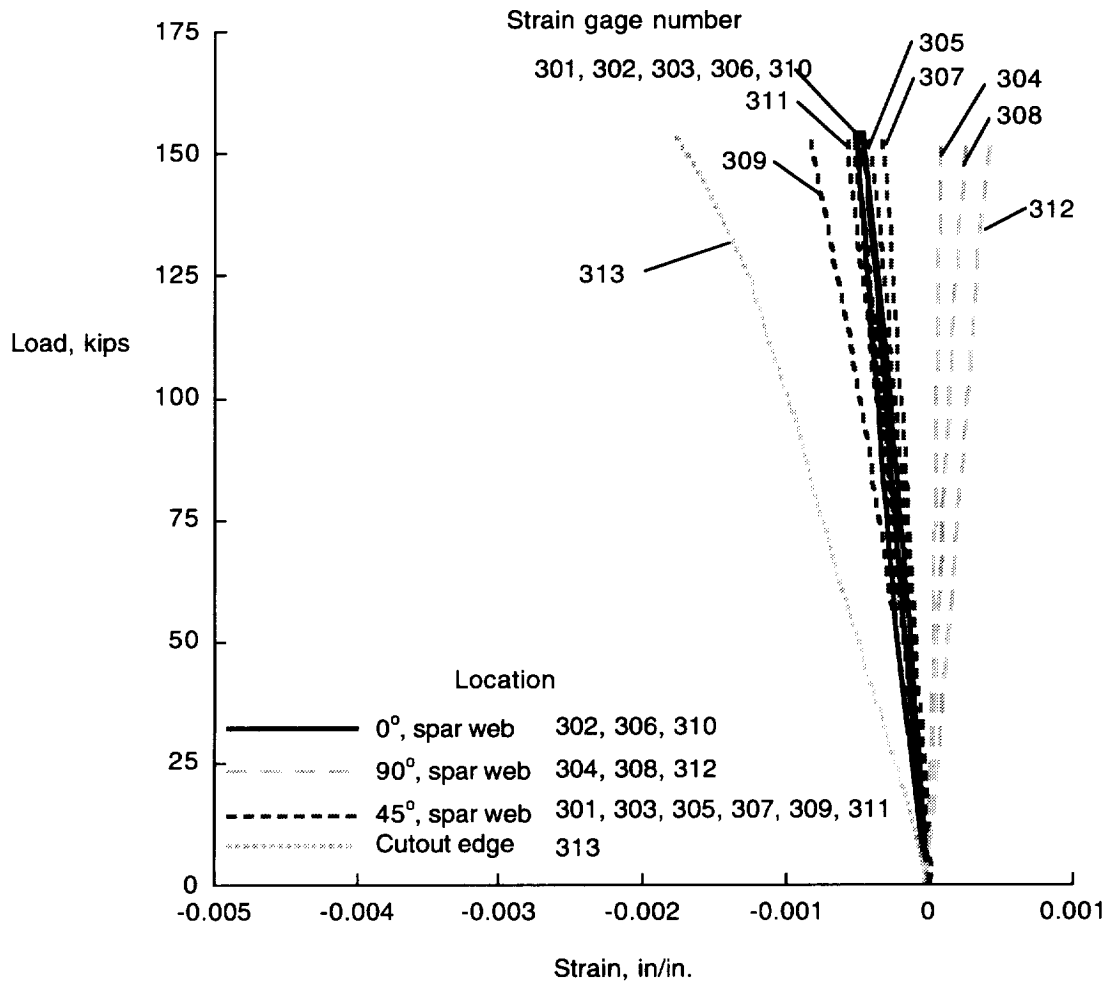
Figure 49. Strain in rear spar.
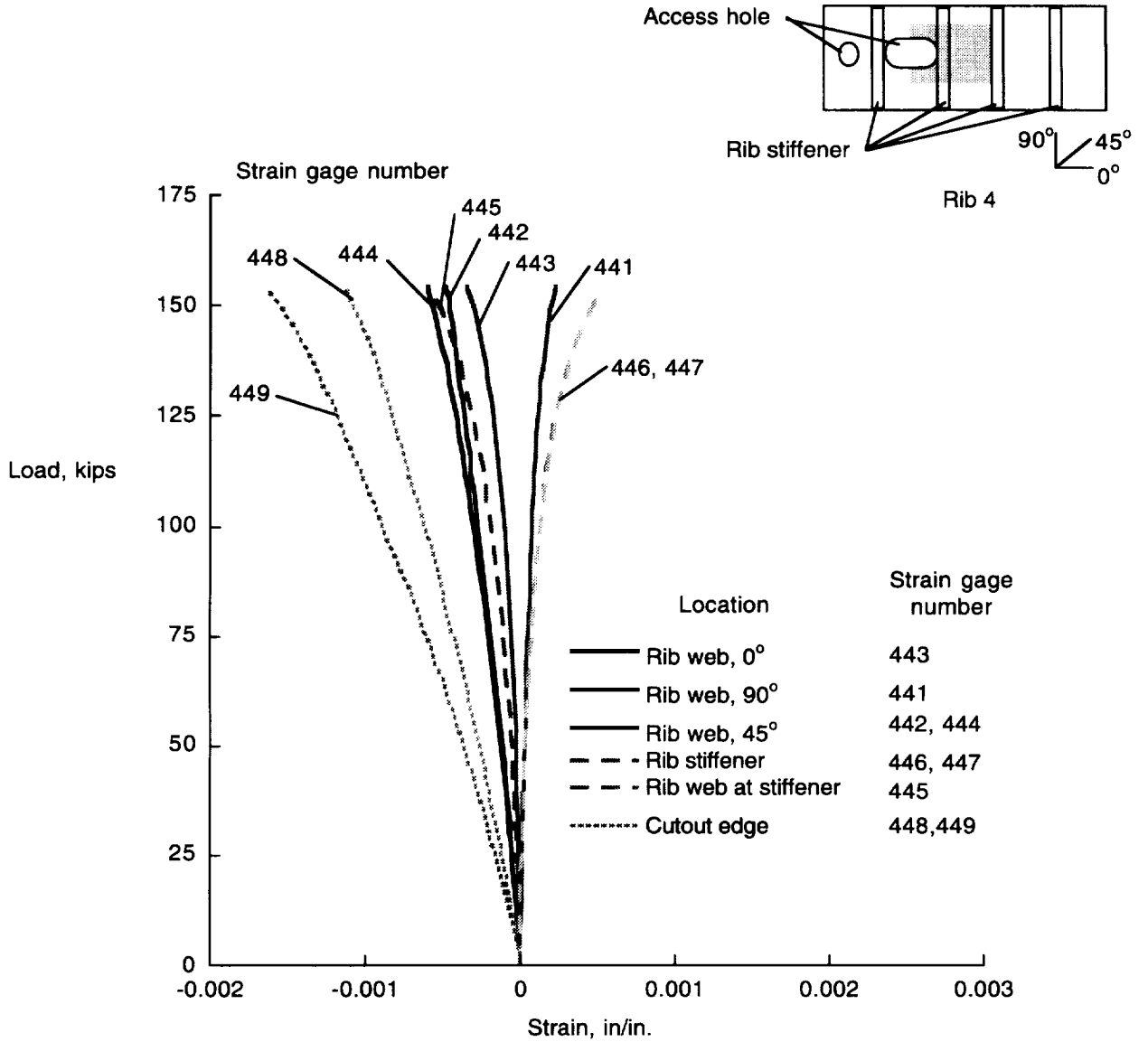
Figure 50. Strains for rib 4.
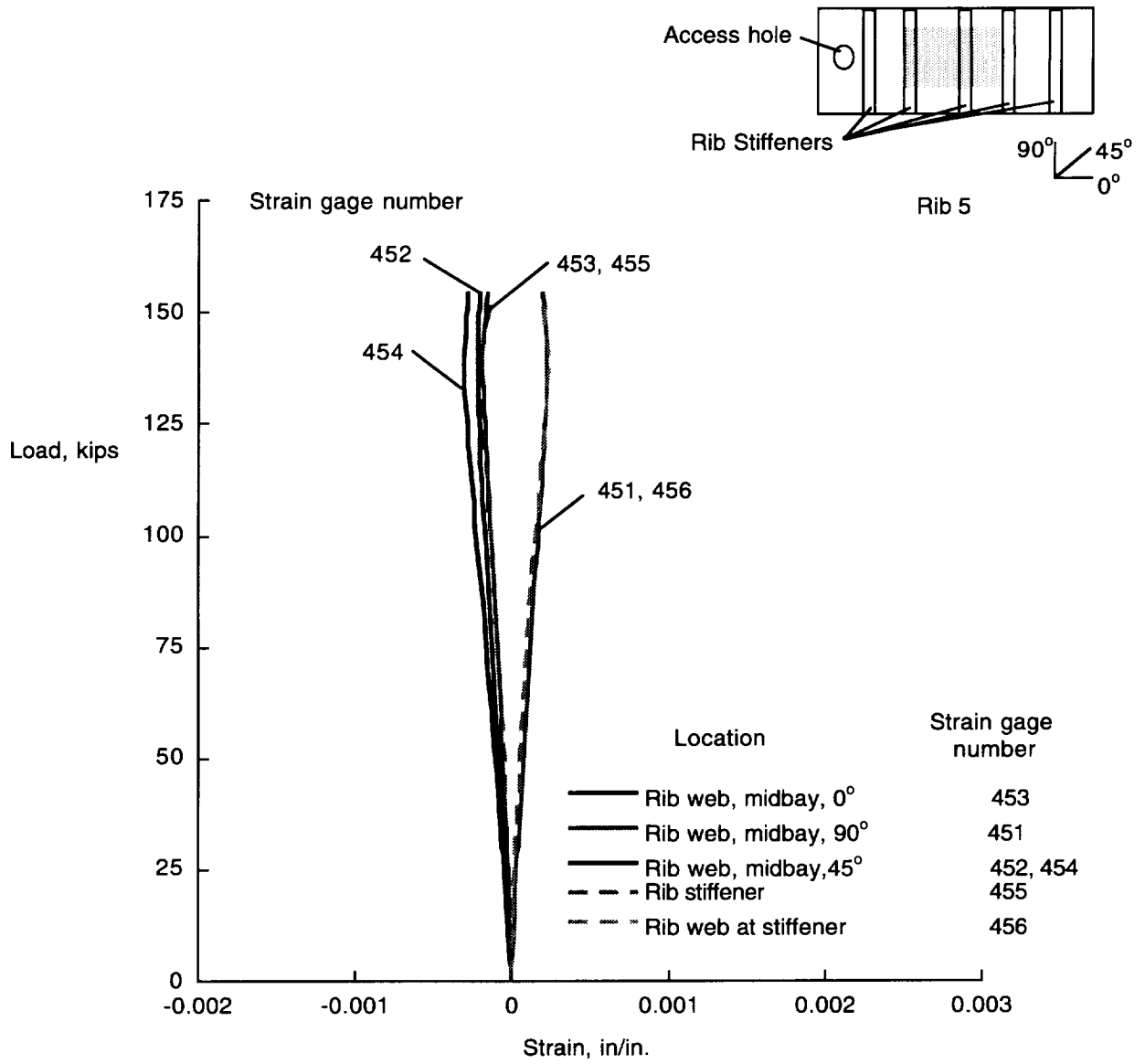
Figure 51. Strains in rib 5.
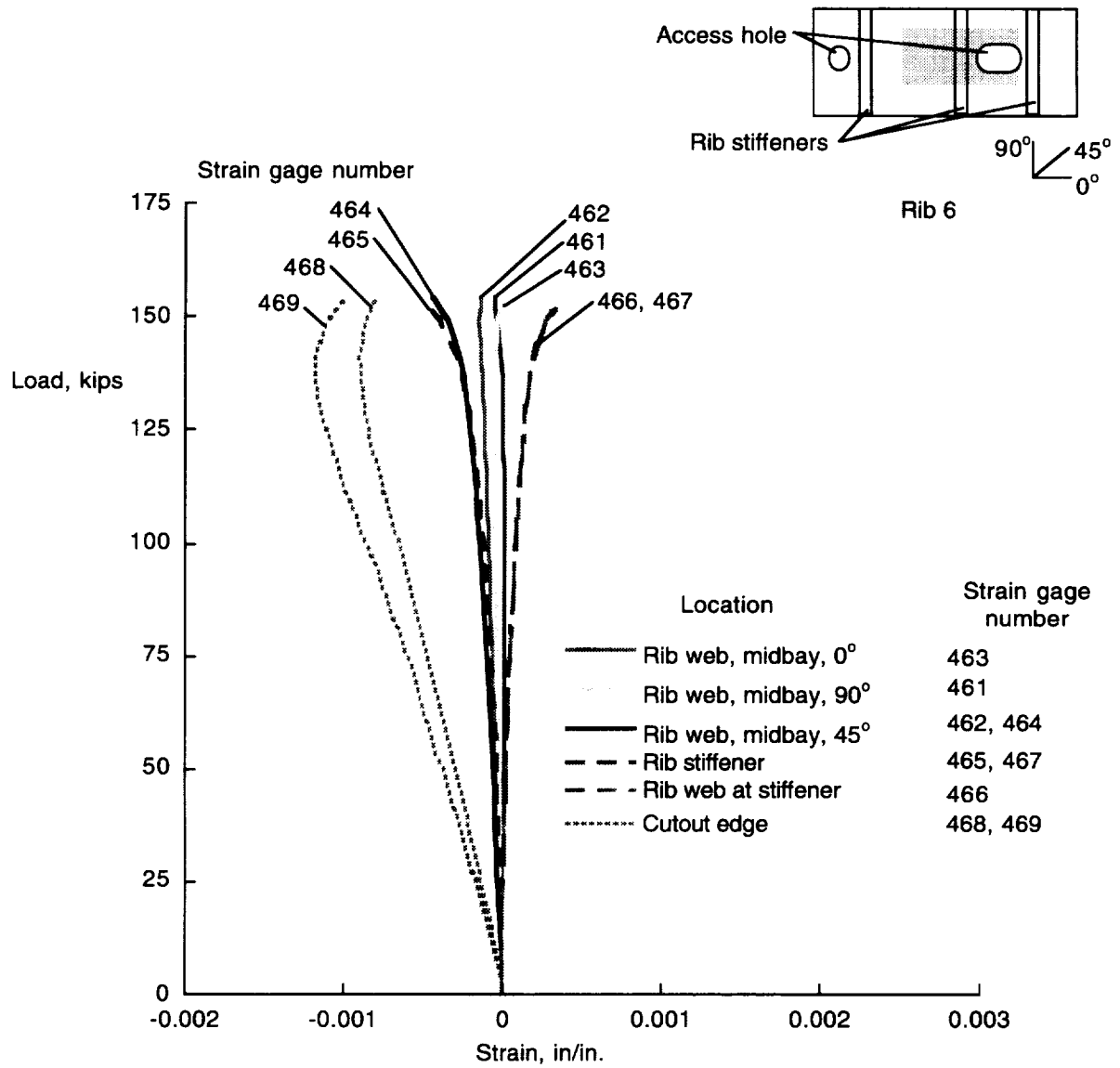
Figure 52. Strains for rib 6.
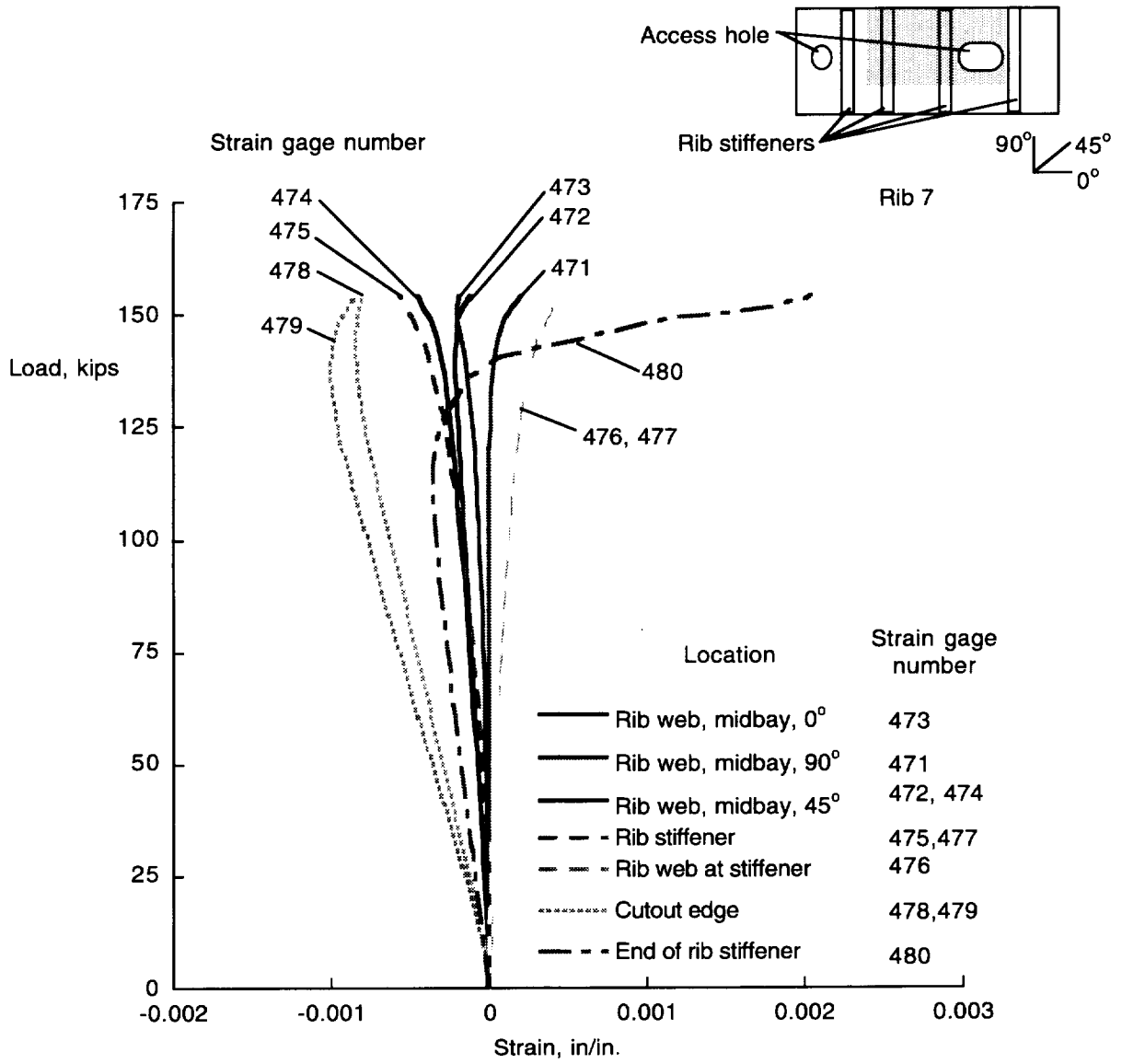
Figure 53. Strains for rib 7.
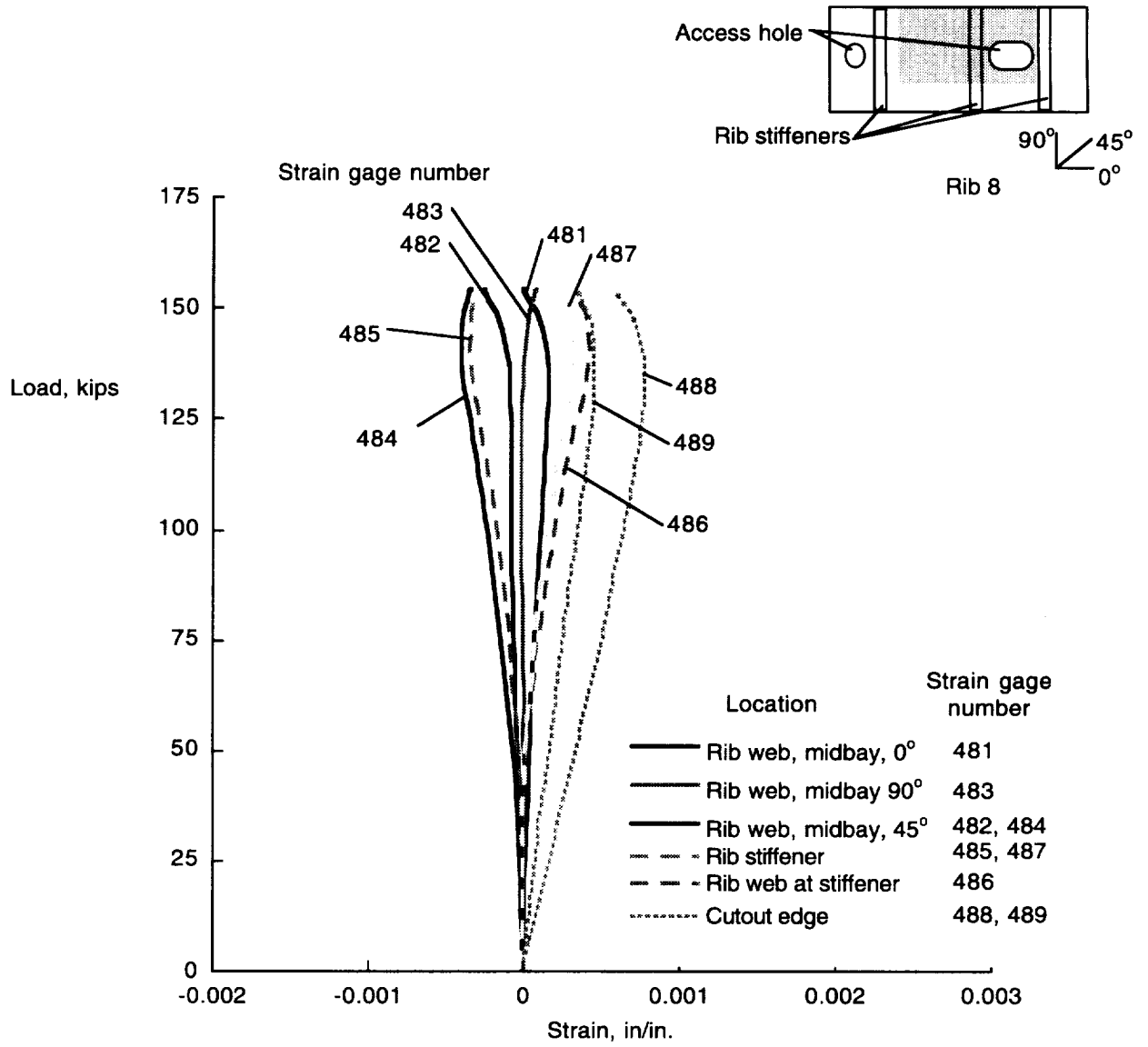
Figure 54. Strains for rib 8.
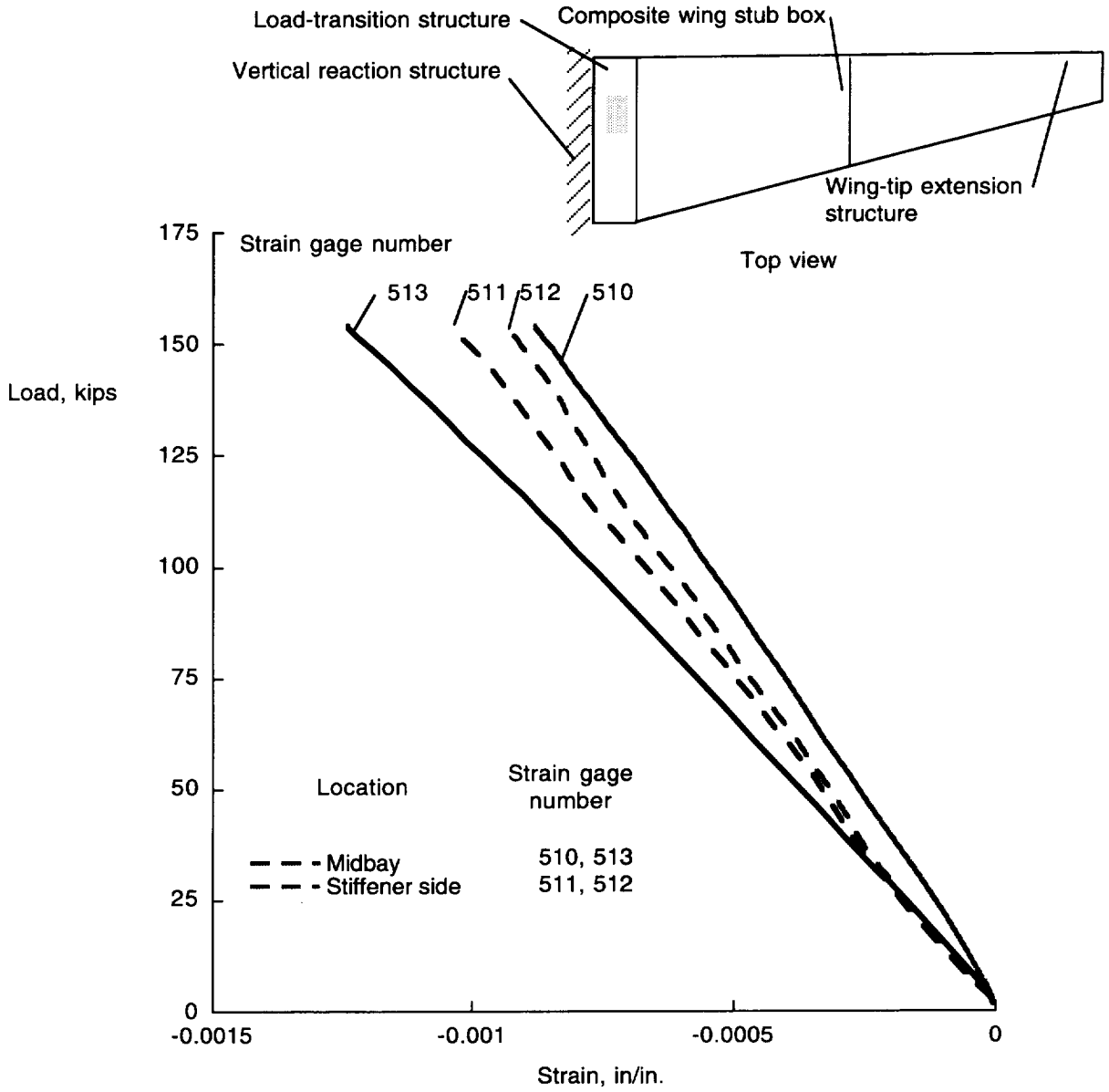
Figure 55. Strains for load-transition structure.
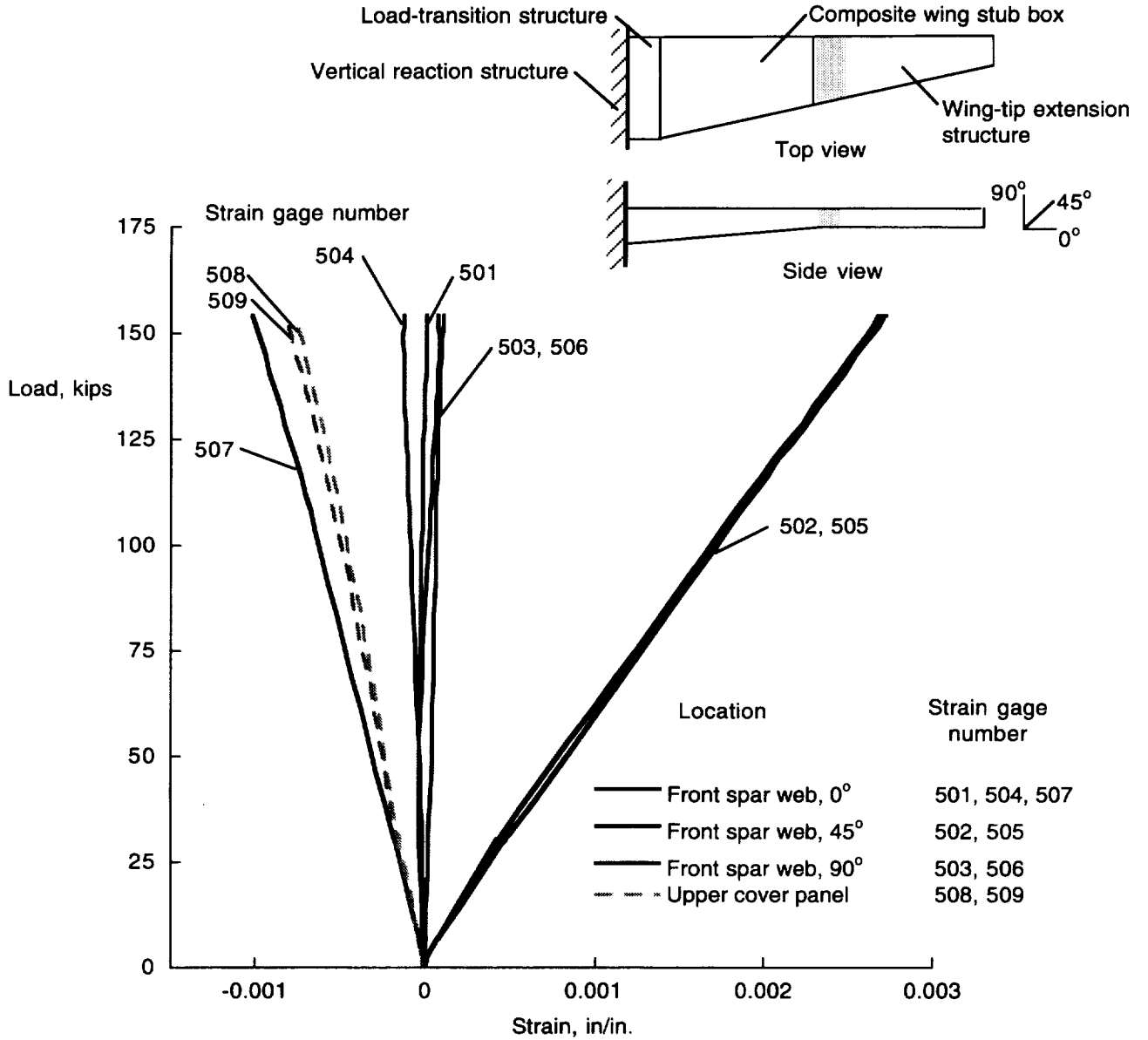
Figure 56. Strains for wing-tip extension structure.
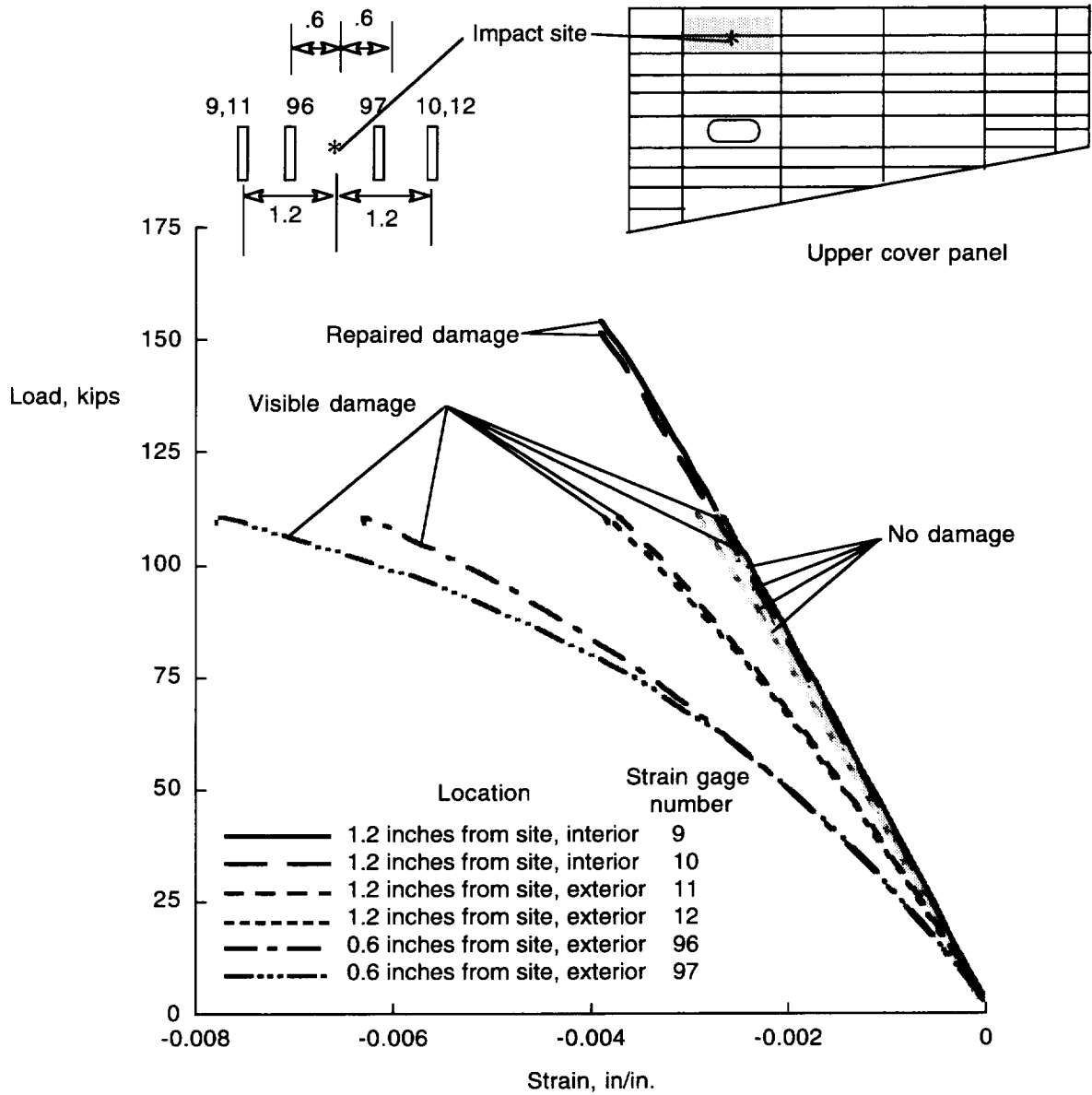
Figure 57. Strains in detectable-damage and repair region during last three tests.
All dimensions are in inches.
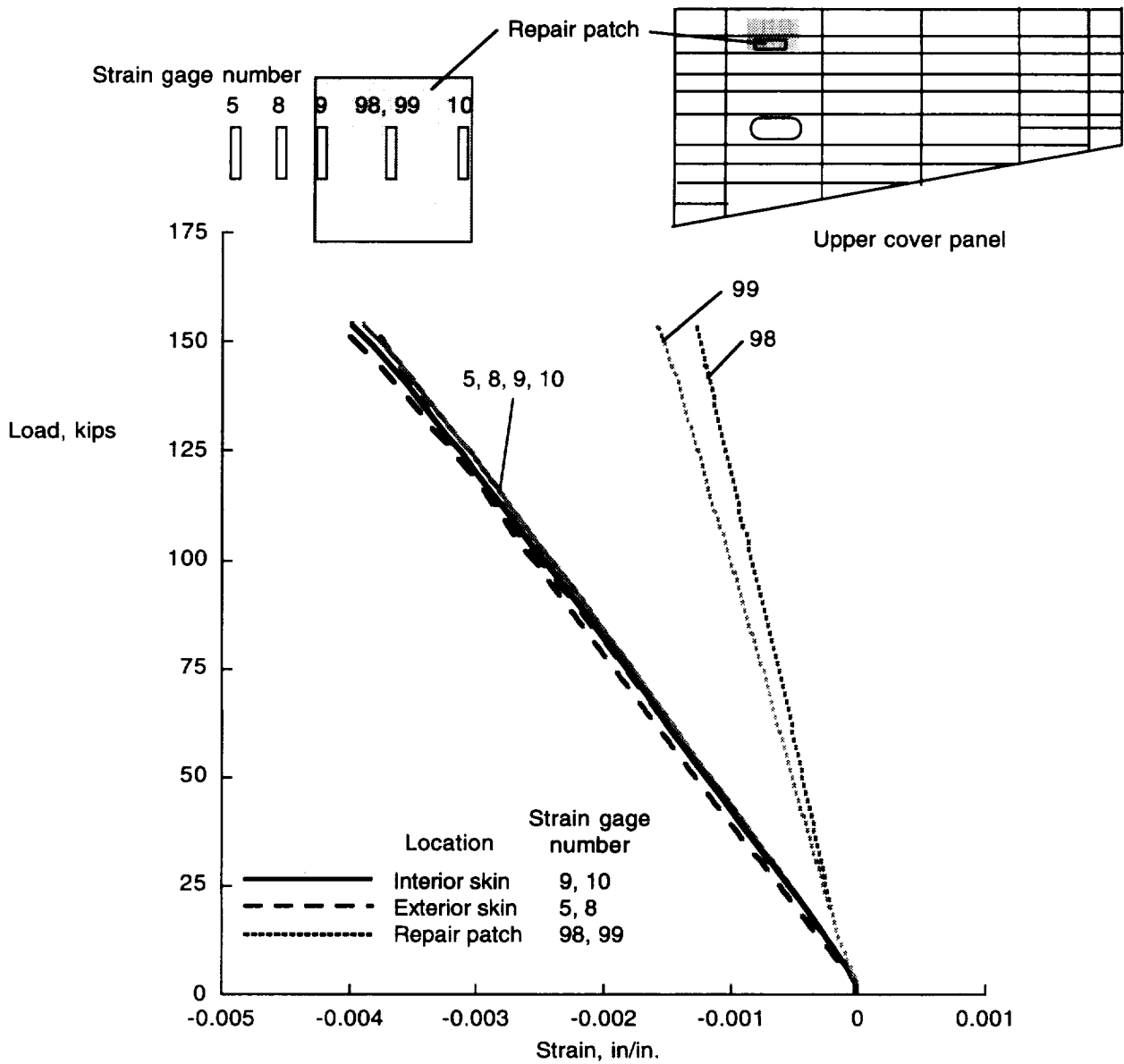
Figure 58. Strains for region of repair.
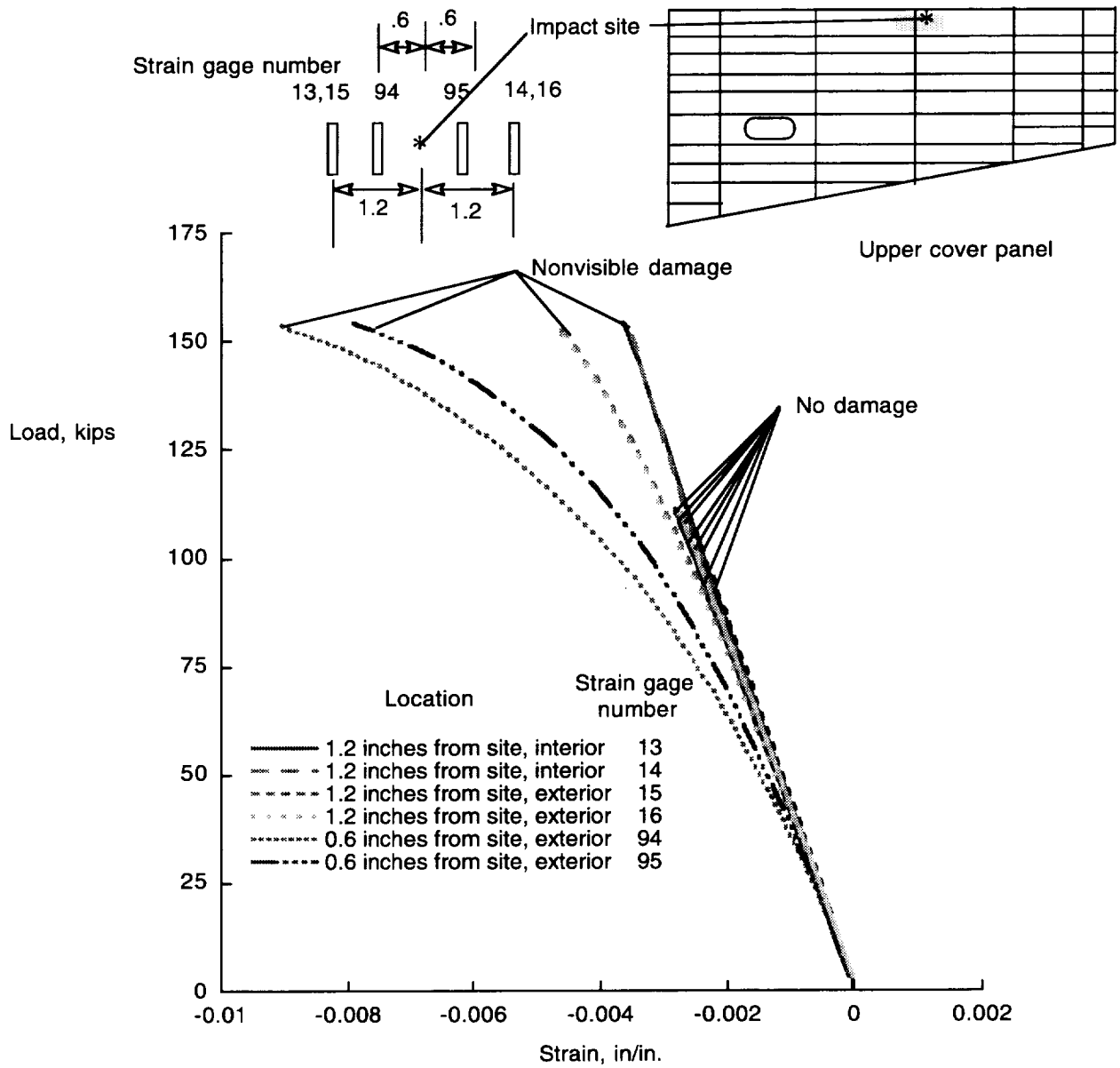
Figure 59. Strains at nonvisible damage site 1 for last three tests. All dimensions are in inches.
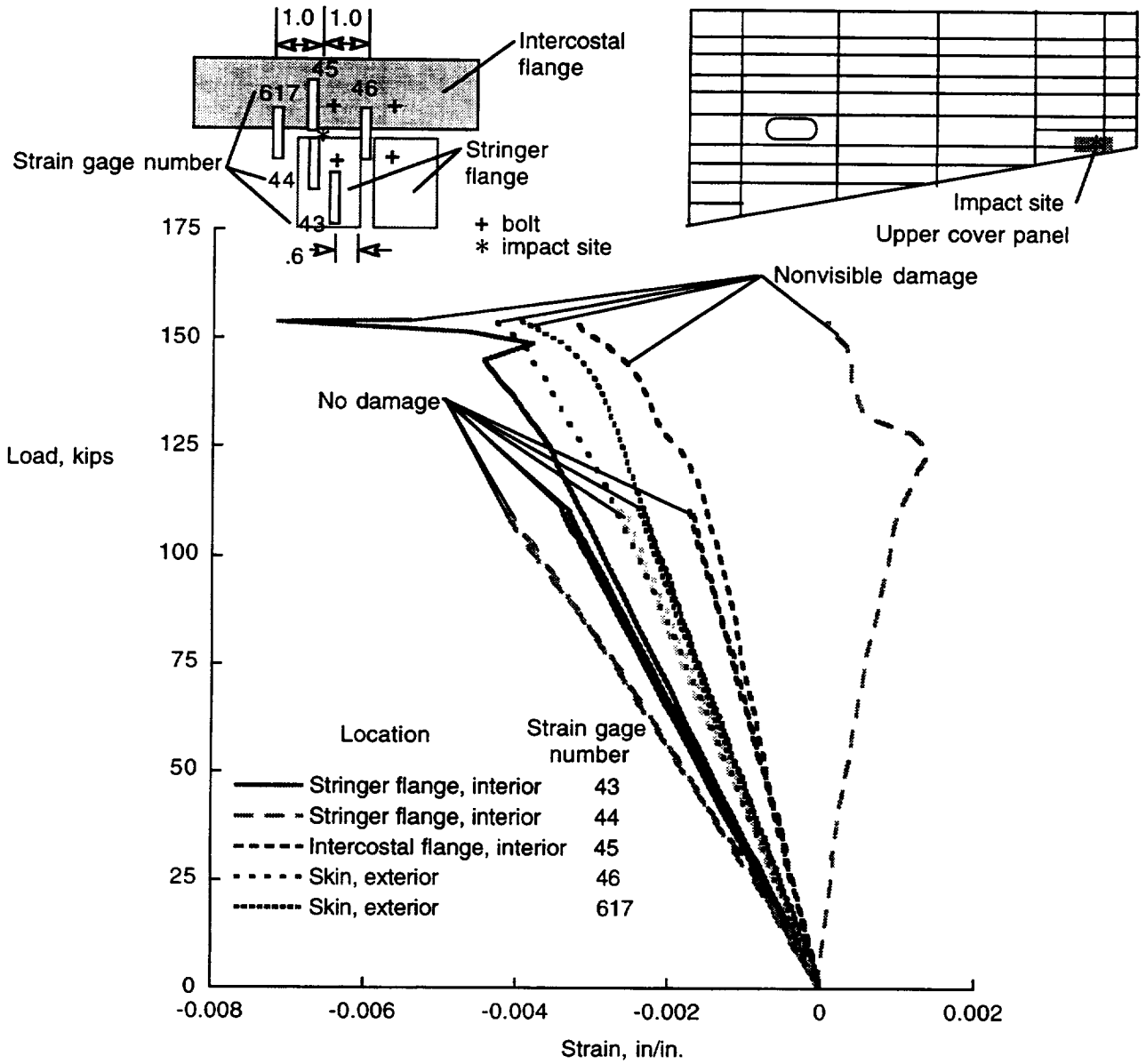
Figure 60. Strains in area around nondetectable damage site 2 for last three tests. All dimensions are in inches.
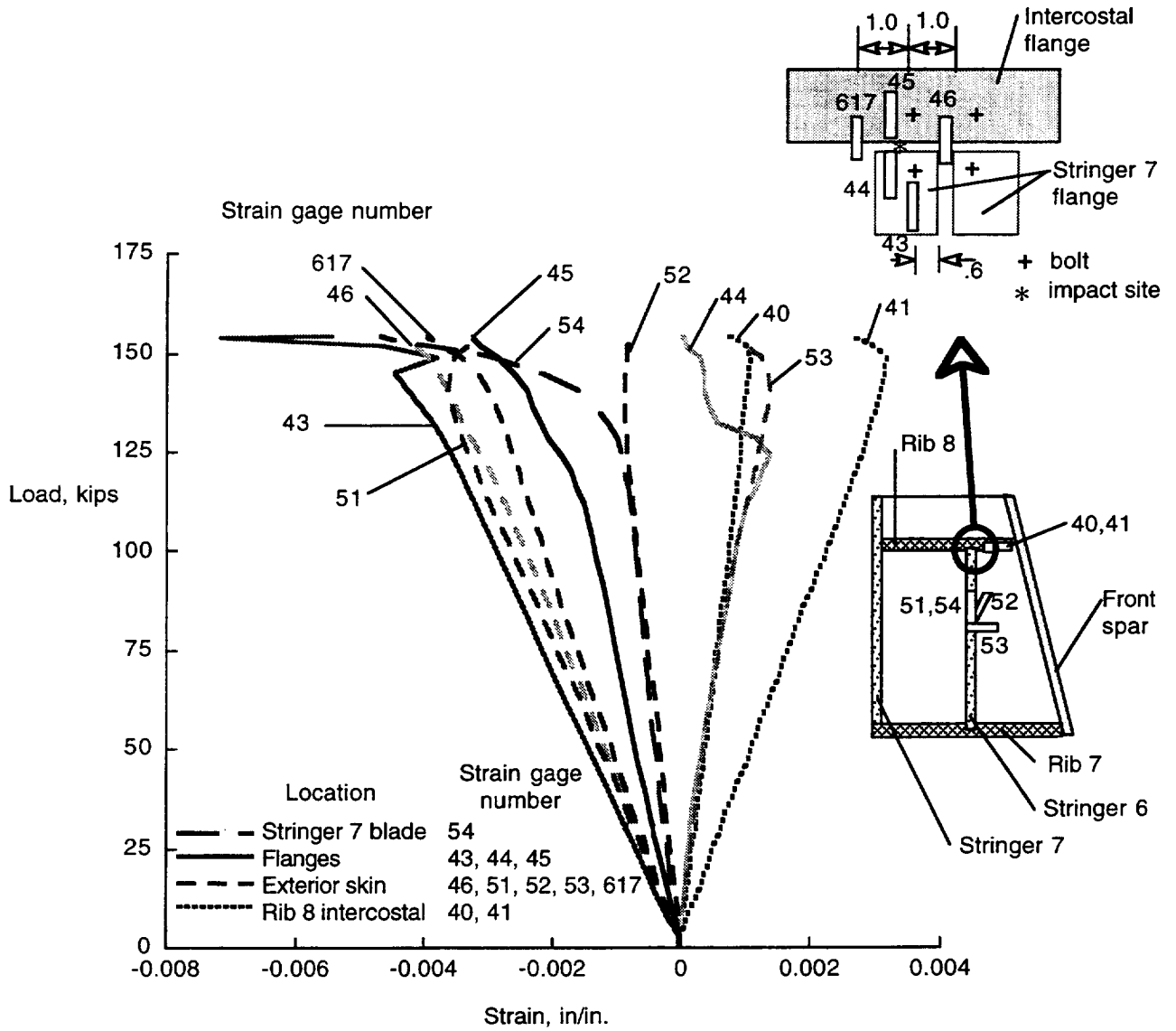
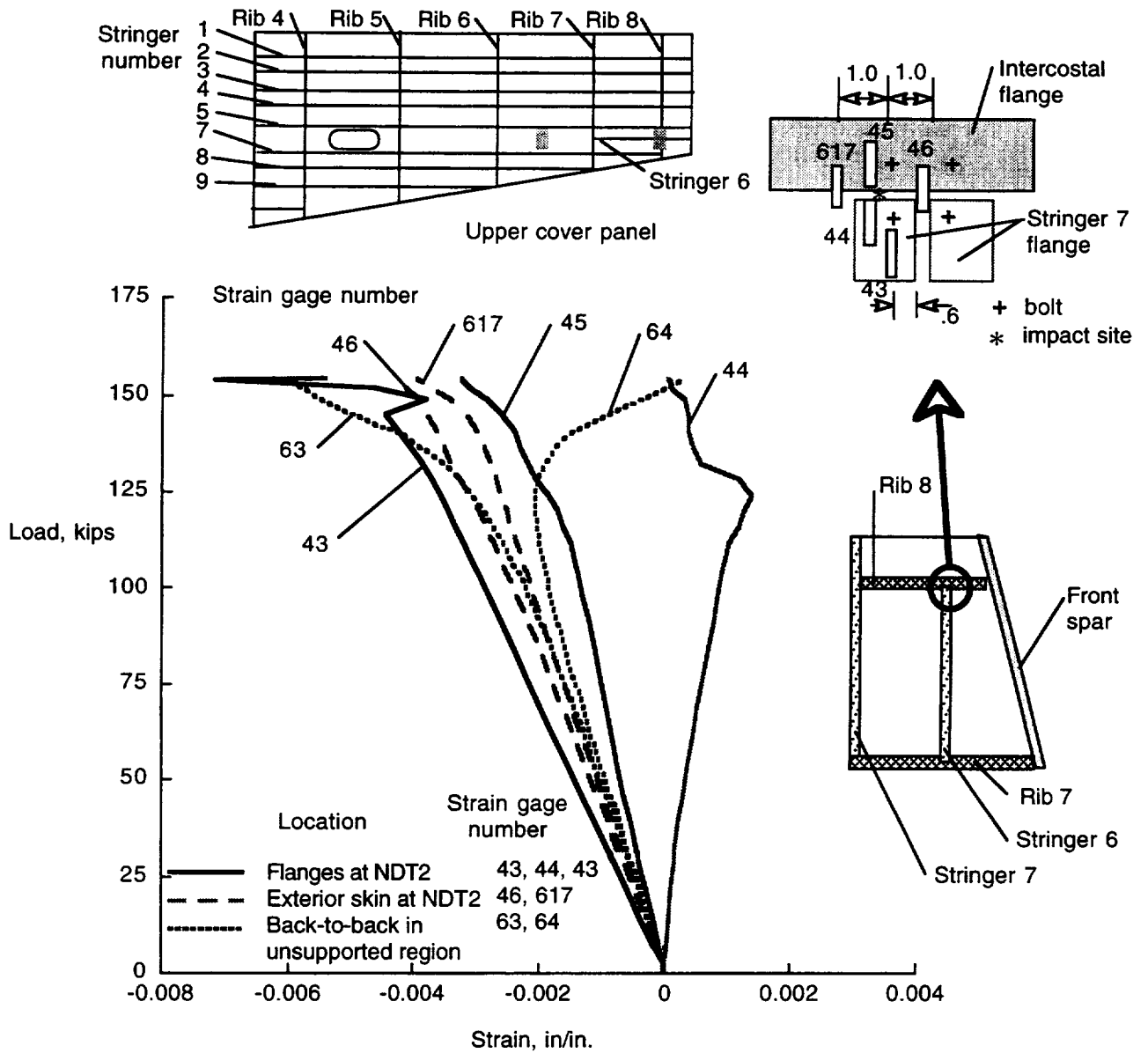Figure 61. Strain in region of nondetectable impact damage site 2. All dimensions are in inches.

Figure 62. Strains in region of nondetectable impact damage site 2 and in unsupported skin region. All dimensions are in inches.
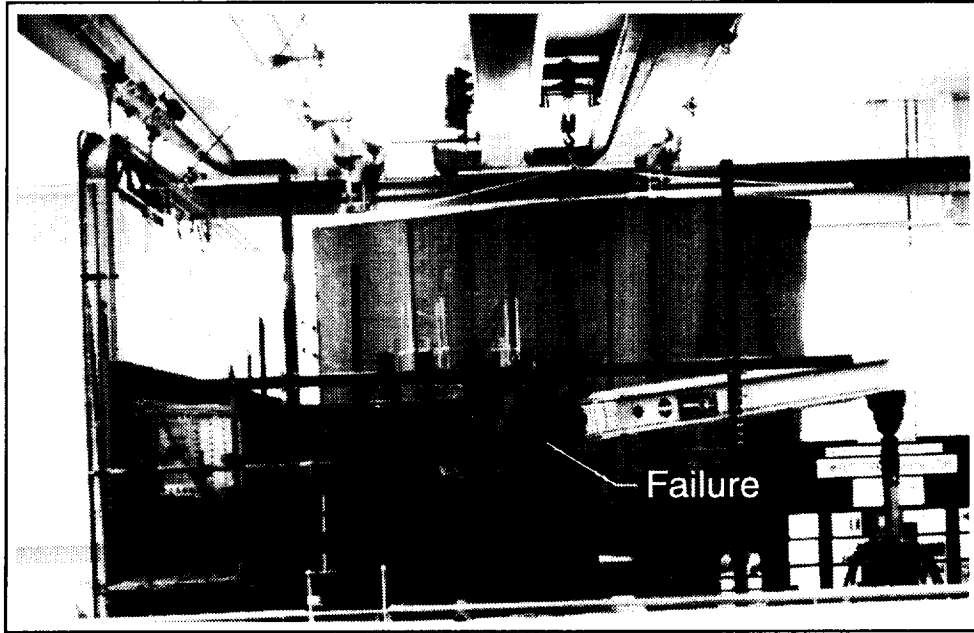
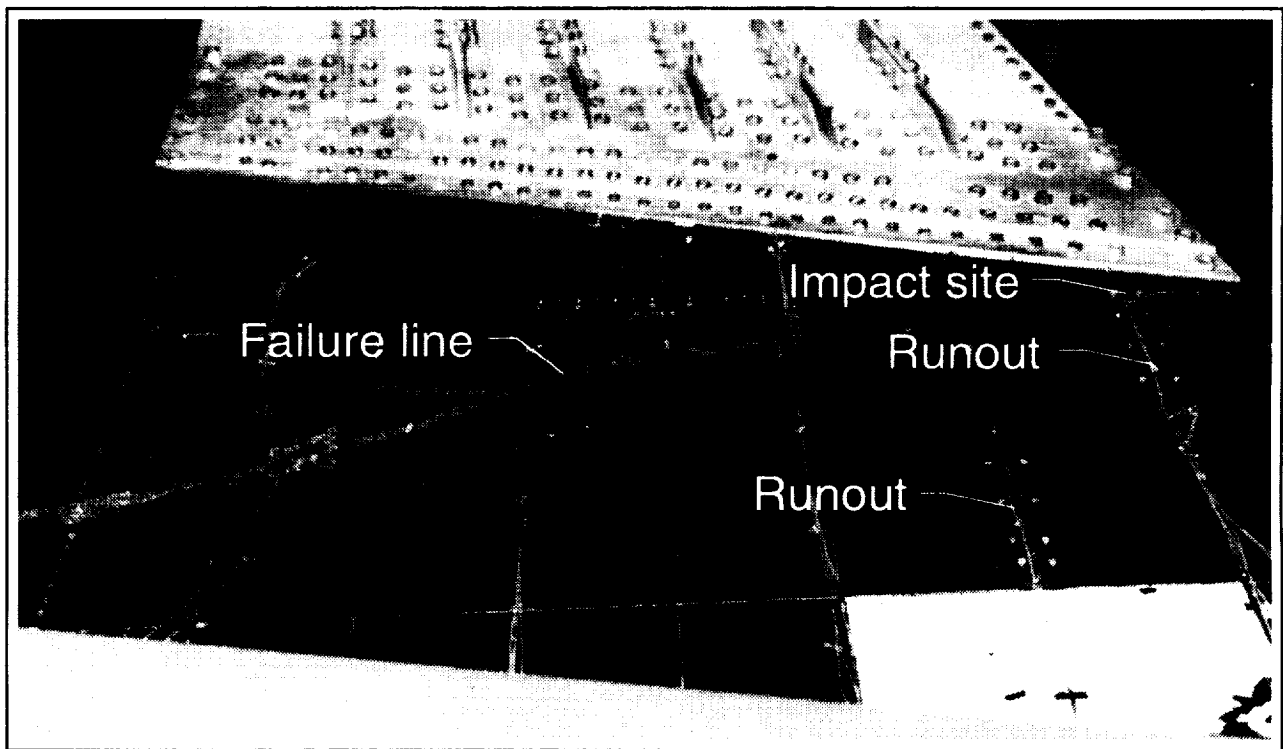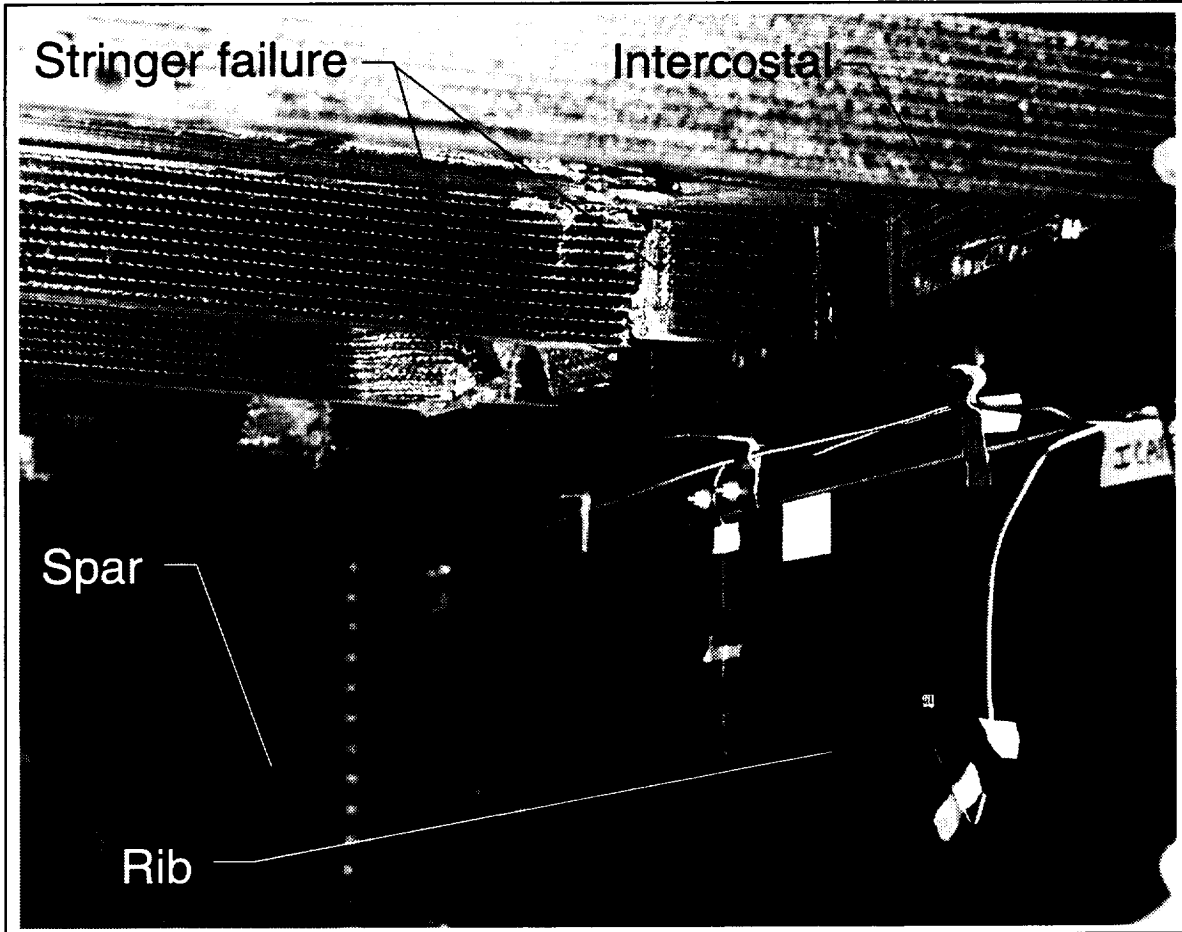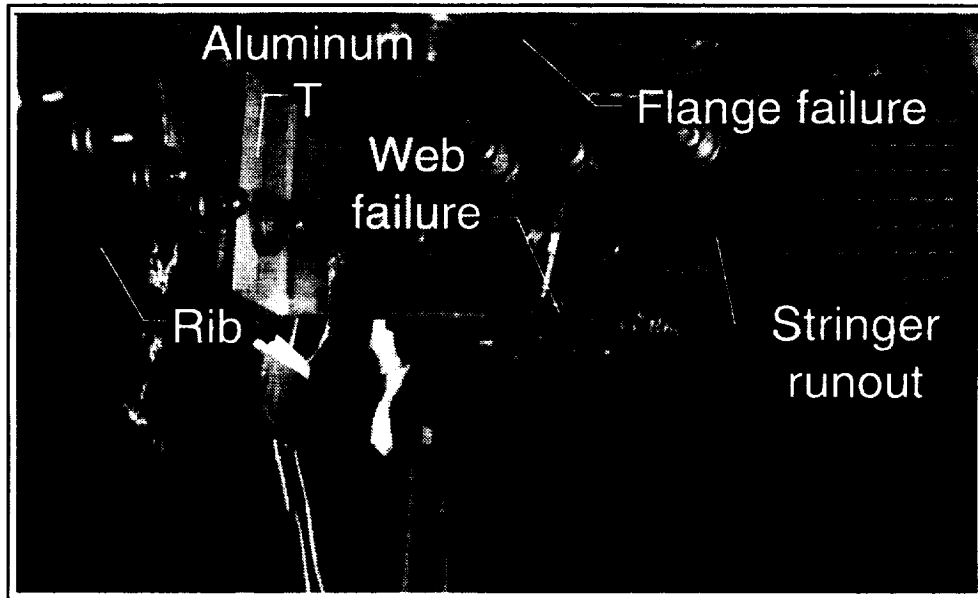Figure 63. Side view of test specimen after failure.

Figure 64. Upper cover after failure of test specimen.

a) Failed stiffeners in upper cover panel

Figure 65. Failed upper cover panel stiffeners.

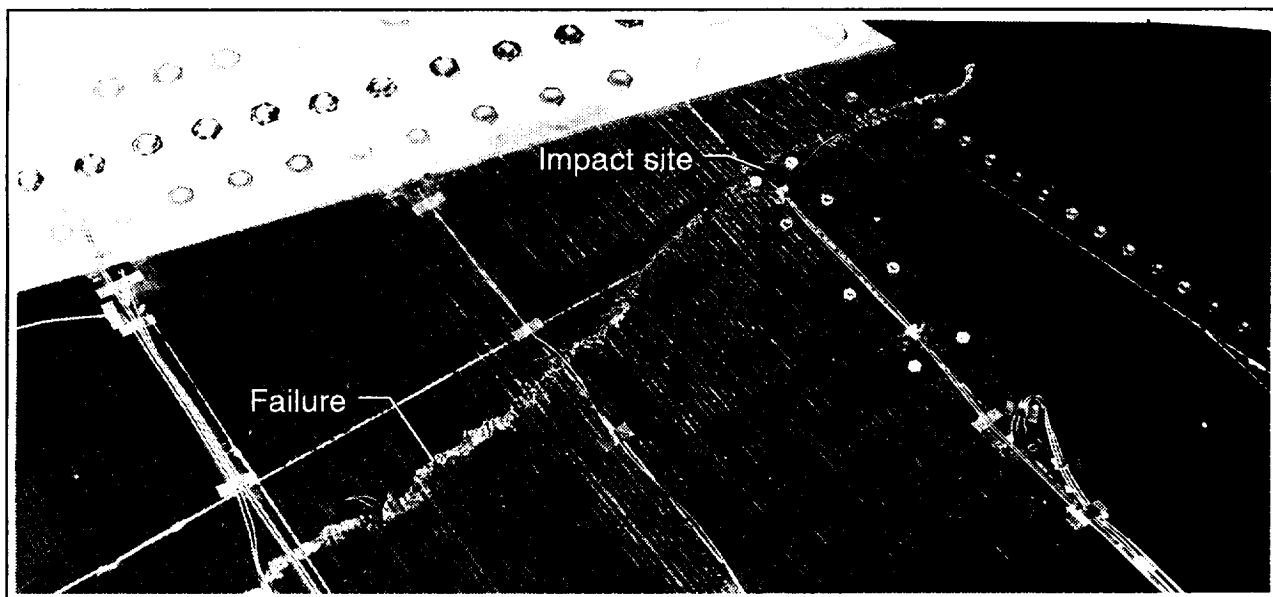b) Failure at runout of stringer 6

Figure 65. Concluded.

Figure 66. Failure through impact damage site NDT2.

REPORT DOCUMENTATION PAGE

Public reporting burden for this collection of information is estimated to average 1 hour per response, including the time for reviewing instructions, searching existing data sources, gathering and maintaining the data needed, and completing and reviewing the collection of information. Send comments regarding this burden estimate or any other aspect of this collection of information, including suggestions for reducing this burden, to Washington Headquarters Services, Directorate for Information Operations and Reports, 1215 Jefferson Davis Highway, Suite 1204, Arlington, VA 22202-4302, and to the Office of Management and Budget, Paperwork Reduction Project (0704-0188), Washington, DC 20503.

1. AGENCY USE ONLY (Leave blank)	2. REPORT DATE	3. REPORT TYPE AND DATES COVERED
	April 1997	Technical Memorandum

4. TITLE AND SUBTITLE
Structural Test Documentation and Results for the McDonnell Douglas All-Composite Wing Stub Box

5. FUNDING NUMBERS
538-10-11-06

6. AUTHOR(S)
Dawn C. Jegley
Harold G. Bush

7. PERFORMING ORGANIZATION NAME(S) AND ADDRESS(ES)
NASA Langley Research Center
Hampton, VA 23681

8. PERFORMING ORGANIZATION REPORT NUMBER

9. SPONSORING / MONITORING AGENCY NAME(S) AND ADDRESS(ES)
National Aeronautics and Space Administration
Washington, DC 20546-0001

10. SPONSORING / MONITORING AGENCY REPORT NUMBER
NASA TM-110204

11. SUPPLEMENTARY NOTES

12a. DISTRIBUTION / AVAILABILITY STATEMENT
Unclassified, Unlimited, Subject Category 39

12b. DISTRIBUTION CODE

13. ABSTRACT (Maximum 200 words)

The results of a series of tests conducted at the NASA Langley Research Center to evaluate the behavior of an all-composite full-scale wing box are presented. The wing stub box is representative of a section of a commercial transport aircraft wing box and was designed and constructed by McDonnell Douglas Aerospace Company as part of the NASA Advanced Composites Technology (ACT) program. Tests were conducted with and without low-speed impact damage and repairs. The structure with nonvisible impact damage carried 140 percent of Design Limit Load prior to failure through an impact site.

14. SUBJECT TERMS
graphite-epoxy   impact damage
stitching
wingbox

15. NUMBER OF PAGES
100

16. PRICE CODE
A05

17. SECURITY CLASSIFICATION OF REPORT	18. SECURITY CLASSIFICATION OF THIS PAGE	19. SECURITY CLASSIFICATION OF ABSTRACT	20. LIMITATION OF ABSTRACT
Unclassified	Unclassified		